Steric and Electronic Effects on the Structures of Substituted Silicon Compounds

Lorna J. McLachlan

A thesis presented for the degree of
Doctor of Philosophy
in the College of Science and Engineering
at the University of Edinburgh, 2004.

Declaration

This thesis has not been submitted, in whole or in part, for any degree at this or any other university. The work is original and my own, carried out under the direction of Prof. D. W. H. Rankin; where this is not so credit has been duly given.

Acknowledgements

I would firstly like to thank my supervisor, Prof. David Rankin, for his constant help and direction over the last four years. I have been amazed by his patience at my grammatical failings and can assure him that I now know "that" and "which" are not interchangeable. I also thank the School of Chemistry for funding.

I'd like to thank everyone in the ed@ed group past and present, especially Sarah, Andy, Carole, Blair, Kostya, Julien, Iain and Derek.

Thanks are due to Claire for always being there to cheer me up when the pressures of top science became too much. The shinty club has been a great help for helping take out any frustrations in a healthy way and for many exciting and interesting bruises. I would also like to thank Phoebe, my long distance flat-mate, who has always been there for me and let me claim to be the chemical consultant for the Harry Potter films.

This PhD would not have been the same without the lunch gang. I would especially like to thank Gordon, Kat, Dave and Robin for many happy times putting off the afternoon's work by drinking tea and playing cards.

My last vote of thanks goes to my parents. This would not have been possible without their constant love and support.

Abstract

Gas-phase electron diffraction is an excellent technique for determining molecular structures free from the intermolecular interactions associated with solid-state techniques. By augmenting our experimental data with information from theoretical calculations, using the SARACEN method, we can now study many compounds that were previously inaccessible to us. This thesis is concerned with the application of the SARACEN method to a range of molecules with interesting structural properties and applications in industry.

The gas-phase structures of a series of compounds have been obtained, combining gas-phase electron diffraction and *ab initio* molecular orbital theory. For each compound a search of the potential energy surface was carried out to investigate the number of conformational minima and to locate the global energy minimum.

The gas-phase structures of *trans*-1,2-dichloro-1,2-disilylethene, 1,1-bromosilylethene and 1,1,1,4,4,4-hexachloro-1,4-disilabutane were determined and *ab initio* calculations on analogous compounds were carried out. This study revealed extreme asymmetry in coordination at carbon, and trends in bond lengths and angles were interpreted in terms of cumulative electronic and steric contributions.

The structure of bistrichlorosilyldimethylgermane [$(Me_2Ge(SiCl_3)_2$] was determined *ab initio* and by gas-phase electron diffraction and compared to that of a previously determined trimethyl analogue. An important difference between experimental and theoretical results was revealed.

Three silylhydrazines, $F_3SiN(Me)NMe_2$, $F_3SiN(SiMe_3)NMe_2$ and $ClH_2SiN(Me)NMe_2$ have been studied *ab initio* and by gas-phase electron diffraction. Solid- and gas-phase investigations of other substituted silylhydrazines revealed unusually narrow Si-N-N bond angles. Structural investigations were initiated for the halogen and bulky alkyl-substituted compounds to gauge the effects of these different substitutions on the Si-N-N bond angles. Further calculations were carried out on similar compounds upon removing the "donor" and "acceptor" atoms, to verify the presence of Si β-N interactions.

Contents

CHAPTER ONE

Introduction and Background Theory

1.1 General Introduction

Knowledge of the structure of a molecule is crucial for understanding all aspects of its chemistry. It is impossible to predict correctly the behaviour of a molecule in a reaction or what its physical properties may be without this information. The basis of all chemistry, *i.e.* the fundamental make-up of molecules, is principally concerned with the connectivity of atoms. The bonds and angles that these atoms make to one another give each molecule an individuality that allows the existence of such a huge variety of chemicals, from sand on the beach to the silicon chip in a computer.

Chemists are now demanding more from a structural determination. It is generally no longer adequate simply to know the connectivity of structures. For example, the structures of other possible conformations and highly accurate bond lengths and angles are also desired. As may be expected from an area so close to the core of chemistry, there are many structural determination techniques in existence. Examples of these are X-ray diffraction (used mainly to obtain solid-state structures), rotational, including microwave, spectroscopy (normally only applicable to very small molecules) and liquid crystal nuclear magnetic resonance spectroscopy (used for geometrical information). From these, it is now possible to get very accurate values for bond lengths and angles. However, the molecular structures determined from some of these techniques may be further complicated. For example, in X-ray diffraction, the structure of the molecule may be affected by its neighbours (due to intermolecular forces and packing forces). If one is concerned solely with the structure of an individual molecule then a technique that allows for the elucidation of structures in the gas phase is ideal, as it is free from these forces.

Gas-phase electron diffraction (GED) is the one of the few experimental techniques that is available for gaseous molecules, such as those studied in this thesis. However, as will be explained later, there are still major limitations with this experimental method, which could render these structures unsolvable, or only partially solvable. We therefore need to look elsewhere for information to supplement our experimental data. *Ab initio* techniques have been developed and improved upon substantially in

recent years. By including calculated data within our structural study, we can now determine accurate molecular structures that would previously have been beyond our capabilities

1.2 *Ab initio* calculations

1.2.1 What is *ab initio* theory? *Ab initio* calculations involve finding a solution to the Schrödinger equation in order to investigate molecule structures. The term "*ab initio*" literally means from the beginning. This signifies that a solution to the Schrödinger equation is obtained using only physical constants, such as Planck's constant, the speed of light, the mass, spin and charge of all the constituent particles and no experimental data. A solution to the Schrödinger equation is very desirable as from this quantum mechanical approach it is possible to predict many molecular and geometrical properties. These calculated values can then be used for many purposes including interpretation of infra-red and Raman spectra, prediction of reaction mechanisms and, as is of specific interest in this research, directing the refinement of structures based on gas-phase electron diffraction data.

1.2.2 Solving the Schrödinger equation. The Schrödinger equation can be written in the form

$$H\Psi = E\Psi \qquad \text{Equation 1}$$

where E = the total molecular energy, Ψ = the total wavefunction and H = the Hamiltonian operator.

In principle, it is only possible to obtain an analytical solution for the Schrödinger equation for one-electron systems (e.g. H and He^+); otherwise it can only be solved numerically. This is due to the difficulties in obtaining solutions for systems involving the interaction of more than two bodies caused by the electrons in the system subject to electrostatic forces from one another. This is known as "the many body perturbation problem".[1] It is therefore necessary to employ approximations for

both the Hamiltonian operator and the wavefunction in order to find a solution to the Schrödinger equation.

1.2.3 Simplifying the Hamiltonian Operator. The Hamiltonian operator, which consists of potential and kinetic energy terms, describes which operations are to be carried out on the wavefunction. The Hamiltonian operator is made up of five terms: the kinetic energy of the electrons and the nuclei, the potential energy of the nuclear repulsion and electronic repulsion and the potential energy of the attraction of electrons to nuclei. In order that a solution to the equation may be obtained, several approximations have to be made. The first of these is the Born-Oppenheimer approximation. This uses the assumption that, as nuclei are many, many times heavier than electrons, they will be moving considerably slower. Therefore, it is reasonable to treat the nuclei as stationary in a field of moving electrons. This means that the kinetic energy term for the nuclei is reduced to zero (as the nuclei are not moving). Thus, the nuclear repulsion potential energy term is a constant and dependent only on the fixed positions of the nuclei.

The only terms of the Hamiltonian operator remaining contain an electronic component and, of these, only one poses any specific problems. This term is the potential energy of electronic repulsion. If the electrons did not repel each other, each electron would behave independently and the Schrödinger equation could be solved as a sum of one-electron equations. Unfortunately, it is not possible to deny that the electrons interact with one another and still get an accurate solution to the Schrödinger equation. The electrostatic interaction between two electrons 1 Å apart is 14 eV (i.e. very large). Ignoring this would result in large errors in any calculation, so instead of ignoring their interaction, their correlation is ignored.[2] This is the basis of Hartree-Fock (or Self-Consistent Field – SCF) theory, the most basic of the *ab initio* methods.

Ignoring correlation results in the electrons moving in a uniform field generated by all the other electrons present, *i.e.* the potential energy field of the electron-electron

is a constant. Surprisingly, using the Hartree-Fock (HF) level of theory can account for nearly all of the energy of a molecule (*ca.* 99%).

Correlation is especially important if the molecule contains areas of high electron density, such as when there are double bonds, aromatic rings or highly electronegative atoms. It can be seen that, although ignoring correlation results in a good first approximation, it does not give a complete reflection of the molecule. For example, ignoring electron correlation in a H_2 molecule would give the same probability of both electrons being located near one atom as one electron being near atom H(1) and the other electron near atom H(2). Obviously, this is not completely representative of the real molecule as repulsion between the two electrons would keep them apart.

In this way, the approximations used in the Hartree-Fock level of theory can be used as a starting point for calculations. However, this method is inadequate and it should not be used to generate the final answer on which all conclusions are based.

1.2.4 Including electron correlation. Fortunately, there are a several methods of including correlation. One of the more common methods is called "perturbation theory". Møller and Plesset first applied this method to the problem of correlation in quantum chemical calculations in 1933.[3] For example, if the solution to the Schrödinger equation is known for one Hamiltonian operator, the solution for a similar Hamiltonian operator can be generated by applying a slight perturbation to the first solution. This method can be used to model a large variety of systems and has been extensively used in this thesis.

Other methods of including correlation are the Configuration Interaction (CI) and Coupled Cluster (CC) theories, which use different approaches from that of the Møller-Plesset series (MPX). The Schrödinger Equation is still solved as a series of one-electron equations, but restrictions are made on where the second electron can be placed. It is not permitted to be in the same orbital as the first electron (see Figure

1). With this restriction in place the electrons may still move independently of each other, but they are prevented from becoming too close to one another.

Figure 1 (a) HF method with unrestricted location of electrons; (b) CI/CC method with electrons placed in different regions of space.

While the CI and CC methods of including electron correlation are effective, they are generally only used for calculations in small molecules. This is because they are much more computationally expensive than the MPX method of including electron correlation, and for our purposes, MPX is normally sufficient.

1.2.5 Simplifying the wavefunction. The electronic wavefunction (Ψ) describes the area of space around the nucleus where electron motion is allowed to take place. We have already discounted the motion of nuclei as according to the Born Oppenheimer approximation they are considered stationary. The electronic wavefunction is generated by a linear combination of basis functions each centred on an atom. This combination of basis functions is known as a basis set, a mathematical representation of molecular orbitals. The basis set defines the probability of finding electrons in certain areas of space. Ideally, a basis set would comprise an infinite number of these functions to model the electron distribution perfectly. However, this is not possible as it would require unrealistic (i.e. infinite) computational resources.

There are various mathematical forms of basis functions. One of the most popular is Gaussian functions. However, Gaussian functions [which generate Gaussian-type orbitals (GTO's)] are not totally accurate in their reflection of the structure of an

atomic orbital. A Slater function [which generates Slater type orbitals (STO's)] is much more representative of atomic orbitals. However, STO's are not commonly used in *ab initio* calculations, as Gaussian functions are much easier to compute.

Figure 2: (a) Slater and (b) Gaussian functions.[4]

From Figure 2, it is possible to see the difference between the shapes of the Slater and Gaussian functions. The Gaussian function lacks the cusp (a discontinuous derivative) of the Slater type function and also can be seen to slope off prematurely. To overcome this fact, a summation of a number of Gaussian functions is used instead (see Figure 3). It is possible to vary the exponent (slope) and coefficient (weighting) of each of the Gaussian functions until their summation gives the most accurate reflection of the radial function. In practise some Gaussian functions are frozen in their relative dependencies and are treated as a single function, giving a contracted basis set. Clearly, with fewer coefficients to optimise, the calculations are less computationally expensive.

Figure 3 Summation of Gaussian functions to give approximation of the atomic radial function.[4]

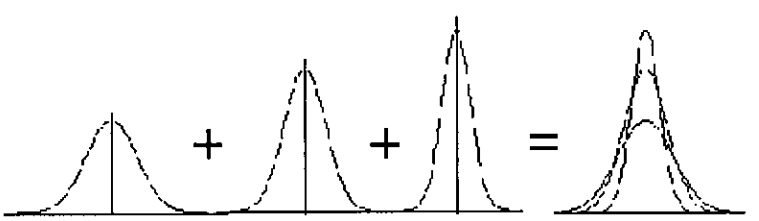

1.2.6 Basis sets. As previously mentioned, it is not possible to use basis sets that model the distribution of the electrons accurately over all space. Instead, a variety of basis set sizes can be used, depending on the accuracy required from the calculation. These range from smaller basis sets (known as single zeta, ζ, basis sets) which only use one basis function to describe each occupied atomic orbital to larger basis sets (for example, triple-ζ or quadruple-ζ basis set) which have three or four functions describing each atomic orbital. The larger the basis set used, the more accurately it reflects the real atomic orbitals.

Minimal basis sets are useful in initial calculations, but should not be used as the final computational solution. Split basis sets are commonly used in calculations to allow for some change in the shape of the orbitals in response to changing molecular environment. They are also commonly used with the introduction of electron correlation, which is only important for the valence electrons involved in bonding. By splitting the basis set into a part for the valence electrons and a part for the core electrons, the inner part can be excluded from correlation calculations, thus saving unnecessary computational expense.

One of the most common small basis sets used is 6-31G,[5-7] in which each of the core orbitals is represented by six Gaussian functions, whilst the inner and outer valence orbitals are represented by three and one Gaussian functions respectively. Another example of a split basis set is 6-311G.[8,9] Here, the core orbitals are represented by six Gaussian functions, the inner valence orbitals are represented by three Gaussian functions, and the outer and the middle orbitals are represented by one Gaussian function each. As the basis sets describe atomic orbitals and not molecular orbitals, it is important to consider any possible changes that the orbital shapes will undergo on bonding. For example, fluorine, the most electronegative element, gains extra electron density in its outermost valence orbitals when it bonds to other atoms. Basis sets, therefore, must be easily adaptable to allow for significant changes in shape or size of these valence orbitals.

It is possible to improve the basis sets further by adding polarisation and diffuse functions. In H_2, for example, adding a *p* orbital to hydrogen allows the atomic orbitals to reflect the shape of the molecular orbital better. This is called a polarisation (denoted by "*") function, and is illustrated in Figure 4

Diffuse functions are larger, more diffuse versions of the basis functions (denoted by "+"). They extend the basis set to give higher electron density in more diffuse regions of space. Including this kind of function is more important when the system of interest contains anions or neutral molecules with lone pairs.

Figure 4 Construction of a molecular orbital for H_2 without polarised function (top) and with the addition of a *p* orbital (bottom).

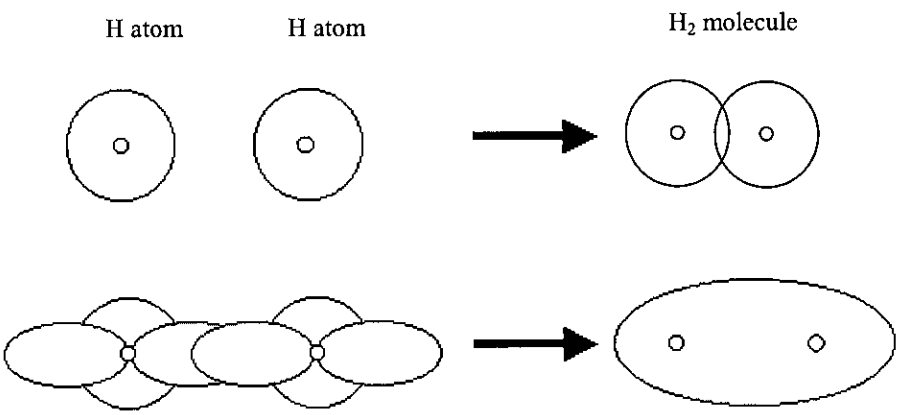

1.2.7 Optimisation procedure. Initially, calculations are carried out on a starting geometry from a Z-matrix, which describes the geometry and symmetry of the molecule, or by identifying the positions of the atoms in the molecule using a set of Cartesian coordinates. The total energy of the system is calculated and minimised. Taking the first derivative of the energy with respect to each nuclear coordinate gives the forces on the atoms. This comes from the gradient of the potential energy surface. The force constants are then estimated and the geometry of the molecule is perturbed and the previous steps repeated. This continues until the forces on the atoms are approximately zero (i.e. $dE / dx = 0$ where x represents the nuclear coordinates).

1.2.8 Other computational methods. As well as Hartree Fock and the Møller-Plesset series, there are other computational methods for calculating the structures of molecules. An example of another method is density functional theory (DFT), which is also in widespread use. In this method, the total energy of the system in expressed as a functional of the total electron density. DFT calculations are generally considered to calculate molecular properties more accurately than HF methods, as electron correlation is taken into account.[10] If the system is large, DFT can be used as a less computationally expensive method to obtain a reliable structure when MP2 calculations would take too long.

Another type of DFT calculation is a plane-wave DFT calculation, which can be used to investigate solid-state crystal structures. In a periodic system, the electrons behave like free particles, i.e. not localised to atomic orbitals. A localised wavefunction (Ψ) would not effectively model this and so a non-localised plane-wave Ψ is combined with a pseudopotential, which describes the core of the system not involved in bonding. A plane-wave DFT study on *N*-methyldichloroacetamide was carried out and the resultant publication is given in Appendix F.[11] It is thought that this paper represents the first publication involving gas- and solid-phase experimental and calculated results together in the one paper.

1.2.9 Conclusions. By utilising a number of approximations, the Schrödinger Equation can be solved for systems containing more than one electron. By increasing the size of the basis set (describing Ψ) and the raising level of theory (describing H), the quality of the approximations used can be improved. In practise, this is achieved by carrying out a series of graded calculations, gradually increasing the basis set and level of theory.

1.3 The theory of Gas-phase Electron Diffraction

One aspect of this research is to compare the calculated structures and molecular geometries obtained from theoretical calculations with those determined by gas-phase electron diffraction.

1.3.1 Early experiments. The theory that light exists as a wave was first suggested by Christiaan Huygans in 1673.[12] This theory however was not immediately accepted as it competed directly with Sir Isaac Newton's theory on the particle nature of light. Indeed, it was not until 100 years later, when Thomas Young conducted his double slit experiment, that compelling experimental evidence was produced and Huygans theory accepted.[13]

In Young's experiment, beams of monochromatic light from a filtered mercury lamp were passed through two slits and the resultant pattern was observed falling on a wall (Figure 5). If the beams of light were particle in nature as previously thought, then the expected pattern would be two bright patches of light on the wall. However, what was actually observed was a pattern of light and dark bands. This can only be explained by considering that the beams of light were acting as waves.

The pattern is generated by different beams of light arriving at the same point on the wall having travelled different distances from the two slits. If the beams arrive in-phase, then there is a bright patch of light on the wall (known as constructive interference). If, however, the beams arrive out-of-phase then a dark patch is generated (destructive interference).

Figure 5 Young's Double Slit Experiment.

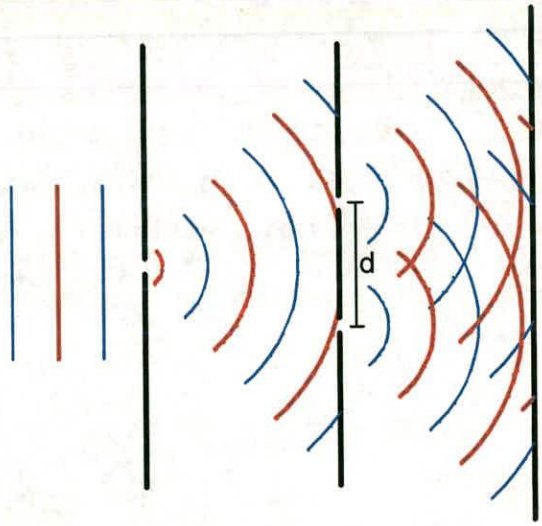

It is possible to calculate the wavelength (λ) of the incident light using the formula (Equation 2)

$$\lambda = d\Delta_{max}/D \qquad \text{Equation 2}$$

where Δ_{max} = the distance between the light and dark maxima, d = slit separation and D = distance from slits to screen.[14]

Following on from this experiment, Louis de Broglie proposed in 1924 that all moving particles also have a wavelength, λ, given by equation 3

$$\lambda = h / p \qquad \text{Equation 3}$$

where λ = wavelength, p = momentum of the particle and h = Planck's constant.[15]

So, whilst a photon can behave as both a wave and a particle, it can also be seen that an electron, normally considered as a particle, could also behave as a wave.

1.3.2 Gas-phase diffraction of electrons. In the case of Young's double slit experiment, for diffraction to be observed it is necessary for the slits to have a separation of similar magnitude to the wavelength of light. Comparisons can be drawn to solid-state structure determination, where X-rays are used as they have a wavelength similar that of the interatomic distances in a crystal. Similarly, moving particles also have wavelengths dependent on their mass and velocity. Electrons accelerated through 50 kV have a suitable wavelength for diffraction by a sample of gas to be studied. [It is usual for the sample being studied to be a gas because electrons (as charged particles) do not pass through solids or liquids very well.] When a beam of electrons is passed through the gas-phase sample, the pairs of atoms in the molecule act like a pair of slits as in Young's experiment. The electrons that are diffracted by the pairs of atoms then interfere with each other and the resultant pattern can be interpreted in order to determine the structure of the molecule. This is

possible as the wavelength of the electrons is known and so the distance between the pairs of atoms can be ascertained from the diffraction pattern.[16]

1.3.3 Experimental set-up. There are two main requirements for a gas-phase electron diffraction experiment; a monochromatic beam of electrons, which interacts with a gas at only one point, and a sample, which must have a sufficient vapour pressure (at least 10 mm Hg for the Edinburgh apparatus) for an electron diffraction pattern of a suitable intensity to be measured. The gas-phase electron diffraction apparatus is shown in Figure 6.

Figure 6 Gas-phase electron diffraction apparatus; details given in text

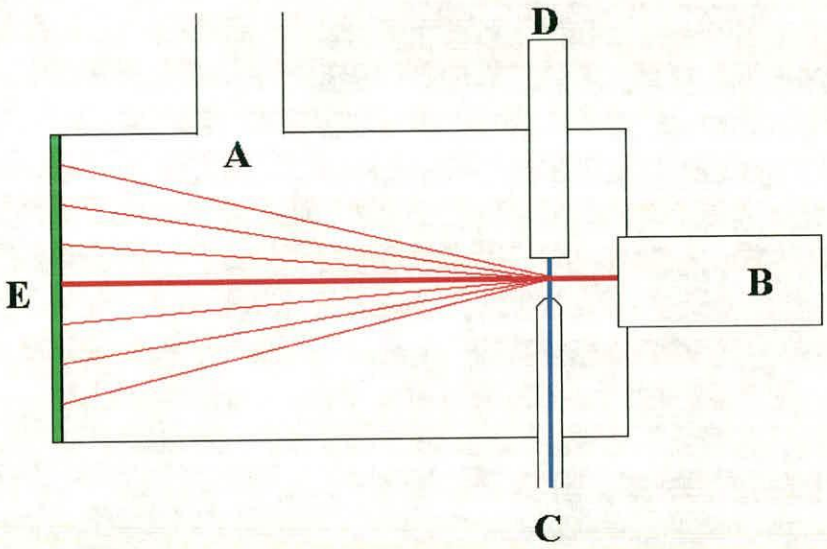

The monochromatic beam of electrons enters the diffraction chamber (B) and interacts with the sample gas (passed out of a fine nozzle, C) at right angles, effectively at a single point. This is ensured by maintaining the whole apparatus under constant vacuum by pumping via a diffusion pump (A). This is to ensure that the electron beam is diffracted at the point where it crosses the sample as it emerges from the nozzle. The diffraction pattern is collected on photographic film (E) and the sample gas is collected in a cold trap (D).

A rotating sector (Figure 7) is to counter the effect of the intensity of the scattered electrons falling off rapidly with scattering angle. The rotating sector, found just before the detector, is shaped so that the width of its opening increases as the fourth power of the distance from its centre. The data are usually collected at two nozzle-to-camera distances, one short and one long. This is to increase the range of angle of the diffraction pattern that can be observed.

The diffraction pattern collected consists of diffuse, concentric rings (see Figure 8). The pattern appears as rings, as opposed to the spots obtained in X-ray crystallography, because in the gaseous sample the molecules are present in random orientations. This pattern must be converted into numerical data before it can be used. This was done using a PDS densitometer at the Institute of Astronomy at the University of Cambridge.[17] The densitometer determines mean intensities as a function of distance from the centre of the diffraction pattern.

Figure 7 Electron diffraction apparatus with rotating sector.[18]

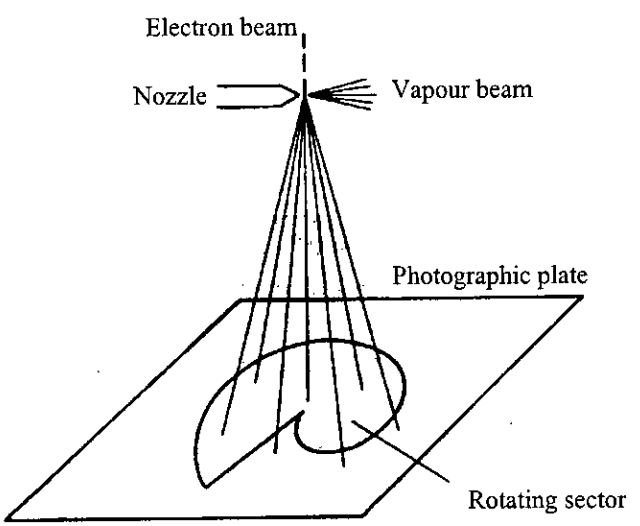

Figure 8 Electron diffraction pattern

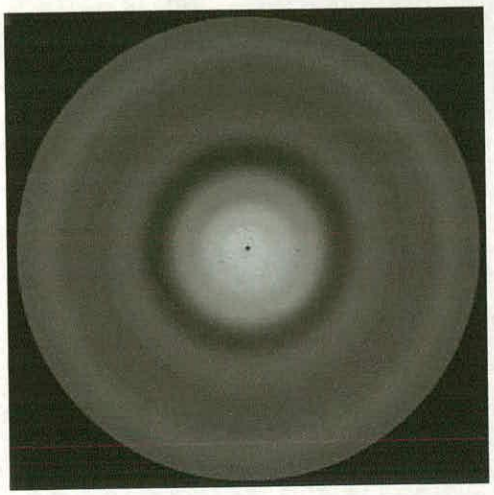

In converting the pattern into numerical data certain facts must be considered, one of which is a blackness correction, which must be carried out to allow for saturation of the photographic emulsion. The diffraction pattern consists of scattering from different sources (Equation 4):

$$I_{tot} = I_{atom} + I_{molec} + I_{bgd} \qquad \text{Equation 4}$$

From this equation, it can be seen that it is possible to obtain the molecular scattering (I_{molec}) by subtracting the atomic (I_{atom}) and the background (I_{bgd}) scattering from the total scattering (I_{tot}). The background intensity is subtracted from the data by using a smooth spline function.[19] The atomic scattering can be calculated as simply being the sum of the contributions from each of the constituent atoms of the molecule.

As can be seen from Figure 9, the total molecular scattering is impossible to interpret. It is necessary to subtract the background and atomic scattering to obtain the molecular intensity scattering curve (Figure 10, NB not the same data as in Figure 9). However, this is also difficult to interpret directly to obtain structural information. The Fourier transform of the molecular scattering curves gives a radial distribution curve. This plots the probability, $P(r)/r$, of finding the distance r plotted against r.

Figure 9 An example of a total intensity scattering curve.

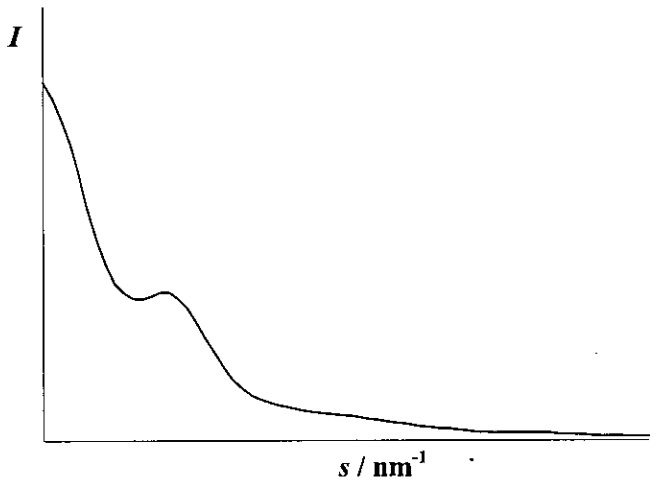

Figure 10 An example of a molecular intensity scattering curve.

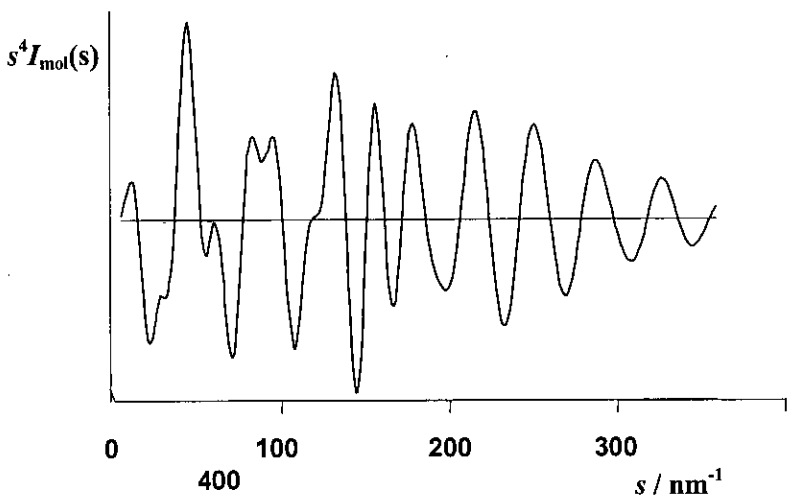

Figure 11 An example of a radial distribution curve, derived from the data shown in Figure 10.

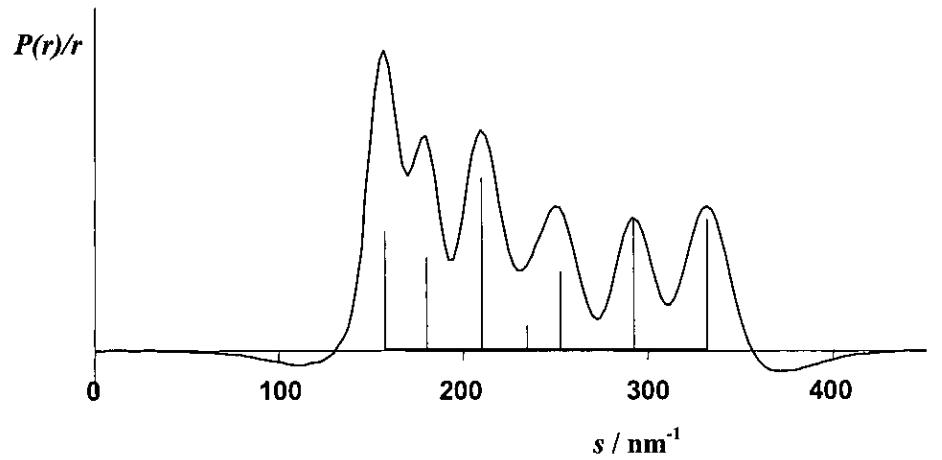

A radial distribution plot is very useful, as an immediate impression of the distances present in the sample molecule is given. As seen in Figure 11, peaks are present centred on internuclear distances. The width of the peak is determined by the amplitude of vibration of the two atoms concerned. It is possible to predict the area under each peak of the radial distribution curve (RDC) by using the formula (Equation 5)

$$area \quad \alpha \quad \frac{Z_i Z_j n_{ij}}{r_{ij}} \qquad \text{Equation 5}$$

where Z_i and Z_j are the atomic numbers of atoms i and j, n_{ij} is the number of times the distance occurs and r_{ij} is the distance.[16]

1.3.4 Structure refinement from electron diffraction data. There are a number of stages in the refinement of a structure based on gas-phase electron diffraction data. First, it is necessary to construct a FORTRAN model of the proposed geometry of the model. *Ab initio* calculations are used to guide the composition of the model, both in a search for conformers and in predicting geometrical properties. The model consists of the molecular structure (atom coordinates) defined by parameters

(generally representing crucial bond lengths and angles) and defines local and total symmetry. This model, along with theoretical amplitudes (also obtained from the *ab initio* calculations), is then refined using a least-squares procedure, allowing the parameters and amplitudes to vary until a best fit with the experimental data is obtained. The quality of fit between the experimental and theoretical data is assessed by two features. The first is a numerical value of the goodness of fit, known as the R_G value, obtained from the least-squares procedure. Another is the difference curve, which is the difference between the experimental and theoretical data sets. This is particularly useful as, when used in conjunction with the radial distribution plot, it is possible to see where the greatest discrepancy between the experimental and theoretical data occurs.

1.3.5 Advantages and disadvantages of electron diffraction. Most electron diffraction is carried out with gaseous samples. This is true of this research. This is beneficial because the molecular structure can be determined free from inter-molecular interactions. It is also useful for direct comparison with the results from theoretical calculations, which also refer to an isolated molecule. Gas-phase electron diffraction (GED) can provide information on inter-nuclear distances in contrast to X-ray diffraction, which measures centres of electron density. In a bond between a hydrogen atom and another atom, the electron density is normally displaced away from the hydrogen towards the other atom. By returning the distance between the centres of electron density an X-ray diffraction study could therefore return a bond that is substantially shorter than the inter-nuclear distance.

However, GED has a number of limitations. The first involves locating the light atoms in a structure. As shown in Equation 5, the area of the peak in the RDC depends on the atomic numbers of the atoms involved. Therefore, if an H - H distance is present in the molecule it would very difficult to distinguish the relevant peak from background noise, and even more so if it overlaps with another peak. Peak overlapping is a distinct problem in itself. When distances of a similar magnitude occur in a molecule, problems can occur in the refinement process. A common method of dealing with the problem of overlapping peaks is by imposing

restraints. By this method, if there are two parameters lying under one peak, it is possible to let them refine and obtain reasonable values. If this method was not used and the parameters were allowed to refine they would be very strongly correlated, and it is possible that they would refine to the same (average) value. However, if parameters are not allowed to refine, the initial parameter value is assumed to be correct and this can lead to unrealistically low estimated standard deviations for correlated parameters.

The SARACEN (**S**tructure **A**nalysis **R**estrained by *Ab initio* **C**alculations for **E**lectron diffractio**N**) method[20] is a way of including in the refinement parameters that would not otherwise have been allowed to refine freely. This involves using a flexible restraint composed of a value (obtained from high level *ab initio* calculations) and an uncertainty (obtained from the level of convergence achieved by that parameter in the calculations) to represent the parameter.

Another problem occurs because of the vibrations of the molecules. Consider the Figure 12; it is possible to see that the average distance between the two blue atoms is less than the actual sum of the two bond distances. This is known as the "shrinkage effect".

Figure 12 Vibrating molecule.

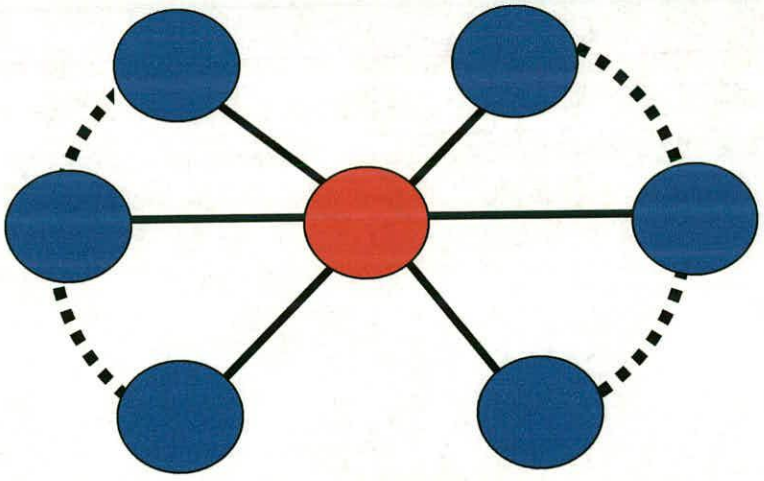

There are two ways of dealing with the shrinkage effect. The first is called rectilinear vibrational corrections (see Figure 13), where the outer (blue) atoms are considered to move in straight lines, based on the direction of motion, for a particular mode, at the equilibrium structure. These corrections are routinely used in the electron diffraction refinements. They are obtained from the output of a program called ASYM40[21], which calculates parallel and perpendicular corrections from a list of *ab initio* calculated frequencies and force constants. Consideration of Figure 13 shows that such vibrational corrections are inadequate. The bonded (blue-red) distance undergoes stretching as the molecule bends, while the non-bonded distance (blue ··· blue) does not change. This is the exact opposite of what really occurs.

Figure 13 Rectilinear corrections.

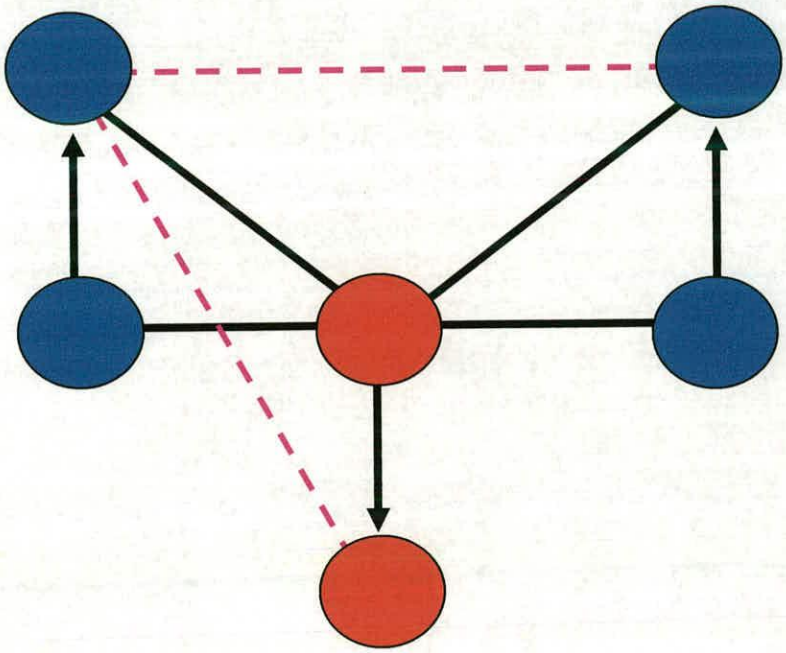

An alternative method involves using curvilinear corrections, and reflects the motion of the atoms in Figure 12. This method is normally only employed when the molecule is floppy, i.e. has a number of low-lying large-amplitude torsional vibrations. The theory of curvilinear corrections can be found in a paper entitled "Calculation of Shrinkage Corrections in Harmonic Approximation" by V.A. Sipachev.[22]

1.4 Aims of Ph.D.

The main aims of this work were to determine the molecular structure of a number of compounds containing silicon by gas-phase electron diffraction. This study was extended by analysing the effects of substituting various groups on the structures to evaluate the effect of increasing or decreasing the electronic or steric presence. This was achieved by conducting *ab initio* calculations on compounds analogous to those determined experimentally.

Some of the compounds showed large differences between the structures calculated *ab initio* and those obtained experimentally. This can be seen to reinforce the necessity for continuing to obtain molecular structures of compounds experimentally instead of simply relying on calculated output.

1.5 References

1. Many Body Problem, "A Dictionary of Science", Oxford University Press, 1999.
2. Gillan, M. J. *Contemporary Physics*, **1997**, ***38(2)***, 115.
3. Møller, C.; Plesset, M. S. *Phys. Rev.* **1934**, *46*, 618.
4. http://www.chem.leeds.ac.uk/boronweb/ormsby/psi-ence/psi-ence.html
5. Hehre, W. J.; Ditchfield, R.; Pople, J. A. *J. Chem. Phys.*, **1972**, *56*, 2257.
6. Hariharan, P. C.; Pople, J. A. *Theor. Chim. Acta*, **1973**, *28*, 213.
7. Gordon, M. S. *Chem. Phys. Lett.*, **1980**, *76*, 163.
8. McLean, A. D.; Chandler, G. S. *J. Chem. Phys. 72*, 5639.
9. Krishnan, R.; Binkley, J. S.; Seeger, R.; Pople, J. A. *J. Chem. Phys. 72*, 650.
10. Hehre, W. J.; Yu, J.; Klunzinger, P. E.; Lou, L. "A Brief Guide to Molecular Mechanics and Quantum Chemical Calculations", Wavefunction, Inc., 1998, p15-17.
11. Hinchley, S. L.; Robertson, H. E.; McLachlan, L. J.; Morrison, C. A.; Rankin, D. W. H.; Simpson, S. J.; Thomas, E. W. *J. Phys. Chem. A.*, **2004**, *108(1)*, 185.
12. http://www.universetoday.com/am/publish/huygens_375_birthday.html
13. Halliday, R. Resnick, J. W. "Fundamentals of Physics", Wiley, 1977, ch. 26-28.
14. http://hep.uchicago.edu/~covault/98/handout112_09/handout112_09.html
15. Atkins, P. W. "Physical Chemistry", Oxford University Press, 1998.
16. Ebsworth, E.; Rankin, D. W. H.; Cradock, S. "Structural Methods in Inorganic Chemistry", Blackwell Scientific Publications, 1991, p304-315
17. Lewis, R.; Brain, P. T.; Rankin, D. W. H. *Spectrum*, **1997**, *15*, 7.
18. Domenicano, A.; Hargittai, I "Accurate Molecular Structures", Oxford University Press, 1992, pg104.
19. http://ego.psych.mcgill.ca/misc/fda/ex-basis-b1.html
20. (a) Blake, A. J.; Brain, P. T.; McNab, H.; Millar, J.; Morrison, C. A.; Parsons, S.; Rankin, D. W. H.; Robertson, H. E.; Smart, B. A. *J. Phys. Chem.*, **1996**, *100*, 12280. (b) Brain, P. T.; Morrison, C. A.; Parsons, S.; Rankin, D. W. H. *J. Chem. Soc., Dalton Trans.*, **1996**, 4589.
21. Hedberg, K.; Mills, I. M. *J. Mol. Struc.*, **1993**, *160*, 117.
22. Sipachev, V. A. J. Mol. Struc. (Theochem), **1985**, 121, 143.

CHAPTER TWO

Highly asymmetric coordination in alkenes: gas-phase structures of *trans*-1,2-dichloro-1,2-disilylethene and 1-bromo-1-silylethene

2.1 Introduction

There are many literature references to the use of polysilylmethanes as precursors for chemical vapour deposition (CVD) of silicon/carbon alloys.[1-6] In a recently developed method of epitaxial deposition of silicon carbide, halogen-containing feedstock gases were introduced to improve reactivity due to increased reversibility during the deposition process. Substituted alkenes are expected to be more suited to epitaxial deposition than the corresponding alkanes, which show low thermal stability. However, although there is already structural information available for silyl alkanes halogenated at the carbon atom,[7,8] there is little on their unsaturated analogues. In the course of this study, the gas-phase electron diffraction structures of *trans*-1,2-dichloro-1,2-silylethene and 1-bromo-1-silylethene were obtained.

These two compounds are also of structural interest because they contain both electron-withdrawing and electron-donating substituents. This leads to extreme asymmetry in the coordination of the carbon atoms. This study was further extended to explore these effects computationally by carrying out *ab initio* calculations on analogous compounds, $(CRX)_2$ and CH_2CRX where R = SiH_3, CH_3 or H, and X = F, Cl, Br or H. It was expected these calculations would reveal even more distorted structures. It is hoped that the asymmetric appearance of these molecules can largely be accounted for by considering valence shell electron pair repulsion (VSEPR) theory or through studying effects of the electronegative atoms on the neighbouring atoms.

2.2 Experimental

2.2.1 Synthesis. Samples of both $(SiH_3)ClC{=}CCl(SiH_3)$ (**1**) and $(SiH_3)BrC{=}CH_2$ (**2**) were prepared by Christoph Rüdinger (Technische Universtät München) according to the literature method,[9] and no further purification was required prior to the electron diffraction experiment.

2.2.2 Computational studies. All calculations were performed on a Dec Alpha 1000A workstation using the Gaussian 98 program.[10] Searches of the torsional potentials of the compounds were conducted at the HF/3-21G* level.[11-13] These resulted in the location of three conformers for **1** and one for **2**. Further optimizations for these four conformers were carried out at HF and MP2(fc) levels of theory using the standard 6-31G* and 6-311G* [14-17] basis sets. Analytical second derivatives of the energy with respect to the nuclear coordinates calculated at HF/6-31G* level for **1** and **2** gave the force fields. These were used, without scaling, to provide estimates of the amplitudes of vibration (u) for use in the gas electron-diffraction (GED) refinements. The force fields for the calculated structures were also used to calculate frequencies, which in turn provided information about the nature of the stationary points. The three conformers of **1** were all confirmed to be minima, two with C_{2h} symmetry and one with C_s, and only differed in the relative positions of the hydrogen atoms of the silyl groups. The sole conformer of **2** was also confirmed as a potential minimum with C_s symmetry. The structure of the lowest energy form of **1** and the only conformer of **2**, with the atom numbering schemes, are shown in Figures 1 and 2.

Figure 1 Molecular structure of *trans*-1,2-dichloro-1,2-disilylethene (**1**) in the gas phase, showing atom numbering.

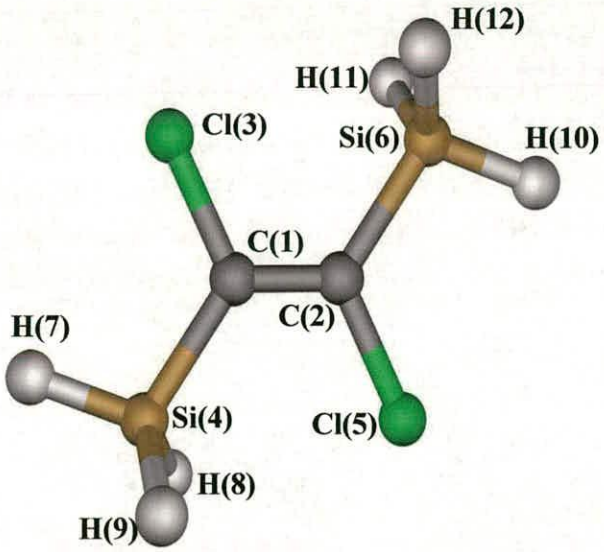

Figure 2 Molecular structure of 1-bromo-1-silylethene (**2**) in the gas phase, showing atom numbering.

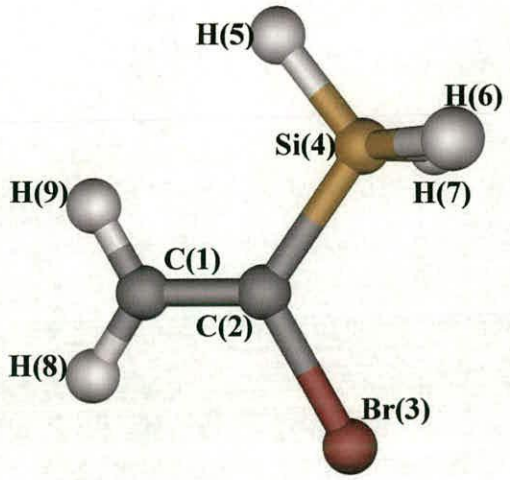

2.2.3 Gas-phase electron diffraction experiment. The Edinburgh gas-diffraction apparatus[18] was used to collect data for both compounds. For **1**, an accelerating voltage of *ca.* 40 kV (electron wavelength *ca.* 6.0 pm) was used, whilst maintaining the sample and nozzle temperatures at 283 and 293 K respectively. Scattering intensities were recorded at nozzle-to-plate distances of 128 and 255 mm on Kodak Electron Image film. Three films were collected at each nozzle-to-plate distance. For (**2**), an accelerating voltage of 40 kV was also used, and the sample and nozzle temperatures were both maintained at 293 K. Scattering intensities were recorded at nozzle-to-plate distances of 128 and 285 mm on Kodak Electron Image film. As with **1**, three films were recorded at each nozzle-to-camera distance. The weighting points for the off-diagonal weight matrices, correlation parameters and scale factors for the two camera distances are given in Table 1. The scattering patterns of benzene were also recorded for the purpose of calibration; these were analyzed in the same way as those for **1** and **2** to minimize systematic errors in wavelengths and camera distances. The electron-scattering patterns were converted into digital form using a PDS densitometer at the Institute of Astronomy in Cambridge with a scanning program described elsewhere.[19] Data reduction and least-

squares refinements were carried out using standard programs,[20,21] employing the scattering factors of Ross *et al.*[22]

Table 1 GED experimental conditions for (**1**) and (**2**).

Compound	(1)		(2)	
camera distance / mm	127.65	255.00	127.71	285.11
Δs / nm^{-1}	4	2	4	2
s_{min} / nm^{-1}	100	40	100	40
s_1 / nm^{-1}	120	60	120	60
s_2 / nm^{-1}	256	128	264	110
s_{max} / nm^{-1}	300	150	308	130
correlation parameter	0.0287	0.4476	-0.2160	0.3252
scale factor	0.762(23)	0.843(12)	0.868(22)	0.847(3)
electron wavelength / pm	0.06016	0.06016	0.06016	0.06016

2.3 Results

2.3.1 Computational Studies for *trans*-1,2-dichloro-1,2-disilylethene. Three minima were located for *trans*-1,2-dichloro-1,2-disilylethene (**1**), varying over an energy range of only 4.2 kJ mol^{-1}. There were also low lying vibrational frequencies (80.8 and 101.5 cm^{-1}) found in the *ab initio* calculations involving a torsion of the silyl groups about H-Si-C=C. However, as the three conformers differ just in the torsional position of the hydrogen atoms on the silyl group (see Figure 3) it was decided that only the lowest energy conformer should be considered in the refinement of the gas-phase data. It was thought that it would not be possible to distinguish between the three conformers using the GED data. Partial geometries obtained from the four highest level calculations for the lowest energy conformer of **1** are given in Table 2. Cartesian coordinates and energies for the three energy minima of **1** are given in Appendix A.

Figure 3 Conformers of **1** showing relative energies

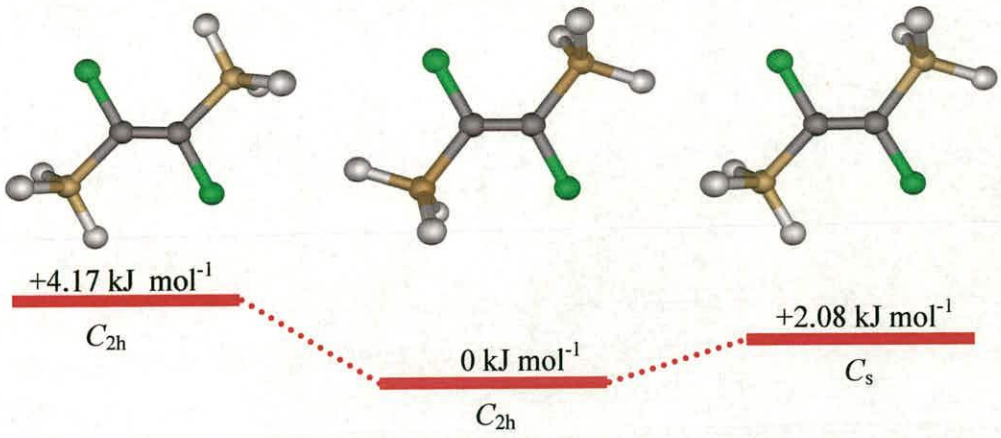

Table 2 Calculated geometric parameters (r_e structure) for the lowest-energy (C_{2h}) structure of $(SiH_3)ClCCCl(SiH_3)$ (**1**) (distances in pm, angles in °).[a]

	Basis set/level of theory			
Parameter	HF/ 6-31G*	MP2/ 6-31G*	MP2/ 6-311G*	MP2/ 6-311+G*
C(2)=C(1)	132.5	135.2	135.2	135.3
Cl(3)-C(1)	176.1	175.2	175.1	175.1
Si(4)-C(1)	190.7	189.8	189.4	189.5
H(7)-Si(4)	146.9	148.0	147.7	147.8
H(8)-Si(4)	147.1	148.2	147.9	147.9
C(2)-C(1)-Cl(3)	117.1	116.9	117.0	116.9
C(2)-C(1)-Si(4)	127.3	126.6	126.2	126.1
Cl(3)-C(1)-Si(4)	115.6	116.5	116.8	117.0
C(1)-Si(4)-H(7)	107.3	107.0	107.0	107.3
C(1)-Si(4)-H(8)	109.4	109.6	109.4	109.3
C(2)-C(1)-Si(4)-H(8)	60.4	60.4	60.2	60.2
Total energy[b]	-1576.0549	-1576.6609	-1576.8006	-1576.8104

[a] See Figure 1 for atom numbering.

[b] Energy in Hartrees with zero point correction applied to HF energies.

As the molecule contains both a double bond and the electronegative chlorine atoms, electron correlation effects are especially important. Inclusion of
electron correlation results in a large increase in the length calculated for the C=C bond (from 132.5 to 135.2 pm) and a decrease in the C-Cl bond length (176.1 to 175.2 pm) from HF/6-31G* to MP2/6-31G*. The MP2/6-311G* calculation shows that basis set convergence has been attained as there is little difference between the values calculated at this and the previous MP2/6-31G* level. A further MP2 calculation was carried out using the 6-311+G* basis set, but this again made very little difference to the values calculated using the 6-311G* basis set. As basis set convergence had been achieved, it was not thought necessary or feasible to continue these calculations to a higher level, although, of course, other types of basis set might produce slightly different parameters.

2.3.2 Computational studies for 1-bromo-1-silylethene. In the study of 1-bromo-1-silylethene **2**, only one conformer was located. Partial geometries obtained from the four highest level calculations for this conformer are given in Table 3. From this it can be seen that, as with **1**, including electron correlation is important for the C=C bond, increasing its length from 131.8 to 134.0 pm. The Hartree Fock method appears to consistently underestimate the C=C distance. Including electron correlation, unlike in the previous case, has very little effect on the C-Br bond distance, probably because bromine is less electronegative than chlorine. Basis set convergence was achieved with the MP2/6-311G* level of calculation, apart from the C-Br bond length, which changed sizeably between the MP2/6-31G* (192.5 pm) and MP2/6-311G* (191.3 pm) calculations. This can attributed to the valence region of the double-zeta basis set being too restrictive for an atom the size of bromine. Addition of a diffuse function by using the 6-311+G* basis set can be seen to have little effect and confirms that basis set convergence was achieved using the MP2/6-311G* level, although, again, it may be possible to produce different results using a very different basis set. Cartesian coordinates for the calculated structure of **2** are given in Appendix A.

Table 3 Calculated geometric parameters (r_e structure) for the C_s structure of SiH_3BrCCH_2 (**2**) (distances in pm, angles in °).[a]

	Basis set/level of theory			
Parameter	HF/ 6-31G*	MP2/ 6-31G*	MP2/ 6-311G*	MP2/ 6-311+G*
C(1)=C(2)	131.8	134.0	134.2	134.3
Br(3)-C(2)	192.3	192.5	191.3	191.4
Si(4)-C(2)	187.9	187.6	187.8	187.9
H(5)-Si(4)	147.6	148.6	148.2	148.2
H(6)-Si(4)	147.2	148.2	147.9	147.9
H(8)-C(1)	107.5	108.6	108.6	108.6
H(9)-C(1)	107.6	108.7	108.7	108.7
C(1)-C(2)-Br(3)	119.1	119.0	119.2	119.1
C(1)-C(2)-Si(4)	127.0	126.1	125.0	125.1
C(2)-Si(4)-H(5)	108.0	108.0	107.4	107.4
C(2)-Si(4)-H(6)	109.7	109.5	109.6	109.5
C(2)-C(1)-H(8)	123.1	123.0	123.0	122.9
C(2)-C(1)-H(9)	120.0	119.6	119.5	119.6
Total Energy[b]	-2937.4856	-2937.8677	-2940.4087	-2940.4128

[a] See Figure 2 for atom numbering.

[b] Energy in Hartrees with zero point correction applied to HF energies.

Ab initio calculations were also carried out for CH_2CRX and $(CRX)_2$ (R = SiH_3, CH_3 or H; X = H, F, Cl, Br) to the MP2/6-311G* level. Basis set convergence had been achieved at this level as with **1** and **2** and no further calculations were felt to be necessary. Partial geometries for the calculations are given in Tables 4 and 5.

Table 4 Selected calculated geometric parameters for CH_2CRX, where R = SiH_3, CH_3 or H and X = H, Br, Cl or F, at the MP2(fc)/6-311G* level. (Distances in pm and angles in °.)

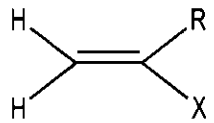

			χ ⟶	
X	H	Br	Cl	F
R = SiH_3				
C(1)=C(2)	134.7	134.3	134.3	133.8
X(3)-C(2)	109.1	191.4	175.2	137.0
Si(4)-C(2)	186.8	187.9	188.0	188.4
C(1)-C(2)-X(3)	117.5	119.1	119.3	118.2
C(1)-C(2)-Si(4)	122.9	125.1	124.8	127.3
R = CH_3				
C(1)=C(2)	134.1	133.9	133.8	133.4
X(3)-C(2)	109.0	191.0	174.7	136.1
C(4)-C(2)	150.1	149.8	149.7	148.9
C(1)-C(2)-X(3)	118.8	119.6	119.9	119.0
C(1)-C(2)-C(4)	126.1	126.0	125.9	124.6
R = H				
C(1)=C(2)	133.8	133.5	133.5	133.0
X(3)-C(2)	108.5	189.0	173.1	134.9
H(4)-C(2)	108.5	108.4	108.4	108.4
C(1)-C(2)-X(3)	121.6	122.9	123.1	121.5
C(1)-C(2)-H(4)	121.6	123.7	123.6	126.3

Table 5 Selected calculated geometric parameters for *trans*-$(CRX)_2$ (R = SiH_3, CH_3 or H; X=H, Br, Cl, or F) at the MP2(fc)/6-311G* level. (Distances in pm and angles in °.)

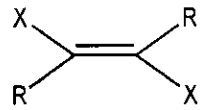

			χ ⟶	
X	H	Br	Cl	F
R = SiH_3				
C(1)=C(2)	135.6	135.4	135.4	134.6
X(3)-C(2)	109.3	191.9	175.1	137.1
Si(4)-C(2)	187.3	189.6	189.5	188.9
C(1)-C(2)-X(3)	117.9	116.4	116.9	116.2
C(1)-C(2)-Si(4)	123.5	127.4	126.1	129.8
R = CH_3				
C(1)=C(2)	134.3	134.8	134.8	133.8
X(3)-C(2)	109.3	191.4	174.7	136.3
C(4)-C(2)	150.1	149.7	149.6	148.5
C(1)-C(2)-X(3)	118.6	118.8	119.1	117.3
C(1)-C(2)-C(4)	124.7	128.8	127.9	128.8
R = H				
C(1)=C(2)	133.8	133.7	133.6	133.1
X(3)-C(2)	108.5	188.5	172.4	134.7
H(4)-C(2)	108.5	108.4	108.4	108.3
C(1)-C(2)-X(3)	121.6	121.2	121.4	119.9
C(1)-C(2)-H(4)	121.6	124.0	123.5	125.6

2.3.3 Electron diffraction analysis for *trans*- 1,2-dichloro-1,2-disilylethene (1). The refinement of the gas-phase structure of **1** was carried out using a model of the lowest energy conformation from the *ab initio* calculations. The model was written using C_2 symmetry, allowing for both twisting of the silyl groups and twisting about the C=C bond, which lowers the molecular symmetry from C_{2h}, as found in the *ab initio*

calculations. The structure was defined in terms of ten independent geometric parameters (Table 6). These comprised four bond lengths, three bond angles and two torsions (one about the C-Si bond, the other about the C=C bond), and a tilt of the silyl group. The four bond lengths were C=C (p_1), Si-H (p_2), C-Cl (p_3) and C-Si (p_4) and independent angles were CCSi (p_5), CCCl (p_6) and CSiH (p_7). The remainder of the parameters were a twist of the silyl group around the x axis (p_8), a tilt of the silyl group in the z direction (p_9) (defined as positive if tilted away from the adjacent chlorine atom) and a Cl-C=C-Cl torsion [180°- (p_{10})]. Although two pairs of two distances overlap in the radial distribution curve (Figure 4), it was found that correlations were lower if these four distances were treated as independent parameters.

The starting values for the ten geometric parameters used in the refinement were taken from the *ab initio* calculation (MP2/6-311G*). Theoretical (HF/6-31G*) Cartesian force fields were obtained and converted into force fields described by a set of symmetry coordinates using ASYM40.[23] The model was refined as an r_a structure (i.e. without any perpendicular amplitude corrections). In total all ten geometric parameters and eleven groups of amplitudes were refined. Flexible restraints were used during the refinement (seven geometric and two amplitude) using the SARACEN[24] method and are listed in Tables 6 and 7.

The final refinement, for which R_G = 0.073 (R_D = 0.052), lead to the satisfactorily small difference curves for the combined molecular scattering intensity (Figure 5) and radial distribution (Figure 4). R_G and R_D represent different measures of the goodness of fit, R_G relates to the number of parameters whereas R_D does not. Although it appears that the short and long data do not overlap well in Figure 5, it should be noted that this is merely due to the scaling of the data with different s intervals. Final refined parameters are listed in Table 6, and interatomic distances and the corresponding amplitudes of vibration in Table 7. The least-squares correlation matrix is given in Table 8.

Table 6 Refined and calculated geometric parameters (r_a structure) from the GED study of $(SiH_3)ClCCCl(SiH_3)$ (**1**) (distances in pm, angles in °).[a, b]

	Parameter	GED	MP2/6-311G*	Restraint
p_1	C-C	134.5(3)	135.2	135.2(10)
p_2	C-Cl	174.9(1)	175.1	
p_3	C-Si	187.9(2)	189.4	
p_4	Si-H	147.4(7)	147.8	147.8(10)
p_5	∠CCSi	128.1(1)	126.2	126.6(3)
p_6	∠CCCl	117.0(2)	117.0	
p_7	∠CSiH	109.6(3)	108.2	108.2(5)
p_8	Φ H-Si-C=C	0.1(11)	0.0	0.1(10)
p_9	SiH_3 tilt	0.4(10)	1.6	0.1(10)
p_{10}	Φ Cl-C=C-Cl	0.1(11)	0.0	0.1(10)

[a] See text for parameter definitions.

[b] Errors in parentheses are standard deviations in terms of the least significant digit.

Figure 4 Experimental and final weighted difference (experimental – theoretical) molecular-scattering intensities for **1**.

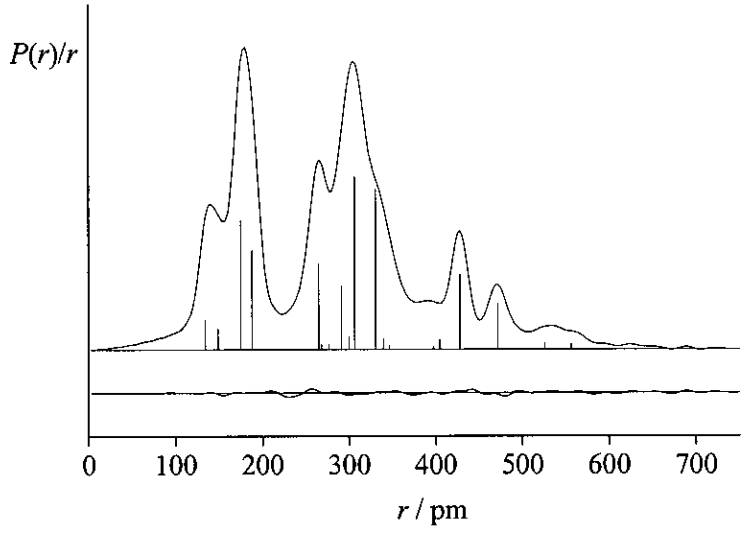

Table 7 Interatomic distances (r_a/pm) and amplitudes of vibration (u/pm) for the restrained GED structure of $(SiH_3)ClCCCl(SiH_3)$ (**1**).

	Atom pair	r_a	u	Restraint
u_1	Cl(5)···Si(4)	329.7	13.9(4)	
u_2	Si(4)···Cl(3)	306.0	7.8(3)	
u_3	Cl(3)-C(1)	174.9	3.7(6)	
u_4	Si(4)-C(1)	187.9	3.8(6)	
u_5	Cl(3)···C(2)	264.6	5.8(3)	
u_6	Cl(5)···Cl(3)	428.1	5.7(3)	
u_7	Si(4) ···C(2)	291.2	6.5(6)	
u_8	Si(6)···Si(4)	471.5	8.1(4)	6.9(7)
u_9	C(2)=C(1)	134.5	3.4(8)	
u_{10}	H(9)-Si(4)	148.6	9.8 (tied to u_{12})	
u_{11}	H(8)-Si(4)	148.6	9.8 (tied to u_{12})	
u_{12}	H(7)-Si(4)	148.6	9.8(6)	
u_{13}	H(8)···Cl(5)	339.1	32.6(32)	36.6(36)
u_{14}	H(9) ···Cl(5)	339.6	32.6 (tied to u_{13})	

Table 8 Least-squares correlation matrix (× 100) for (**1**).[a]

	p_4	p_5	p_7	u_2	u_3	u_4	u_7	u_9	u_{12}	k_1	k_2
p_2	50	-	-	-	-	-	-	-	-	-	-
p_3	-	-57	69	-	-56	-55	-	-	-	-	-
p_4	-	-	56	-	-	-	-	-	-	-	-
p_5	-	-	-81	-	-	-	-	-	-	-	-
u_1	-	-	-	61	-	-	-	-	-	-	-
u_2	-	-	-	-	-	-	75	-	-	-	-
u_3	-	-	-	-	-	93	-	62	-	65	50
u_4	-	-	-	-	-	-	-	53	-	64	51
u_5	-	-	-	-	-	-	-	-	-	61	-
u_6	-	-	-	-	-	-	-	-	-	64	-
u_9	-	-	-	-	-	-	-	-	58	-	-

[a] Only elements with absolute values ≥ 50% are shown. k_1 and k_2 are scale factors.

Figure 5 Experimental and difference (experimental – theoretical) radial-distribution curves, $P(r)/r$, for (**1**). Before Fourier inversion the data were multiplied by $s \cdot \exp(-0.00002s^2)/(Z_{Cl}-f_{Cl})/(Z_{Si}-f_{Si})$.

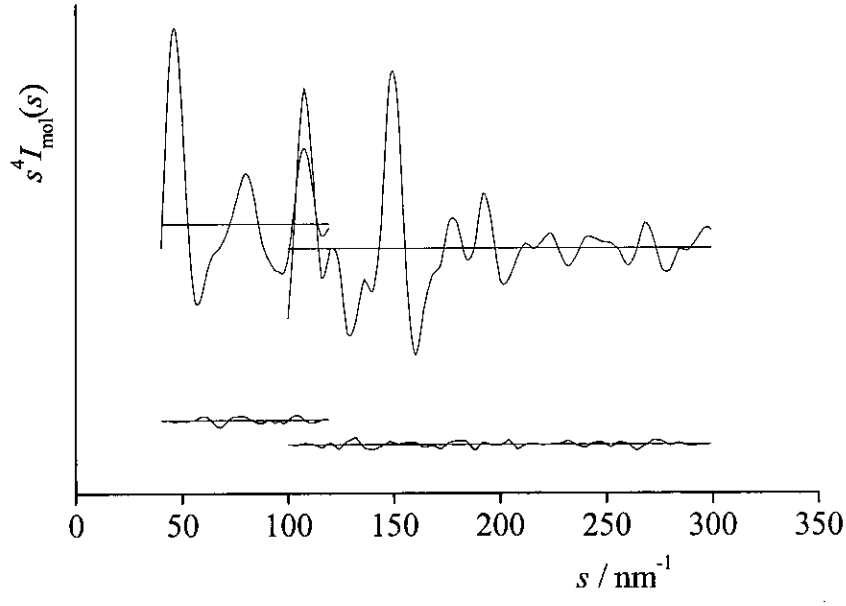

2.3.4 Electron diffraction analysis for 1-bromo-1-silylethene (2). The refinement of the gas-phase structure of (2) was carried out using a model of C_s symmetry, assuming local C_{3v} symmetry within the silyl group and C_{2v} for $C{=}CH_2$. The structure was defined using twelve independent geometric parameters, comprising five bond lengths, four bond angles and two torsions (one about the C-Si bond and one about the C=C bond) and a tilt of the silyl group. The five bond lengths were Si-H (p_1), C-Si and C-Br [which were described in terms of the average of the two distances (p_2) and the difference between them (p_3)] C-C (p_4) and C-H (p_5). The average value was used for the CSiH (p_6) angles, thus defining HSiH, although the CSiH were subsequently changed as the group was tilted. The angles CCBr(p_7), CCSi (p_8) and CCH (p_9) were also used in the model description. The remaining parameters were a twist of the silyl group around the x axis (p_{10}), a tilt of the silyl group in the z direction (p_{11}) (defined as positive if tilted away from the adjacent bromine atom) and a C=C torsional parameter around the x axis (p_{12}).

The starting values for the geometric parameters were obtained from the *ab initio* calculations (MP2/6-311G*) and the theoretical force field was obtained and refined exactly as described previously. In total all twelve geometric parameters and seven groups of amplitudes were refined. Flexible restraints were used during the refinement (eight on geometric parameters and two on amplitudes), again using the SARACEN[24] method, and are listed in Tables 9 and 10.

In the final refinement R_G was 0.054 (R_D = 0.046). The experimental and final difference combined molecular scattering intensity curves are shown in Figure 5 and the radial distribution curves in Figure 6. Refined parameters are listed in Table 9 and interatomic distances and the corresponding amplitudes of vibration in Table 10. The correlation matrix can be found in Table 11.

Table 9 Refined and calculated geometric parameters (r_a structure) from the GED study of SiH_3BrCCH_2 (**2**) (distances in pm, angles in °).[a]

	Independent parameters	GED	MP2/6-311G*	Restraint
p_1	Si-H	150.0(5)	148.0	
p_2	C-Si/C-Br average	189.1(1)	189.6	
p_3	C-Si/C-Br difference	3.8(6)	3.5	3.5(8)
p_4	C-C	133.4(2)	134.2	
p_5	C-H	109.0(6)	108.7	108.6(3)
p_6	∠CSiH	108.2(4)	108.9	108.9(5)
p_7	∠CCBr	120.7(4)	119.2	
p_8	∠CCSi	125.0(4)	125.0	125.0(5)
p_9	∠CCH	120.9(4)	121.3	121.3(5)
p_{10}	Φ H-Si-C=C	1.0(10)	0.0	1.0(10)
p_{11}	SiH_3 tilt	0.2(8)	1.5	1.0(10)
p_{12}	Φ Br-C=C-H	1.0(10)	0.0	1.0(10)

	Dependent parameters		
p_{13}	C-Si	187.2(3)	187.8
p_{14}	C-Br	191.0(3)	191.3

[a] See text for parameter definition

Table 10 Interatomic distances (r_a/pm) and amplitudes of vibration (u/pm) for the restrained GED structure of SiH_3BrCCH_2 (**2**).

	atom pair	r_a	u	Restraint
u_1	Si(3)···Br(4)	317.7	8.5(1)	
u_2	Br(3)-C(2)	191.0	5.4(2)	
u_3	Br(3)···C(1)	283.4	5.2(2)	
u_4	Si(4)-C(2)	187.2	5.3 (tied to u_2)	
u_5	Si(4) ···C(1)	285.5	6.0 (tied to u_3)	
u_6	H(5)-Si(4)	150.0	9.9(5)	
u_7	C(2)-C(1)	133.4	4.3(3)	4.0(4)
u_8	H(8)-C(1)	109.0	7.3(4)	
u_9	H(8)···Br(3)	295.6	14.2 (fixed)	
u_{10}	H(7)···Br(3)	350.1	18.3(10)	21.5(20)
u_{11}	H(6)···Br(3)	352.2	18.3 (tied to u_{10})	

Table 11 Least-squares correlation matrix (× 100) for **2**.[a]

	p_8	u_2	u_3	k_2
p_2	50	72		54
p_3		-56		
p_7	-98		75	
p_8			-75	
u_1				65
u_2				58

[a] Only elements with absolute values ≥ 50% are shown. k_2 is a scale factor.

Figure 5 Experimental and final weighted difference (experimental – theoretical) molecular-scattering intensities for **2**.

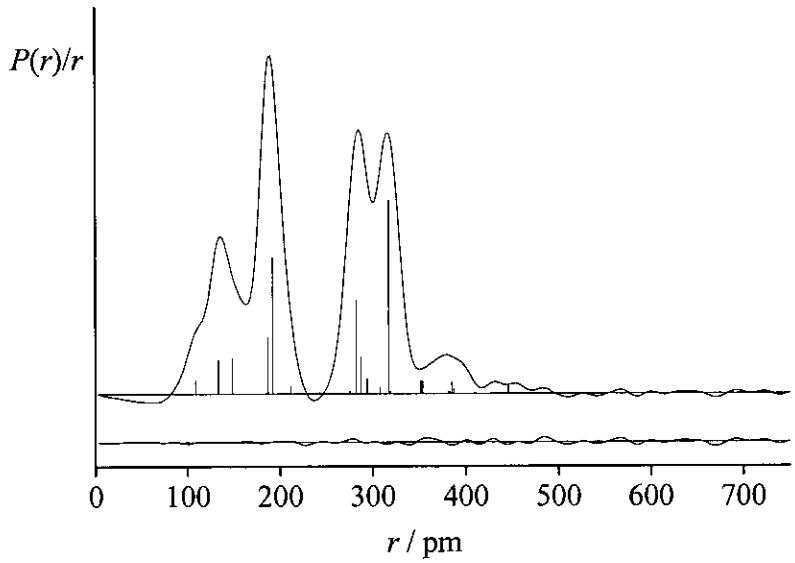

Figure 6 Experimental and difference (experimental – theoretical) radial-distribution curves, $P(r)/r$, for **2**. Before Fourier inversion the data were multiplied by $s \cdot \exp(-0.00002s^2)/(Z_{Br}-f_{Br})/Z_{Si}-f_{Si})$.

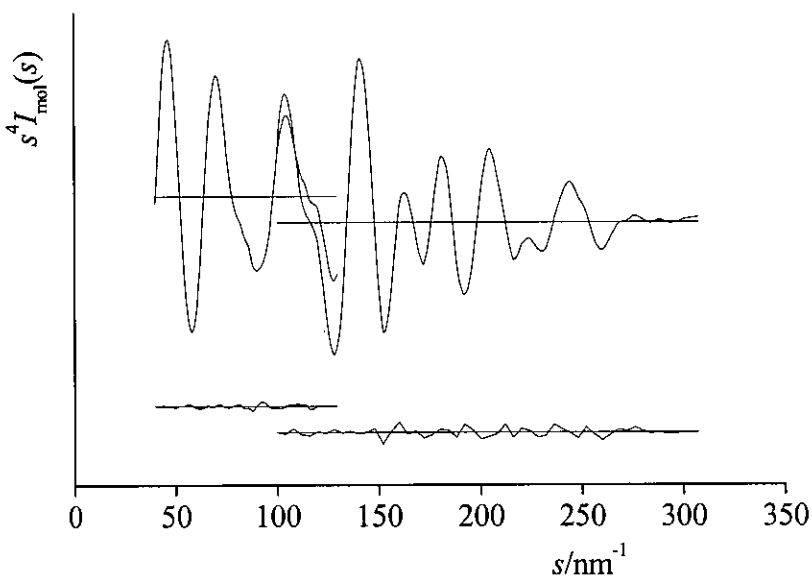

2.4 Discussion

2.4.1 Experimental results. The results from the GED and *ab initio* calculations for **1** and **2** show very asymmetric coordination about the C=C bond. In **1**, the difference between ∠CCSi and ∠CCCl is 11.1°/9.2° (GED/*ab initio*) and in **2** the difference between ∠CCSi and ∠CCBr is 4.8°/5.8° (GED/*ab initio*). It is expected that the compound which is substituted at both ends of the C=C bond will have a larger asymmetry than the singly substituted compound. This is because increasing the CCSi angle, forces the CCCl angle to get smaller, which in turn encourages the CCSi angle to the silyl group on the neighbouring carbon to get larger and so on.

2.4.2 Asymmetry in series CH_2CRX and *trans*-$(CRX)_2$. The same asymmetry about the carbon-carbon double bond found in **1** and **2** is noticeably present in the results of the calculations for the series of analogous compounds, CH_2CRX and *trans*-$(CRX)_2$ (Tables 4 and 5).

The largest difference (13.6°) between ∠CCX and ∠CCR is found in *trans*-$[C(SiH_3)F]_2$, with the angle CCSi 129.8° and CCF 116.2°, the largest and smallest angles in the whole group of compounds. This can be explained by looking at the electron density, which in the C-F bond is pulled towards the fluorine atom, whereas in the C-Si bond the electron density is closer to the carbon atom. The angle at the carbon atom to the silyl group must therefore increase, while the angle to the fluorine atom must reduce. This high asymmetry is less extreme but still present in other molecules in the series *trans*-$[C(SiH_3)X]_2$ (see Table 11). The difference between the CCSi and CCBr angles in *trans*-$[C(SiH_3)Br]_2$ (127.4° and 116.4°) is greater than the equivalent difference in *trans*-$[C(SiH_3)Cl]_2$, suggesting that the effects of the electronegativities of the substituents are partially countered by steric effects of the large bromine atom. A similar trend is noticed in the series *trans*-$[C(CH_3)X]_2$, with the largest difference between the CCC and CCX angles occurring when X = F. These, and other trends, are consistent with valence shell electron pair repulsion theory (VSEPR).

Table 11 Selected calculated geometric parameters for *trans*-$[CRX]_2$, where R= SiH_3 or CH_3 and X = H, Br, Cl or F, at the MP2/6-311G* level. (Angles measured in °.)

		$\chi\longrightarrow$		
X	H	Br	Cl	F
$R=SiH_3$				
C(1)-C(2)-X(3)	117.9	116.4	116.9	116.2
C(1)-C(2)-Si(4)	123.5	127.4	126.1	129.8
Δ^a	5.6	11.0	9.2	13.6
$R=CH_3$				
C(1)-C(2)-X(3)	118.6	118.8	119.1	117.3
C(1)-C(2)-C(4)	124.7	128.8	127.9	128.8
Δ	6.1	10.0	8.8	11.5

[a] Δ is defined as C(1)-C(2)-R(4) minus C(1)-C(2)-X(3)

The asymmetry is also present in the series of compounds studied that are only substituted at one end of the carbon-carbon double bond, CH_2=CRX. As with the previous examples, the highest asymmetry is exhibited in CH_2=C(SiH_3)F, where the difference between the CCSi and CCF angles is 9.1° (127.3° and 118.2°, respectively). It is also worth noting that the CCX angles are slightly larger than in the *trans*-$(CRX)_2$ analogues. This is in all likelihood due to the lack of steric repulsion from the hydrogen atoms at the non-substituted end of the carbon-carbon double bond, allowing the CCX angle to increase to avoid the R substituent.

2.4.3 Variations in C=C, C-X and C-R bond lengths. The experimental C=C bond length obtained for 1-bromo-1-silylethene (**2**) [133.4(2) pm] is about 1 pm less than that observed for **1**. This can be attributed to the presence of another electron-donating silyl group in **1** increasing the C=C bond length, overriding the effect of an additional electron-withdrawing atom. Having observed this shortening of C=C in **2** compared to **1** it is appropriate to extend the discussion to the series of compounds CH_2=CRX (R =

CH_3, SiH_3, H; X = H, F, Cl, Br) (Table 4). By observing how the C=C bond length varies on changing R and X, we can gain an understanding of how the effects of electronegativity of X compare with the consequences of changing the R group. We have also extended these calculations to XRC=CRX analogues (Table 5), to complete our understanding of these effects.

For the series CH_2=CRX, when X is varied and R = SiH_3 (Table 12), we see the expected systematic decrease in the length of the C=C bond as the electronegativity of X increases. This is accompanied by a lengthening of the C-X bond compared to the same bonds in $CHXCH_2$, where there is no electron-donating group next to X. This illustrates the two competing electron-donating/withdrawing effects, as there was no effect on the neighbouring bond lengths from the electron-donating, then the C-X bond should be approximately the same length in CH_2CHX compared to $CH_2C(CH_3)X$ and $CH_2C(SiH_3)X$ (see table 11).

Table 12 Length of C=C and C-X bond when R = H, CH_3 or SiH_3 in CH_2CRX where X= H, Br, Cl or F.

			$\chi\longrightarrow$	
X	H	Br	Cl	F
R = H				
C=C	133.8	133.5	133.5	133.0
C-X	108.5	189.0	173.1	134.9
R=CH_3				
C=C	134.1	133.9	133.8	133.4
C-X	109.0	191.0	174.7	136.1
R=SiH_3				
C=C	134.7	134.3	134.3	133.8
C-X	109.1	191.4	175.2	137.0

Similar consequences of varying X are observed when R = CH_3. Again, the C=C bond shortens as the electronegativity of X increases, while the C-X bond is longer than in the analogous compounds with R = H (see Table 11). The results for R = CH_3 show that bromine and chlorine have approximately the same effect, slightly decreasing the length of the C=C bond compared to X = H, reflecting their similar electronegativities. Hydrogen, which is less electronegative, gives a longer C=C bond length, whereas fluorine, which is much more electronegative, is seen to promote a shorter C=C bond length.

For R = CH_3 and H the C-R bond length decreases as the electronegativity of X increases. However, for R = SiH_3, the opposite occurs, with the C-Si bond length actually increasing as the electronegativity of X increases. This can be attributed to electrostatic repulsion occurring between the carbon and silicon atoms. As the electronegativity of X increases, more electron density is drawn away from carbon making it more electropositive. This in turn repels the positive silyl group, making the C-Si bond longer. This is not observed when R = CH_3 or H as neither is as positive as the SiH_3 group.[28]

Similar trends are observed in a series of calculations carried out on XRC=CRX (R = SiH_3, CH_3, H; X = H, F, Cl, Br). Comparing the lengths of the C=C bonds in CH_2CH_2, $[C(SiH_3)H]_2$ (both Table 5) and $(SiH_3)HCCH_2$ (Table 4), an increase from 133.8 pm and 134.7 pm to 135.6 pm is observed. This is expected, as the addition of another electron-donating silyl group further increases the length of the neighbouring C=C bond.

However, unlike the examples of the ethenes substituted on one side of the C=C bond, the lengths of the Si-C bonds in Table 5 do not show the same increase as the electronegativity of X increases. In fact, the Si-C bond length in $[C(SiH_3)F]_2$ is shorter than that of $[C(SiH_3)Br]_2$ and $[C(SiH_3)Cl]_2$. This can be attributed to having competing effects at the two ends of the carbon-carbon double bond. Although both the carbon atoms in the double bond are slightly positive due to the electron- withdrawing effect of

the fluorine atoms, the effect is not as pronounced as in the other examples as it is not possible to have two substantial positive charges on adjacent carbon atoms.

2.5 Conclusions

Overall, high-level calculations provide excellent estimates of differences between geometrical parameters for series of related molecules, but absolute values of some parameters are significantly unreliable. At the other extreme, VSEPR theory gives a simple explanation of many of the observed features. These simple molecules, perhaps the simplest showing such extreme distortions from idealised symmetric coordination at the central atom, provide an elegant illustration of VSEPR theory.

2.6 References

1. Beyer, W.; Hager, R.; Schmidbaur, H.; Winterling, G. *Appl. Phys. Lett.*, **1989**, *54*, 1666.

2. Hölsch, J.; Rübel, H. Schade, H. *Appl. Phys. Lett.*, **1992**, *61*, 3029.

3. Rübel, H.; Hölsch, J.; Schade, H. *Solid State Comm.*, **1993**, *85*, 593.

4. Zech, J.; Schmidbaur, H. *Eur. J. Solid State Inorg. Chem.*, **1992**, *29*, 5.

5. Zech, J.; Schmidbaur, H. *Chem. Ber.*, **123**, 1990, 2087.

6. Bommers, S.; Schmidbaur, H. *Z. Naturforsch*, **1994**, *49b*, 337.

7. Fritz, G.; Matern, E. *Z. Anorg. Allg. Chem.*, **1976**, *426*,28.

8. Fritz, G.; Arnason, I. *Z. Anorg. Allg. Chem.*, **1976**, *419*, 213.

9. Rüdinger, C.; Beruda H.; Schmidbaur, H. *Z. Naturforsch., B: Chem. Sci.*, **1994**, *49*, 1348.

10. Gaussian 98 (Revision A.7), Frisch, M. J.; Trucks, G. W.; Schlegel, H. B.; Scuseria, G. E.; Robb, M. A.; Cheeseman, J. R.; Zakrzewski, V. G.; Montgomery, J. A.; Stratman, R. E.; Burant, J. C.; Dapprich, S.; Milliam, J. M; Daniels, A. D.; Kudin, K. N.; Strain, M. C.; Farkas, O.; Tomasi, J.; Barone, V.; Cossi, M.; Cammi, R.; Mennucci, B.; Pomelli, C.; Adamo, C.; Clifford, S.; Ochterski, J.; Petersson, G. A.; Ayala, P.Y.; Cui, Q.; Morokuma, K.; Malick, D. K.; Rabuck, A. D.; Raghavachari, K.; Foresman, J. B.; Cioslowski, J.; Ortiz, J. V.; Baboul, A. G.; Stefanov, B. B.; Liu, C.; Liashenko, A.; Piskorz, P.; Komaromi, I.; Gomperts, R.; Martin, R. L.; Fox, D. J.; Keith, T.; Al-Laham, M. A.; Peng, C. Y.; Nanayakkara, A.; Gonzalez, C.; Challacombe, M.; Gill, P. M. W.; Johnson, B. G.; Chen, W.; Wong, M. W.; Andres, J. L.; Gonzales, C.; Head-Gordon, M.; Replogle, E. S.; Pople, J. A. Gaussian, Inc., Pittsburgh PA, **1998**.

11. Binkley, J. S.; Pople, J. A.; Hehre, W. J. *J. Am. Chem. Soc.*, **1980**, *102*, 939.

12. Gordon, M. S.; Binkley, J. S.; Pople, J. A.; Pietro, W. J.; Hehre, W. J. *J. Am. Chem. Soc.*, **1982**, *104*, 2979.

13. Pietro, W. J.; Francl, M. M.; Hehre, W. J.; DeFrees, D. J.; Pople, J. A.; Binkley, J. S. *J. Am. Chem. Soc.*, **1982**, *103*, 5039.

14. Hehre, W. J.; Ditchfield, R.; Pople, J. A. *J. Chem. Phys.*, **1972**, *56*, 2257.

15 Hariharan, P. C.; Pople, J. A. *Theor. Chim. Acta*, **1973**, *28*, 213.

16. Gordon, M. S. *Chem. Phys. Lett.*, **1980**, *76*, 163.

17. Krishnan, R; Binkley J. S.; Seeger, R; Pople, J. A. *J. Chem. Phys.*, **1980**, *72*, 650.

18. Huntley, C. M.; Laurenson, G. S.; Rankin, D. W. H. *J. Chem. Soc., Dalton Trans.*, **1980**, 954.

19. Lewis, J. R.; Brain, P. T.; Rankin, D. W. H. *Spectrum*, **1997**, *15*, 7.

20. Cradock, S.; Koprowski, J. *J. Mol. Struct.*, **1982**, *77*, 113.

21. Boyd, A. S. F.; Laurenson, G. S.; Rankin, D. W. H. *J. Mol. Struct.*, **1981**, *71*, 217.

22. Ross, A. W.; Fink M.; Hilderbrandt, R. in *International Tables for Crystallography*, ed. A. J. C. Wilson, Vol. C, Kluwer Academic Publishers, Dordrecht, **1992**, p.245.

23. Hedberg, L.; Mills, I. M. *J. Mol. Struct.*, **1993**, *160*, 117.

24. Blake, A. J.; Brain, P. T.; McNab, H.; Millar, J.; Morrison, C. A.; Parsons, S.; Rankin, D. W. H.; Robertson, H. E.; Smart, B. A. *J. Phys. Chem.*, **1996**, *100*, 12280; Brain, P. T.; Morrison, C. A.; Parsons, S.; Rankin, D. W. H. *J. Chem. Soc., Dalton Trans.*, **1996**, 4589.

25. Huismann, P. A. G.; Mijlhoff, F. C. *J. Mol. Struct.*, **1979**, *54*, 145.

26. Bartell, L. S.; Roth, E. A.; Hollowell, C. D. *J. Chem. Phys.*, **1965**, *42*, 2683.

27. Schäfer, L.; Ewbank, J. D.; Siam, K.; Paul, D. W.; Monts, D. L. *J. Mol. Struct.*, **1986**, *145*, 135.

28. Rempfer, B.; Pfafferott, G.; Oberhammer, H.; Beckers, H.; Bürger, H.; Eujen, R. Boggs, J. *Rev. Chim. Miner.*, **1986**, *23*, 551.

CHAPTER THREE

The molecular structure of 1,1,1,4,4,4-hexachloro-1,4-disilabutane by gas-phase electron diffraction and *ab initio* calculations

3.1 Introduction

The solid-state structure of 1,1,1,4,4,4-hexachloro-1,4-disilabutane (**1**)[1] and the gas-phase and solid-state structures of 1,4-disilabutane[2] and 1-silabutane[3] have been published. These are examples of simple carbosilane molecules which, along with their halogen derivatives, are thought to be useful as pre-cursors for the epitaxial growth of β-SiC layers by chemical vapour deposition (CVD).[3] Although this work is primarily concerned with analysing the gas-phase experimental structures and exploring the effects of different substituents, (of **1** and related compounds) accurate knowledge of the structure may also lead to a better understanding of the complex decomposition chemistry that occurs in the CVD process.

Much work has previously been carried out on butane and its derivatives as this is the simplest alkane which exists as two conformers. Conformational analysis is of interest to a large area of pharmaceutical research, concerned with conformers of molecules and the implications of conformer stability on properties. The gas- and solid-phase structures of 1,4-disilabutane and gas-phase structure of 1-silabutane were previously determined with a view to studying the conformations and the effects of substitution on other compounds.[2,3] This study is an extension of this work and compares the results from the two previous papers with the gas-phase and *ab initio* results for **1**.

3.2 Experimental

3.2.1 Synthesis. The sample of **1** used for the gas-phase electron diffraction experiment was prepared by Prof. N. W. Mitzel from TUM according to the previously published method and used without further purification.[1]

3.2.2 Computational studies. All *ab initio* molecular orbital calculations were carried out on a DEC Alpha 1000A workstation using the Gaussian 98 program.[4] A search of the torsional potential of **1** was conducted at the Hartree Fock (HF) level of the theory with the 3-21G* basis set [5-7] and only one conformer was found. Further

6-31G*[8-10] and 6-311G*[11] basis sets with various additional polarisation and diffuse functions. Analytical second derivatives with respect to the nuclear co-ordinates calculated at the HF/6-31G* level gave the equilibrium, harmonic force field, which was used to obtain estimates for the amplitudes of vibration (u) used in the refinement of the gas-phase electron diffraction (GED) data. The molecular structure of **1** with atom numbering scheme is shown in Figure 1.

Figure 1 Molecular structure of $SiCl_3CH_2CH_2SiCl_3$ (**1**) in the gas phase showing atom numbering.

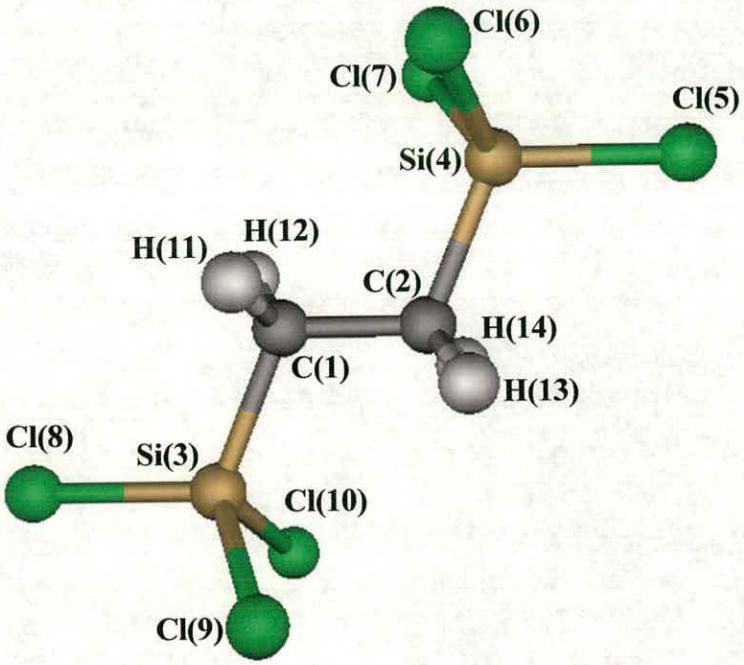

3.2.3 Gas-phase electron diffraction experiment. The Edinburgh gas diffraction apparatus[12] was used for the collection of the data for **1**. An accelerating voltage of *ca.* 40 kV (electron wavelength *ca.* 6.0 pm) was used. Scattering intensities were recorded at two nozzle-to-film distances (98 and 253 mm), with three films being exposed at each distance. The sample and nozzle temperatures were held at 359 and 360 K respectively for the short distance, and 331 and 346 K respectively for the long data collection. The weighting points for the off-diagonal weight matrices, correlation parameters and scale factors for the two camera distances are given in

correlation parameters and scale factors for the two camera distances are given in Table 1. The scattering patterns of benzene were also recorded for the purpose of calibration; these were analysed in the same way as the data for **1** in order to minimise any systematic errors in wavelengths and camera distances. The electron-scattering patterns were converted into digital form using a PDS densitometer at the Institute of Astronomy in Cambridge with a scanning program described elsewhere.[13] Data reduction and least-squares refinements were carried out using standard programs, [14,15] utilising the scattering factors of Ross *et al.*[16]

Table 1 GED experimental conditions for $SiCl_3CH_2CH_2SiCl_3$.

camera	weighting functions /nm^{-1}					correlation	scale factor	electron
distance/mm	Δs	s_{min}	s_1	s_2	s_{max}	parameter		wavelength/pm
97.63	4	120	140	304	356	0.4048	0.777(19)	6.016
252.90	2	40	60	134	158	0.4395	0.863(9)	6.016

3.3 Results

3.3.1 Computational studies. A search of the torsional potential of the Si-C-C-Si dihedral angle at the HF/6-31G* level revealed the presence of two minima, representing *anti* (ϕSi-C-C-Si of 180.0°) and *gauche* (ϕSi-C-C-Si of 80°) conformers. There is a significant energy difference calculated between the two conformers of 19.2 kJ mol^{-1}, and so it would be expected that only the *anti* conformer would be found in the gas-phase experiment. However, further calculations carried out at a higher level only returned one minimum, during the optimisation procedure the *gauche* conformer converted to the *anti* conformer. Cartesian coordinates for the *anti* conformer are given in Appendix B.

Partial geometries from the four highest level calculations can be found in Table 2. It can be seen that basis set convergence had been mostly achieved by MP2/6-311+G*, with only ∠CCSi changing noticeably from 113.1 to 112.4° (MP2/6-311G* to MP2/6-311+G*). A further calculation with the addition of polarisation functions on the hydrogen atoms (MP2/6-311+G**) had, as might be expected, little effect on the relevant parameters. There are substantial changes in the C-Si bond length,

∠CCSi and both CSiCl angles upon improving the level of theory from Hartree Fock to MP2, thus including electron correlation. The Si-Cl and C-Si bond lengths decrease significantly upon improving the basis set from MP2/6-31G* to MP2/6-311G* (from 204.1 to 203.3 pm and 186.3 to 185.2 pm respectively), but the bond lengths seem relatively insensitive to further increases in basis set size.

Table 2 Calculated geometric parameters (r_e structure) for $SiCl_3CH_2CH_2SiCl_3$ (distances in pm, angles in °).[a]

Parameter	Level of Theory / Basis set			
	HF/ 6-31G*	MP2/ 6-31G*	MP2/ 6-311G*	MP2/ 6-311+G*
C(1)-C(2)	154.4	154.0	154.1	154.1
C(1)-Si(3)	187.1	186.3	185.2	185.2
C(1)-H(11)	108.7	109.7	109.6	109.7
Si(3)-Cl(8)	204.3	204.1	203.3	203.4
Si(3)-Cl(9)	204.5	204.4	203.6	203.8
C(2)-C(1)-Si(3)	114.5	112.9	113.1	112.4
C(2)-C(1)-H(11)	110.7	110.8	110.8	110.8
C(1)-Si(3)-Cl(8)	109.5	110.1	110.2	110.7
C(1)-Si(3)-Cl(9/10)	110.6	109.9	109.9	109.7
Si(3)-C(1)-C(2)-Si(4)	180.0	180.0	180.0	180.0
C(2)-C(1)-Si(3)-Cl(9)	60.1	59.8	59.8	59.6
Si(3)-C(1)-C(2)-H(11)	121.1	120.8	120.9	120.9
Total energy[b]	-3413.1314	-3414.3222	-3414.5931	-3414.6181

[a] See Figure 1 for atom numbering.

[b] Energy in Hartrees with zero-point correction applied.

3.3.2 Electron diffraction analysis. The initial geometry for the refinement of the structure was taken from the results of the *ab initio* calculations. The model has overall C_{2h} symmetry, with local C_{3v} symmetry assumed for the $SiCl_3$ groups and local C_s symmetry assumed for the CCH_2Si groups. The assumptions of local symmetry were used as there is little variation in the calculated values for the two different SiCl distances and the three CSiCl angles differ by less than a degree in the

calculations. The molecule was defined using eleven independent geometric parameters, comprising four bond lengths, three bond angles, three torsions and a tilt of the silyl group. The bond lengths used were *r*SiC (p_1), *r*SiCl (p_2), *r*CH (p_3) and *r*CC (p_4). The angles used were ClSiCl angles (p_5) as well as ∠CCH (p_6) and ∠CCSi (p_7). The hydrogen atoms in the CH_2 group were moved into position using a Si-C-C-H torsion (p_8) and a torsion around the C-C bond was included (Si-C-C-Si) (p_9). Torsion (Cl-Si-C-C) (p_{10}) and tilt (p_{11})parameters for the $SiCl_3$ group were also included. This last parameter was defined as the angle between the local C_3 axis of the $SiCl_3$ group and Si-C bond, tilting in the CCSi plane, positive if towards to the hydrogen atoms on the adjacent carbon.

The starting values for the eleven geometric parameters used in the refinement were taken from results of the *ab initio* calculations (MP2/6-311G*). The theoretical (HF/6-31G*) Cartesian force field was obtained and, using ASYM40,[17] converted into a force field described by a set of symmetry coordinates. The model was refined as an r_α (r_{h0}) structure (i.e. with rectilinear perpendicular distance corrections). It should be noted that the model was also refined using curvilinear corrections (r_{h1} structure) generated using the methods of Siphachev.[18] This, however, resulted in a less satisfactory fit to the experimental data than was obtained using rectilinear perpendicular distance corrections. In total, all eleven geometric parameters and nine groups of amplitudes were refined. Flexible restraints were used during the refinement (eight geometric, shown in Table 3, and three amplitude, shown in Table 4) defined using the SARACEN method.[19]

In the process of the refinement, two of the three films from the short nozzle-to-film distance were ignored. This was because there appeared to be impurities or imperfections present on the films causing disagreement between them. A low scale factor for two of the three short films was noticed and on removing them from the refinement, an improvement in R_G value and removal of discrepancies from the difference curve from the radial distribution curve were noticed.

The molecular scattering intensities (Figure 2) and the radial distribution curve (Figure 3) can be used to judge the success of the final refinement for which R_G = 0.048 (R_D = 0.035). Final refined parameters are listed in Table 3, and interatomic distances and the corresponding amplitudes of vibration in Table 4. The least-squares correlation matrix is shown in Table 5.

Table 3 Refined geometric parameters from the GED study of $SiCl_3CH_2CH_2SiCl_3$ (distances in pm, angles in °).

	Independent Parameters	GED (r_{h0})	Restraint
p_1	*r*SiCl	199.7(1)	
p_2	*r*CSi	184.1(4)	
p_3	*r*CH	109.4(5)	109.7(5)
p_4	*r*CC	154.2(4)	154.1(5)
p_5	∠ClSiCl	107.8(2)	
p_6	∠CCH	110.7(4)	110.8(4)
p_7	∠CCSi	112.6(4)	112.4(10)
p_8	Si(3)-C(1)-C(2)-H(11)	120.0(9)	120.0(10)
p_9	Si(3)-C(1)-C(2)-Si(4)	180.0(15)	180.0(15)
p_{10}	Cl(5)-Si(4)-C(2)-C(1)	1.2(19)	1.0(20)
p_{11}	$SiCl_3$ tilt	1.6(3)	1.0(20)
	Dependent Parameters		
p_{12}	∠C(2)Si(4)Cl(5)	112.6(4)	
p_{13}	∠C(2)Si(4)Cl(6)	110.3(4)	

Figure 2 Experimental and final weighted difference (experimental – theoretical) molecular-scattering intensities for **1**.

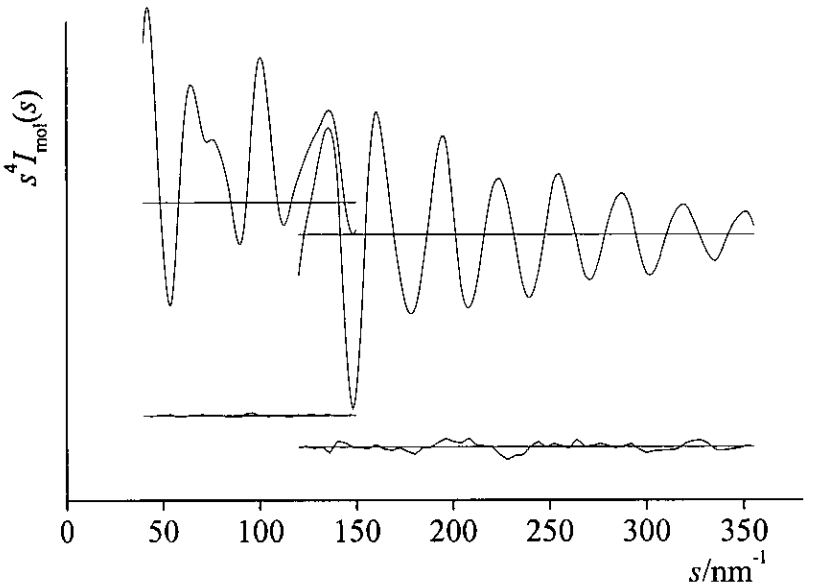

Figure 3 Experimental and difference (experimental – theoretical) radial distribution curves, $P(r)/r$, for **1**. Before Fourier inversion the dataset was multiplied by $s\exp(-0.00002s^2)/(Z_{Cl}-f_{Cl})(Z_{Si}-f_{Si})$.

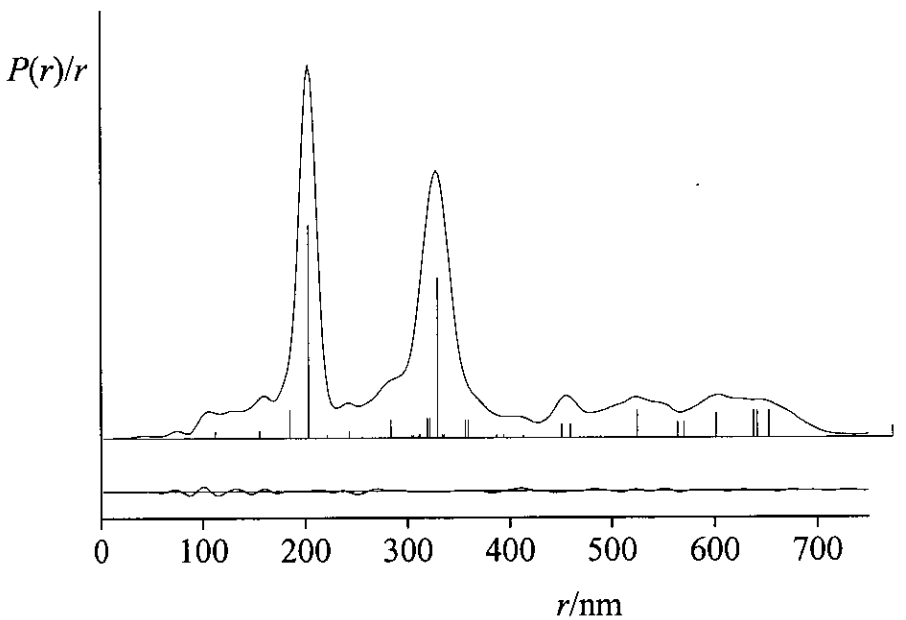

Table 4 Interatomic distances (r_a/pm) and amplitudes of vibration (u/pm) for the restrained GED structure of $SiCl_3CH_2CH_2SiCl_3$.[a,b]

	Atom pair	r_a / pm	u / pm	Restraint
u_1	Cl(5)-Si(4)	202.9(1)	4.8(1)	
u_2	Cl(6)··Cl(5)	329.0(3)	9.9(1)	
u_3	Cl(8)··Cl(6)	637.1(58)	37.4 (tied to u_8)	
u_4	Cl(7)··Si(3)	525.6(63)	26.1(10)	
u_5	Cl(6)··Si(3)	523.7(30)	26.1 (tied to u_4)	
u_6	Cl(8)··Cl(7)	642.5(39)	37.4 (tied to u_8)	
u_7	Si(3)-C(1)	185.1(4)	8.7(7)	
u_8	Cl(9)··Cl(7)	652.7(42)	21.7(8)	
u_9	Cl(5)··Si(3)	601.6(53)	15.0(8)	
u_{10}	Cl(6)··C(2)	319.2(26)	11.6 (tied to u_{12})	
u_{11}	Cl(7)··C(2)	319.3(25)	11.6(tied to u_{12})	
u_{12}	Cl(5)··C(2)	321.8(51)	11.8(9)	
u_{13}	Si(3)··C(2)	283.0(4)	8.0(*fixed*)	
u_{14}	Cl(6)··C(1)	356.0(33)	22.3(17)	
u_{15}	Cl(7)··C(1)	358.7(62)	22.3 (tied to u_{14})	
u_{16}	Cl(10)··Cl(7)	567.0(41)	44.9(41)	43.2(40)
u_{17}	Cl(9)··Cl(6)	567.7(42)	44.9 (tied to u_{16})	
u_{18}	C(2)-C(1)	112.2(5)	7.8(6)	7.5(8)
u_{19}	H(11)-C(1)	155.5(4)	4.9(5)	5.1(5)

[a] See Figure 1 for atom numbering.

[b] Other amplitudes were included but not refined and fixed at HF/6-31G* values.

Table 5 Least-squares correlation matrix (× 100) for $SiCl_3CH_2CH_2SiCl_3$.[a]

	u_{12}	k_3	k_4
p_2	-	-	-51
p_5	-88	-	-
u_1	-	81	-
u_2	-	53	-

[a] Only elements with absolute values ≥50% are shown; k_3 and k_4 are scale factors.

3.4 Discussion

The results of the MP2/6-311+G* calculations in general agree well with those obtained from the gas-phase electron diffraction refinement. The most notable difference is in *r*SiCl, which is 4 pm shorter in the gas phase than is calculated by MP2/6-311+G* (199.7 and 203.7 pm respectively). Initially, it was thought that this was due to the fact that *r*SiCl lies under the same peak in the radial distribution curve as *r*CSi. Two distances occurring under the same peak can sometimes be strongly correlated, and so may refine to values towards the average of the two distances. Attempts were made to overcome this by refining the two distances in terms of the average of the two distances and the difference between them. However, the results from this refinement did not constitute an improvement in the values obtained for the two distances and as a result it was not deemed necessary to continue with a refinement using average and difference values. Further evidence for this is present in the value obtained for *r*CSi, which would be higher than expected if overlapping peaks were the cause of the problem. As can be seen from Table 3, this is in fact not the case, the *r*CSi distance being slightly shorter than is predicted by the *ab initio* calculations. This is a common problem for distances between second row atoms which are consistently overestimated by MP2 level of calculations, even when using a large basis set.

Table 6 shows the differences between the calculated, experimental gas-phase and X-ray structures for **1**. There is, in general, good agreement between the values obtained from all three techniques. However, it can bee seen that there is a large difference between the value for *r*SiCl from GED and those from the other two methods. The gas-phase distance is also shorter than previous literature values [e.g. 202.8(2) pm in Cl_3SiCH_2Cl[20] and 206.0(5) in $Cl_3Si\text{-}CH{=}CH_2$[21]]. As this distance occurs six times in the molecule and involves the heaviest atoms, it should be well defined by GED and so this short *r*SiCl must be indeed be genuine. Other, less extreme differences between the GED and the XRD values can be seen in the angles CCSi and CSiCl, where the values from the two techniques differ by over a degree. The increased ∠CCSi causes the narrowing of ∠CSiCl(8) (though slight in the GED

structure) to allow the bulky $SiCl_3$ group sufficient room from the backbone CH_2 group.

With an increased ∠CCSi in the crystal, it would be expected that the corresponding C(1)Si(3)Cl(8) angle would also increase. However, as can be seen from Table 5, the C(1)-Si(3)-Cl(8) angle is, in fact, larger than the calculated value in both the crystal and gas-phase structures.

Table 6 Refined and calculated geometric parameters from the GED and XRD study of $SiCl_3CH_2CH_2SiCl_3$ (distances in pm, angles in °).

	MP2/6-311+G*	GED	XRD[1]
C(1)-C(2)	154.1	154.2(7)	153.6(3)
C(1)-Si(3)	185.2	184.0(4)	184.7(2)
C(1)-H(11)	109.7	109.4(5)	
Si(3)-Cl(8)	203.3	199.7(1)	202.8(1)
Si(3)-Cl(9)	203.8	199.7(1)	202.3(1)
C(2)-C(1)-Si(3)	112.4	112.8(2)	113.9(1)
C(2)-C(1)-H(11)	110.8	110.7(4)	
C(1)-Si(3)-Cl(8)	110.7	112.6(4)	111.4(1)
C(1)-Si(3)-Cl(9)	109.7	110.3(4)	109.8(1)

Comparing the results for this compound (**1**) with those available in the literature for 1,4-disilabutane[2] ($SiH_3CH_2CH_2SiH_3$) and 1-silabutane[3] ($CH_3CH_2CH_2SiH_3$) it is possible to see one immediate difference, in that **1** only has one conformer where both $SiH_3CH_2CH_2SiH_3$ and $CH_3CH_2CH_2SiH_3$ have two (one *anti* and one *gauche*). A conformational analysis was carried out on these three compounds as well as butane, $CCl_3CH_2CH_2CCl_3$, $CCl_3CH_2CH_2SiCl_3$ and $SiCl_3CH_2CH_2CH_3$ by varying the (Si/C)-C-C-(Si/C) dihedral angle from 0.0 to 180.0° in steps of 10°. The results from all sets of seven calculations can be seen in Figure 4. Cartesian coordinates for the minima of all seven compounds are given in Appendix B.

Figure 4 Potential energy plots (HF/6-31G*) for $SiCl_3CH_2CH_2SiCl_3$ (black) (**1**), $SiH_3CH_2CH_2SiH_3$ (green), $CH_3CH_2CH_2SiH_3$ (blue), $CH_3CH_2CH_2CH_3$ (red), $SiCl_3CH_2CH_2CH_3$ (purple), $CCl_3CH_2CH_2SiCl_3$ (cyan) and $CCl_3CH_2CH_2CCl_3$ (orange). [a,b]

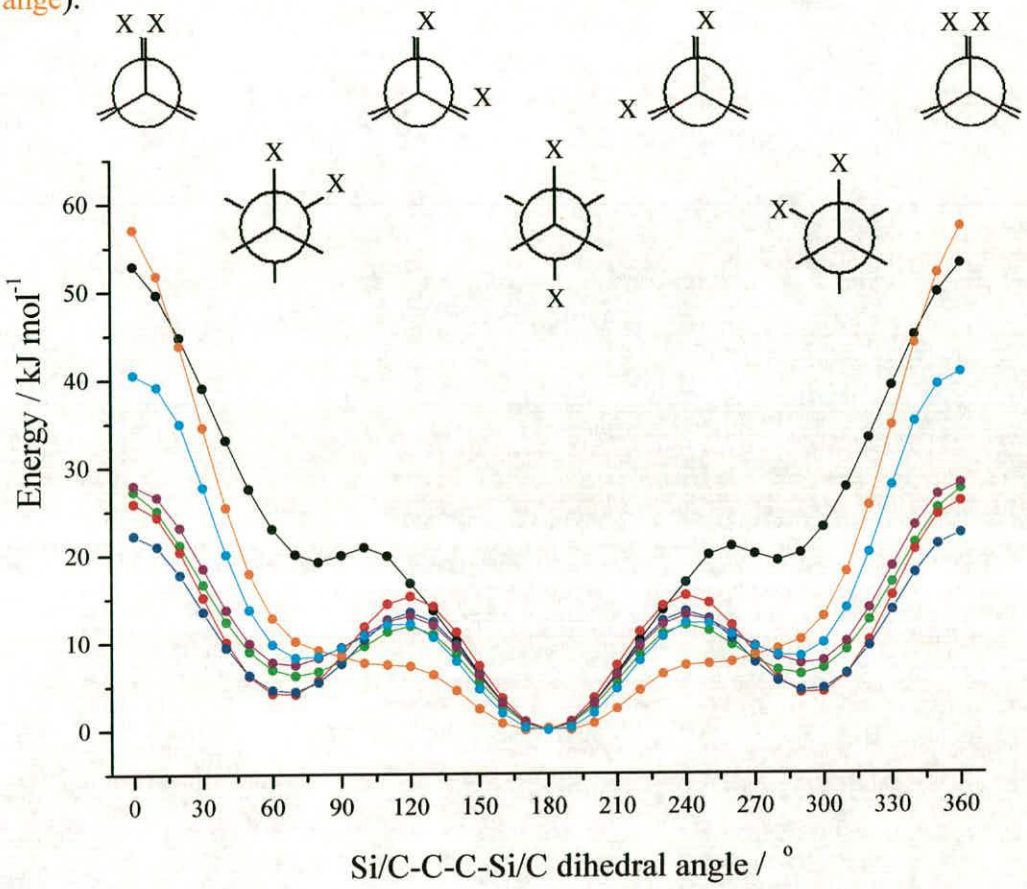

[a] X represents $SiCl_3$, SiH_3 or CH_3 in the Newman projections.

[b] All curves were normalised to their own zero for plotting purposes.

It is immediately obvious in Figure 4 that there is a large difference between the curve for **1** and the majority of the other molecules as the minimum that is present at approximately 70° is not as prominent in **1**. This minimum is also much higher in energy, thus showing that it is unlikely that the *gauche* conformer would ever actually exist. This is easily explained by the increase in steric bulk caused by the $SiCl_3$ groups; in the *gauche* conformer, chlorine atoms from the two $SiCl_3$ groups would be forced into close proximity and the electrostatic repulsion raises the energy of the system.

This is corroborated by considering the curve for $CCl_3CH_2CH_2CCl_3$, where the minimum at around 70° is also less distinct than even that present in **1**. This can be attributed to the steric repulsion between the chlorine-substituted groups. It can also be seen that the three compounds that are substituted with either $SiCl_3$ or CCl_3 groups at both ends of the carbon carbon bond [$SiCl_3CH_2CH_2SiCl_3$ (**1**), $SiCl_3CH_2CH_2SiCl_3$ and $SiCl_3CH_2CH_2SiCl_3$] have the highest energies when the two groups are eclipsed, again due to the high steric repulsion between the $SiCl_3$ and CCl_3 groups. The compound with the highest energy conformer at torsion angle of 360° is $CCl_3CH_2CH_2CCl_3$. This is to be expected as the C-Cl bond distance is shorter than that of the Si-Cl, which forces the two end trichloro substituted groups into even closer contact than would be the case for $SiCl_3$ substituted groups. The remaining four compounds ($SiH_3CH_2CH_2SiH_3$, $CH_3CH_2CH_2CH_3$, $CH_3CH_2CH_2SiH_3$ and $SiCl_3CH_2CH_2CH_3$) trace similar curves with two minima present, at 70 / 290° and 180° at approximately the same energy differences.

Table 7 shows selected parameters for the *anti* and *gauche* conformers of the majority of the compounds as calculated during the search of the (Si/C)-C-C-(Si/C) torsional potential at the HF/6-31G* level. This allows comparison between values calculated for bond lengths and angles in the *anti* and *gauche* conformers.

From Table 7 it is possible to notice several interesting trends. In every molecule, the ∠CC(Si/C) angle is larger in the *gauche* conformer than in the *anti*. Predictably, the two molecules with the largest difference between the values calculated for the *gauche* and *anti* conformers were those with chlorine-substituted end groups (with differences in both cases of over 7°). This is expected, as bringing the two $SiCl_3$ or CCl_3 groups into closer proximity would encourage a larger ∠CC(Si/C) to limit the steric crowding. In both $CCl_3CH_2CH_2CCl_3$ and $SiCl_3CH_2CH_2SiCl_3$, the C-Si and C-C bond lengths are considerably longer in the *gauche* conformer than in the *anti*. This can be again attributed to limiting the steric interference of the two large $SiCl_3$ or CCl_3 groups in the *gauche* conformer, by extending the distance between the

carbon backbone and the bulky groups both by increasing the bond distance and the angle.

Table 7 Selected parameters calculated at HF/6-31G* (distances in pm, angles in °).

	$SiCl_3CH_2CH_2SiCl_3$		$CH_3CH_2CH_2SiCl_3$	
	anti	*gauche*	*anti*	*gauche*
*r*CC	154.3	154.5	154.0	154.1
*r*CSi	187.1	187.7	186.5	187.0
*r*SiCl(8)	204.3	204.8	204.9	205.1
∠CCSi	114.5	121.6	115.8	118.7
∠CSiCl(8)	109.5	107.2	109.8	108.7
ϕ(Si/C)CCSi	180.0	70.0	180.0	70.0
	$SiH_3CH_2CH_2SiH_3$		$CH_3CH_2CH_2SiH_3$	
	anti	*gauche*	*anti*	*gauche*
*r*CC	154.7	154.6	153.7	154.0
*r*CSi	189.4	189.7	189.3	189.6
*r*SiH(8)	147.9	147.8	147.9	147.9
∠CCSi	113.6	116.8	114.5	116.5
∠CSiH(8)	110.8	109.4	110.5	109.6
ϕ(Si/C)CCSi	180.0	70.0	180.0	70.0
	$CCl_3CH_2CH_2CCl_3$		$CH_3CH_2CH_2CH_3$	
	anti	*gauche*	*anti*	*gauche*
*r*CC	153.1	153.6	153.0	153.3
*r*CC(4)	152.5	153.6	152.8	153.0
*r*C(Cl/H)(8)	178.0	177.9	108.6	108.8
∠CCC(4)	111.7	118.4	113.1	114.3
∠CC(Cl/H)(8)	110.0	107.9	111.3	110.9
ϕCCCC	180.0	70.0	180.0	70.0

As might be expected, the smallest change in ∠CC(Si/C) between *gauche* and *anti* conformer is in $CH_3CH_2CH_2CH_3$, where the ∠CCC(4) angle increases by 1.22° between the two conformers and there is also a moderate increase in *r*CC(4). This is

because of a lesser steric effect upon changing between the *gauche* and *anti* conformers than is present in other molecules in this study. There is less steric bulk associated with both the CH_3 groups as compared to their chlorine-substituted analogues. Also as expected, it can be seen from Table 7 that molecules substituted at only one end of the molecule by silyl or chlorine-substituted groups have the smallest change in values calculated for ∠CC(Si/C) between the two conformers.

It is also possible to compare values for the bond lengths and angles obtained from the gas-phase refinements of **1**, $SiH_3CH_2CH_2SiH_3$[2] and $CH_3CH_2CH_2SiH_3$.[3] The silicon-carbon bond length was found to be a shorter in **1** than in either $SiH_3CH_2CH_2SiH_3$ or $CH_3CH_2CH_2SiH_3$ [184.0(4), 188.2(1) and 187.4(2) pm respectively]. This can be attributed to the fact that **1** has electronegative chlorine atoms attached to the silicon whereas $SiH_3CH_2CH_2SiH_3$ and $CH_3CH_2CH_2SiH_3$ have simple silyl groups. Therefore, in removing electron density away from the silicon towards the chlorine atoms, the C-Si bond length in **1** decreases notably.

The other main difference is in the values obtained for ∠CCSi, which is larger in **1** than in $SiH_3CH_2CH_2SiH_3$ [112.8(2) and 110.7(2)° respectively]. This can be attributed to the steric bulk of the $SiCl_3$ groups, which take up more space than the silyl groups on $SiH_3CH_2CH_2SiH_3$. However, the ∠CCSi in $CH_3CH_2CH_2SiH_3$ is approximately the same as that in **1** [113.0(6) and 112.8(2)° respectively]. This is most likely due to the fact that $CH_3CH_2CH_2SiH_3$ only has one silyl group and is more free to increase the size of ∠CCSi without having steric implications at the other end of the molecule than would be the case in the other two molecules, which are substituted at both ends of the C-C bond.

3.5 Conclusion

The gas-phase structure of **1** has been determined using electron diffraction. It is found to exist in only one *anti* conformation, thus differing from other substituted ethanes. Studying the potential energy plots of seven compounds, each with varying degrees of end-substitution by varying the (Si/C)-C-C-(Si/C) torsion angle from 0.0

to 360.0° confirmed differences in the energies for different conformers. From these calculations it was possible to see that the compounds substituted on both ends of the molecule with either CCl_3 or $SiCl_3$ groups had a less discernable minimum present at torsion angle of 70°. This lack of *gauche* conformer can be attributed to steric hindrance between the trichloro substituents at the two ends of the molecule.

3.6 References

1. Mitzel, N. W.; Riede, J.; Schmidbaur, H. *Acta Cryst. C*, **1997**, *C53*, 1335.

2. Mitzel, N. W.; Smart, B. A.; Blake, A. J.; Robertson, H. E.; Rankin, D. W. H. *J. Phys. Chem.*, **1996**, *100*, 9339.

3. Arnason, I.; Oberhammer, H. *J. Phys. Chem. A*, **2003**, *107*, 243.

4. Gaussian 98 (Revision A.7), Frisch, M. J.; Trucks, G. W.; Schlegel, H. B.; Scuseria, G. E.; Robb, M. A.; Cheeseman, J. R.; Zakrzewski, V. G.; Montgomery, J. A.; Stratman, R. E.; Burant, J. C.; Dapprich, S.; Milliam, J. M; Daniels, A. D.; Kudin, K. N.; Strain, M. C.; Farkas, O.; Tomasi, J.; Barone, V.; Cossi, M.; Cammi, R.; Mennucci, B.; Pomelli, C.; Adamo, C.; Clifford, S.; Ochterski, J.; Petersson, G. A.; Ayala, P.Y.; Cui, Q.; Morokuma, K.; Malick, D. K.; Rabuck, A. D.; Raghavachari, K.; Foresman, J. B.; Cioslowski, J.; Ortiz, J. V.; Baboul, A. G.; Stefanov, B. B.; Liu, C.; Liashenko, A.; Piskorz, P.; Komaromi, I.; Gomperts, R.; Martin, R. L.; Fox, D. J.; Keith, T.; Al-Laham, M. A.; Peng, C. Y.; Nanayakkara, A.; Gonzalez, C.; Challacombe, M.; Gill, P. M. W.; Johnson, B. G.; Chen, W.; Wong, M. W.; Andres, J. L.; Gonzales, C.; Head-Gordon, M.; Replogle, E. S.; Pople, J. A. Gaussian, Inc., Pittsburgh PA, **1998**.

5. Binkley, J. S.; Pople, J. A.; Hehre, W. J. *J. Am. Chem. Soc.*, **1980**, *102*, 939.

6. Gordon, M. S.; Binkley, J. S.; Pople, J. A.; Pietro, W. J.; Hehre, W. J. *J. Am. Chem. Soc.*, **1982**, *104*, 2979.

7. Pietro, W. J.; Francl, M. M.; Hehre, W. J.; DeFrees, D. J.; Pople, J. A.; Binkley, J. S. *J. Am. Chem. Soc.*, **1982**, *103*, 5039.

8. Hehre, W. J.; Ditchfield, R.; Pople, J. A. *J. Chem. Phys.*, **1972**, *56*, 2257.

9. Hariharan, P. C.; Pople, J. A. *Theor. Chim. Acta*, **1973**, *28*, 213.

10. Gordon, M. S. *Chem. Phys. Lett.*, **1980**, *76*, 163.

11. Krishnan, R; Binkley J. S.; Seeger, R; Pople, J. A. *J. Chem. Phys.*, **1980**, *72*, 650.

12. Huntley, C. M.; Laurenson, G. S.; Rankin, D. W. H. *J. Chem. Soc., Dalton Trans.*, **1980**, 954.

13. Lewis, J. R.; Brain, P. T.; Rankin, D. W. H. *Spectrum*, **1997**, *15*, 7.

14. Cradock, S.; Koprowski, J. *J. Mol. Struct.*, **1982**, *77*, 113.

15. Boyd, A. S. F.; Laurenson, G. S.; Rankin, D. W. H. *J. Mol. Struct.*, **1981**, *71*, 217.

16. Ross, A. W.; Fink M.; Hilderbrandt, R. in *International Tables for Crystallography*, ed. A. J. C. Wilson, Vol. C, Kluwer Academic Publishers, Dordrecht, **1992**, p.245.

17. Hedberg, L.; Mills, I. M. *J. Mol. Struct.*, **1993**, *160*, 117.

18. Vilkov, L. V.; Mastryukov, V. S.; Akishin, P.A., *Z. Strukt. Khim.*, **1964**, *5(2)*, 183.

19. (a) Blake, A. J.; Brain, P. T.; McNab, H.; Millar, J.; Morrison, C. A.; Parsons, S.; Rankin, D. W. H.; Robertson, H. E.; Smart, B. A. *J. Phys. Chem.*, **1996**, *100*, 12280. (b) Brain, P. T.; Morrison, C. A.; Parsons, S.; Rankin, D. W. H. *J. Chem. Soc., Dalton Trans.*, **1996**, 4589.

20. Vajda, E.; Székely, T.; Hargittai, I.; Maltsev, A. K.; Baskir, E. G.; Nefedov, O. M., *J. Org. Chem.*, **1980**, *188(3)*, 321.

CHAPTER FOUR

The molecular structure of bistrichlorosilyldimethylgermane $[Me_2Ge(SiCl_3)_2]$ by gas-phase electron diffraction and *ab initio* calculations

4.1 Introduction

Previous work, carried out in collaboration with Prof. W. W. du Mont, of the Technische Universität Braunschweig in Germany, on bis(trichlorosilyl)*tert*-butylphosphine [$PBu^t(SiCl_3)_2$] has revealed asymmetric bonding around the phosphorus atom.[1] This has been attributed to the electron withdrawing nature of the $SiCl_3$ groups as well as the steric effect of the bulky tertiary butyl groups.

The structure of bistrichlorosilyldimethylgermane [$Me_2Ge(SiCl_3)_2$] was investigated by gas-phase electron diffraction and *ab initio* studies. The structure can be compared to the previously determined structure of the germane with only one $SiCl_3$ group, $Me_3GeSiCl_3$. This will allow investigation into the effect of electron withdrawing groups on the structure

4.2 Experimental

4.2.1 Synthesis. A sample of $Me_2Ge(SiCl_3)_2$ was prepared by Emma Seppälä from the Technische Universität Braunschweig, Germany. The sample was used in the gas-phase experiment without further purification.

4.2.2 Computational studies. All geometry optimisation and frequency calculations for $Me_2Ge(SiCl_3)_2$ were carried out on a dual-processor Pentium III 1000 MHz workstation using the Gaussian 98 program.[2] An extensive search of the potential energy hypersurface of $Me_2Ge(SiCl_3)_2$ was undertaken at the Hartree Fock (HF) level using the 3-21G*[3-5] basis set and one minimum was located. The structure of this minimum with atom numbering is shown in Figure 1. Further geometry optimisations were undertaken at the HF and MP2(fc) levels using the standard 6-31G*[6-8] basis set, and at the MP2 level using the 6-311G*[9,10] and 6-311+G* basis sets. Analytical second derivatives with respect to the nuclear coordinates calculated at the HF/6-31G* level gave the force field which was used to obtain estimates for the amplitudes of vibration (u) and curvilinear corrections (k), used

in the refinement of the GED data. The force fields were also used to calculate the frequencies for all the optimised structures, which in turn provided information about the nature of stationary points. This is important in order to determine if the stationary point found in the potential energy surface is, in fact, a minimum or if it represents an imaginary structure or transition state. Cartesian coordinates for the two lowest energy structures can be found in Appendix C.

As well as one minimum located during the search of the torsional potentials of $Me_2Ge(SiCl_3)_2$, several transition state structures were also found. Each of these represented a different orientation of the $SiCl_3$ and methyl groups and in total span an energy difference of 42.9 kJ mol^{-1}. The lowest energy transition state structure is 4.11 kJ mol^{-1} higher in energy and has low-lying vibrational modes (13*i* and 28 cm^{-1}) which both involve torsional motions of the $SiCl_3$ groups. The lowest lying frequencies of the global minimum (8 and 29 cm^{-1}) also involve torsional motions of the $SiCl_3$ group. This indicates that there is very little barrier to rotation of the $SiCl_3$ groups which can have major implications during the refinement of the gas-phase data and will be discussed later in this chapter.

Figure 1 Lowest energy molecular structure of $Me_2Ge(SiCl_3)_2$.

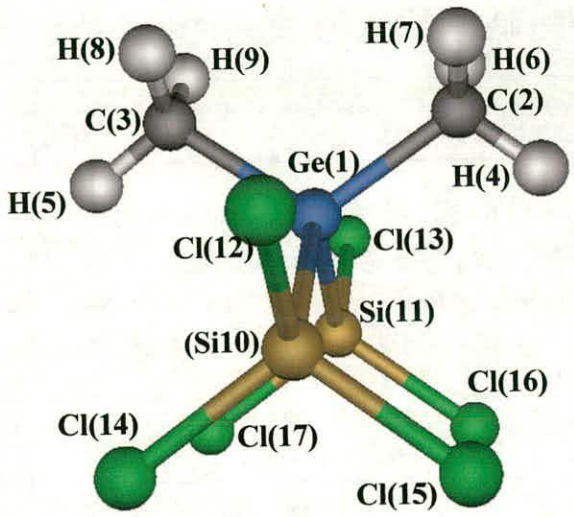

4.2.3 Gas-phase electron diffraction experiment. Data were collected for $Me_2Ge(SiCl_3)_2$ using the Edinburgh gas diffraction apparatus.[11] An accelerating voltage of *ca.* 40 kV (electron wavelength *ca.* 6.0 pm) was used. Sample and nozzle temperatures were maintained at 345 K and 353 K respectively and the scattering intensities were recorded on Kodak Electron Image plates at nozzle-to-plate distances of 94.7 and 256.8 mm. The weighting points for the off-diagonal weight matrices, correlation parameters and scale factors for the two camera distances for each molecule are given in Table 1, together with electron wavelengths, which were determined from the scattering patterns of benzene vapour, recorded immediately after the compound patterns and analysed in exactly the same way to minimise systematic errors in wavelengths and camera distances. A PDS microdensitometer was used to convert the intensity patterns into digital form.[12] Data reduction and least-squares refinements were carried out using standard programs,[13,14] utilising the scattering factors of Ross *et al.*[15]

Table 1 Nozzle-to-plate distances (mm), weighting functions (nm^{-1}), correlation parameters, scale factors and electron wavelengths (pm) used in the gas electron diffraction study of $Me_2Ge(SiCl_3)_2$.

camera distance/mm	weighting functions /nm^{-1}					correlation parameter	scale factor	electron wavelength/pm
	Δs	s_{min}	s_1	s_2	s_{max}			
94.71	4	80	100	288	308	0.2204	1.040(57)	6.016
256.82	2	20	40	88	108	0.4615	0.769(12)	6.016

4.3 Results

4.3.1 Computational Studies. The lowest energy structure of $Me_2Ge(SiCl_3)_2$ on the potential energy hypersurface at the HF/3-21G* level was found to possess C_{2v} symmetry. The effect of improving the basis set and level of theory was studied using a series of graded calculations at the HF/6-31G*, MP2/6-31G*, MP2/6-311G* and MP2/6-311+G* levels. Partial geometries from the four highest level calculations can be found in Table 2.

From Table 2, it can be seen that the Si-Ge-C, Ge-C-H and Ge-Si-Cl angles were virtually unaffected by improving the basis set or including electron correlation. The mean C-H distance underwent its largest change upon the introduction of correlation (from 108.3 to 109.2 pm) whereupon it became stable and hardly changed with subsequent improvements in the basis set. The Si-Cl distances varied only slightly with improved basis set, decreasing in size by 0.6 pm from MP2/6-31G* to MP2/6-311G*, and virtually no change was observed upon the addition of diffuse functions on the heavy atoms. Significant changes were observed for values calculated for the remaining bond distances. For example, Ge-Si decreased by 2.0 pm with the inclusion of correlation and then increased by 1.4 pm from MP2/6-31G* to MP2/6-311G*. The Ge-C bond length increased by only 0.3 pm with the inclusion of correlation, but increased by a further 1.6 pm from MP2/6-31G* to MP2/6-311G*. The values calculated for the Ge-Si and Ge-C distances were not affected by the addition of diffuse functions on the heavy atoms.

As previously stated, there are low-lying vibrational motions of the $SiCl_3$ groups, which it is important to reflect in the model for the refinement of the gas-phase electron diffraction data. In the lowest energy real structure of $Me_2Ge(SiCl_3)_2$, the two lowest energy vibrations involve motions of the $SiCl_3$ groups (the vibration at 8 cm^{-1} involves rotation of the two $SiCl_3$ groups in opposite directions and the vibration at 29 cm^{-1} involves rotation in the same direction). The lowest energy transition state also has low-energy vibrations that involve the $SiCl_3$ groups. The vibration at $13i$ cm^{-1} involves one of the $SiCl_3$ groups rotating whereas the vibration at 28 cm^{-1} involves both of the $SiCl_3$ groups rotating in opposite directions. All four of these vibrations also involve motions of the two methyl groups.

Table 2 Molecular geometry of the lowest energy structure of $Me_2Ge(SiCl_3)_2$ (distances in pm, angles in °).[a,b]

Parameter	HF/6-31G*	MP2/6-31G*	MP2/6-311G*	MP2/6-311+G*
C-H mean	108.3	109.2	109.2	109.3
Ge-C	194.9	194.6	196.2	196.2
Ge-Si	239.8	236.8	238.2	238.2
Si-Cl(12)	205.9	205.6	205.0	205.0
Si-Cl(14)	205.2	204.8	204.2	204.3
Ge-C-H mean	109.9	109.5	110.2	110.3
Ge-Si-Cl(12)	108.4	108.2	108.8	108.8
Ge-Si-Cl(14)	112.1	111.3	111.7	111.7
Si-Ge-C	108.3	108.5	108.8	108.6
C(2)-Ge(1)-Si(10)-Cl(12)	60.0	61.5	61.4	61.7
H(4)-C(1)-Ge(1)-C(3)	180.0	180.0	180.0	180.0
Energy[c]	-5487.4900	-5488.8628	-5491.1746	-5491.2009

[a] See Figure 1 for atom numbering.

[b] Energy in Hartrees and corrected for zero point energy.

4.3.2 Electron diffraction analysis

The refinement of $Me_2Ge(SiCl_3)_2$ was carried out using a model of approximate C_s symmetry. The structure was defined using thirteen independent geometric parameters, comprising four bond lengths, four bond angles and five torsions. An average and difference were used to describe the Si-Cl and Ge-C bond lengths ($p_{1\text{-}2}$). The other bond lengths used were Ge-Si (p_3) and C-H (p_4). The independent bond angle parameters were ∠Ge-Si-Cl (p_5), ∠Si-Ge-Si (p_6), ∠CGeC (p_7) and ∠GeCH (p_8). Five bond torsions were also included: ϕC-Ge-Si-Cl for each of the two $SiCl_3$ groups ($p_{9\text{-}10}$) ($SiCl_3$ group torsion), a tilt of each of the $SiCl_3$ groups ($p_{11\text{-}12}$) [defined as positive if tilted in the y direction, local y-axis defined as in the Ge-Si-Cl(12/13) plane] and ϕH-C-Ge-Si (methyl group torsion) (p_{13}).

The starting parameters for the r_{h1} refinement were taken from the theoretical geometry optimised at the MP2/6-311G* level. A theoretical (HF/6-31G*) Cartesian force field was obtained and converted into a force field described by a set of symmetry coordinates using the SHRINK program which generated both the amplitudes of vibration (u) and the curvilinear corrections (k).[16]

Figure 2 shows a perspective view of (a) the calculated and (b) the GED molecular structures. The success of the final refinement, for which $R_G = 0.090$ ($R_D = 0.070$), can be assessed on the basis of the radial distribution curve [Figure 3] and the molecular scattering intensity curves [Figure 4]. In total, twelve of the thirteen geometric parameters and eight groups of vibrational amplitudes were refined. Final refined parameters are listed in Table 3, interatomic distances and the corresponding amplitudes of vibration in Table 4 with the least-squares correlation matrix shown in Table 5. Flexible restraints were employed during the refinement using the SARACEN method.[17] Altogether, five geometric and two amplitude restraints were employed and these are listed in Tables 3 and 4.

Figure 2 Molecular structure of $Me_2Ge(SiCl_3)_2$ (a) as calculated (MP2/6-311+G*) and as refined using GED data (b).

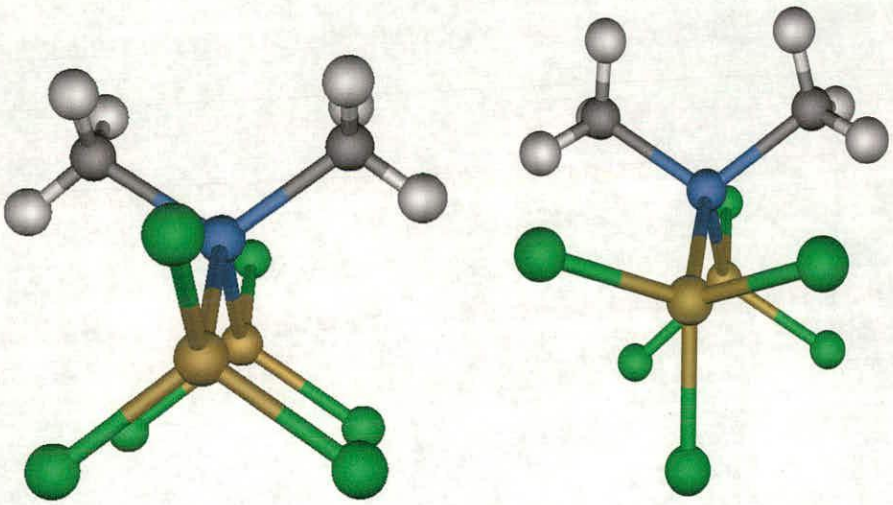

(a) (b)

Table 3 Refined (r_{h1} structure) and calculated (MP2/6-311+G*) geometric parameters from the GED study of $Me_2Ge(SiCl_3)_2$ (distances in pm and angles in °).

Independent Parameters		MP2/6-311+G*	GED	Restraint
p_1	(Si-Cl + Ge-C) / 2	200.4	199.8(5)	200.4(10)
p_2	Si-Cl minus Ge-C	8.3	11.5(10)	8.3(20)
p_3	Ge-Si	238.2	238.1(3)	
p_4	C-H	109.3	109.2(5)	109.3(5)
p_5	Ge-Si-Cl	110.5	111.1(1)	
p_6	Si-Ge-Si	109.2	112.6(6)	
p_7	C-Ge-C	113.1	112.7(10)	112.8(10)
p_8	Ge-C-H	110.3	109.3(9)	109.6(10)
p_9	ϕCl(12)-Si(10)-Ge(1)-C(2)	61.7	67.4(17)	
p_{10}	ϕCl(13)-Si(11)-Ge(1)-C(2)	-61.7	-115.8(20)	
p_{11}	$SiCl_3$ tilt	-	3.6(10)	
p_{12}	other $SiCl_3$ tilt	-	-3.8(10)	
p_{13}	ϕH(4)-C(2)-Ge(1)-Si(10)	0.0	0.1(fixed)	
Dependent Parameters				
p_{14}	Si-Cl	204.5	205.5(1)	
p_{15}	Ge-C	196.2	194.0(9)	

[a] See text for parameter definitions.

Table 4 Interatomic distances (r_a/pm) and amplitudes of vibration (u/pm) for the restrained GED structure of $Me_2Ge(SiCl_3)_2$.

No.	Atom pair	r_a / pm	u / pm[b]	Restraint
u_1	Cl(14)...Si(10)	205.6(1)	5.2(3)	
u_2	Cl(12)...Cl(14)	331.5(2)	10.5(3)	
u_3	Si(10)...Ge(1)	238.1(3)	6.3(4)	
u_4	C(2)...Ge(1)	192.1(9)	5.6(tied to u_1)	
u_5	Cl(14)...Ge(1)	368.8(9)	12.4(6)	
u_6	Cl(13)...Ge(1)	362.2(13)	10.5(tied to u_5)	
u_7	Cl(17)....Ge(1)	373.6(22)	13.4(tied to u_5)	
u_8	Cl(12)...Ge(1)	357.6(25)	13.4(tied to u_5)	
u_9	Cl(15)...Ge(1)	369.8(10)	13.4(tied to u_5)	
u_{10}	Si(10)...C(2)	349.8(10)	12.3(tied to u_5)	
u_{11}	Cl(16)...Cl(12)	723.9(35)	21.7(tied to u_{12})	
u_{12}	Cl(17)...Cl(14)	433.21(74)	21.7(22)	
u_{13}	H(4)...Ge(1)	250.9(15)	11.9(11)	11.3(11)
u_{14}	Cl(16)...Cl(15)	537.8(55)	98.1(fixed)	
u_{15}	Cl(16)...Si(10)	544.3(32)	35.5(fixed)	
u_{16}	Cl(14)...Si(11)	454.4(31)	37.4(33)	35.5(36)

Table 5 Least-squares correlation matrix (× 100) for $Me_2Ge(SiCl_3)_2$.[a]

	p_2	p_{10}	p_{12}	u_1	u_3	u_5	k_2
p_1	-97	-	-	-58	-63	-	-72
p_2	-	-	-	66	61	-	79
p_3	-	-	-	-	-	-	-53
p_5	-	53	-58	-	-	-	-
p_6	-	-	56	-	-	67	-
p_{10}	-	-	-63	-	-	-	-
p_{11}	-	-	-	-	-	-51	-
p_{12}	-	-	-	-	-	51	-
u_1	-	-	-	-	-	-	93
u_2	-	-	-	53	-	54	56
u_3	-	-	-	-	-	-	60

[a] Only elements with absolute values ≥50% are shown; k_2 is a scale factor.

Figure 3 Experimental and difference (experimental - theoretical) radial-distribution curves, $P(r)/r$, for $Me_2Ge(SiCl_3)_2$. Before Fourier inversion the data were multiplied by $s.\exp(-0.00002s^2)/(Z_{Ge}-f_{Ge})/(Z_{Cl}-f_{Cl})$.

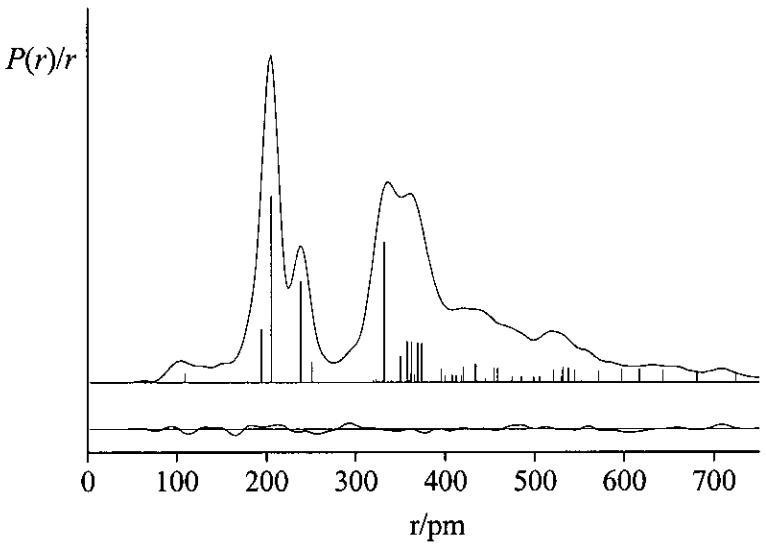

Figure 4 Experimental and final weighted difference (experimental - theoretical) molecular-scattering intensities for $Me_2Ge(SiCl_3)_2$.

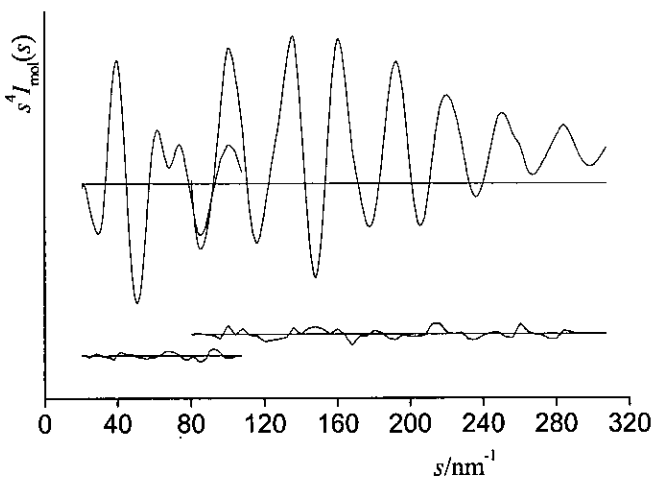

4.4 Discussion

4.4.1 Experimental Results. It can be seen from studying Table 3 that there is a discrepancy between the calculated and experimental structures. The major difference between the calculated and observed structure is in the torsion angle Cl(12)-Si(10)-Ge(1)-C(2). The results from the *ab initio* calculations suggest the $SiCl_3$ groups eclipse one another when viewed along the Si···Si axis, whereas the GED results suggest a 60° increase in the Cl(12)-Si(10)-Ge(1)-C(2) torsion angle, resulting the two $SiCl_3$ groups being in a staggered conformation with respect to one another (see Figure 2).

It is interesting to note that the calculations suggested that the structure returned by the GED experiment exists as a stationary point on the potential energy surface, but it does not represent a minimum. An *ab initio* conformational analysis was carried out at the HF/6-31G* level on $Me_2Ge(SiCl_3)_2$ by varying the Cl-Si-Ge-C torsion angle from 0.0 to 180.0° in steps of 10°. The result from this calculation can be seen in Figure 6, and implies that the observed structure found in the GED experiment is not a minimum on the potential energy surface.

It is interesting to note that the maximum shown with a Cl-Si-Ge-C torsion angle of 120.0° is only 4.1 kJ mol^{-1} higher in energy than the predicted global minimum with a torsion angle of 60.0°. The minimum found at Cl-Si-Ge-C = 120° is the same structure as that with a torsion angle of 60.0°. Therefore, it is possible that the $SiCl_3$ group is freely rotating and the structure returned by the GED study represents the average structure. This is corroborated by the low vibrational frequencies found in the *ab initio* calculations.

Figure 5 One-dimensional *ab initio* energy plot (HF/6-31G*) for variation of the Cl(12)-Si(10)-Ge(2)-C(1) dihedral angle in $Me_2Ge(SiCl_3)_2$.

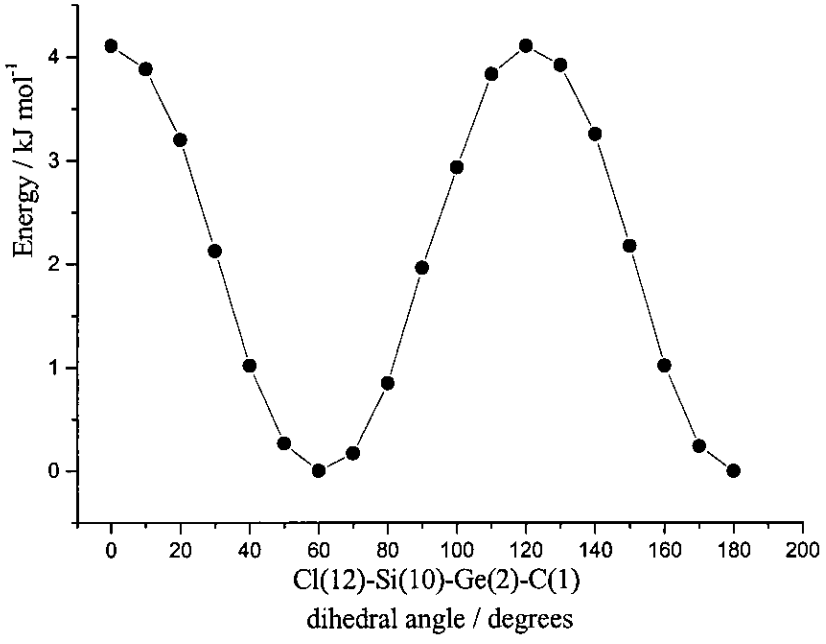

The torsion for the $Si(10)Cl_3$ group was not the only parameter to disagree with the *ab initio* predicted structure, although other deviations were less dramatic. For example, the values obtained for the Si-Cl and Ge-C distances (expressed in terms of an average and difference for the refinement) are both quite different from the calculated values, the Si-Cl distance being found to be 1 pm longer and the Ge-C distance 1.8 pm shorter than the calculated values. However, the other distance parameters (Ge-Si and C-H) are both in good agreement with the calculated values.

The values obtained from the GED refinement for the angles are, in general, also in good agreement with the *ab initio* results. The Si-Ge-Si angle is, perhaps, the exception to this as it differs from the calculated value by 3.4°. However, this angle will be directly affected by the orientation of the $SiCl_3$ groups relative to one another and, as discussed above, these were found to be quite different in the GED structure as compared to the *ab initio* structure.

4.3.2 Comparison with similar molecules. The structure of a related compound, $Me_3GeSiCl_3$, has already been determined by GED by Dr. Sarah Hinchley of the University of Edinburgh. In this case, the structure predicted by *ab initio* calculations was found to agree very well with that determined experimentally. Table 6 shows selected geometric parameters for both $Me_3GeSiCl_3$ and $Me_2Ge(SiCl_3)_2$ to allow a comparison of the GED and *ab initio* results obtained. Figure 6 gives an simple illustration of the difference in orientation between the predicted and experiment structure of $Me_2Ge(SiCl_3)_2$ and $Me_3GeSiCl_3$.

Figure 6 Molecular structure of (a) $Me_2Ge(SiCl_3)_2$ (MP2/6-311+G*), (b) $Me_2Ge(SiCl_3)_2$ (GED) and (c) $Me_3GeSiCl_3$ (GED)

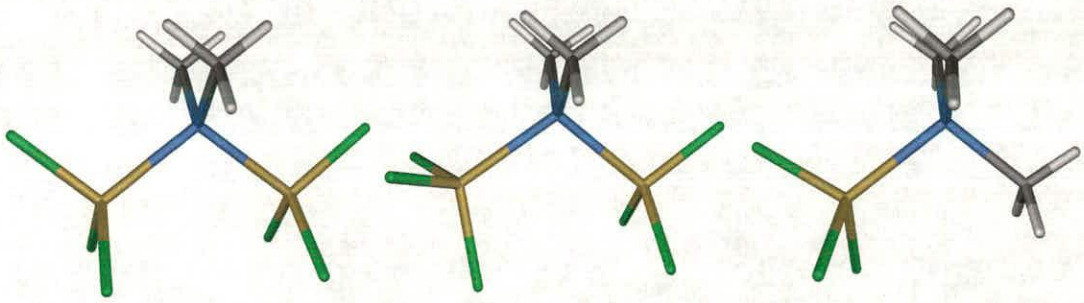

(a) (b) (c)

Table 6 Refined (r_{h1} structure) and calculated (MP2/6-311+G*) geometric parameters for $Me_2Ge(SiCl_3)_2$ and $Me_3GeSiCl_3$ (distances in pm and angles in °).

	$Me_2SiGe(SiCl_3)_2$		$Me_3GeSiCl_3$	
	ab initio	GED	*ab initio*	GED
*r*GeSi	238.2	238.1(3)	238.8	239.3(3)
*r*SiCl	204.5	205.5(1)	205.3	208.7(1)
*r*GeC	196.2	194.0(9)	196.2	196.8(2)
∠ GeSiCl	110.5	111.1(1)	111.4	114.5(1)
ϕCl(12)Si(10)Ge(1)C(2)	61.7	115.8(20)	60.0	43.5(18)

Comparing the two GED refined structures for $Me_3GeSiCl_3$ and $Me_2Ge(SiCl_3)_2$ it is possible to see some notable differences. The Si-Cl distance is 3.2 pm larger in $Me_3GeSiCl_3$ than in $Me_2Ge(SiCl_3)_2$. This difference is mirrored in the *ab initio* predicted Si-Cl distance (MP2/6-311+G*), although it is not so large [rSiCl is 0.8 pm longer in $Me_3GeSiCl_3$ than $Me_2Ge(SiCl_3)_2$]. Steric hindrance can account for the difference in the ∠GeSiCl angle, which is, as expected, larger in $Me_3GeSiCl_3$ than in $Me_2Ge(SiCl_3)_2$ [114.5(1) and 111.1(1)° respectively].

Looking at the variation of the torsions for the $SiCl_3$ groups (ϕCl-Si-Ge-C) between the compounds, in $Me_3GeSiCl_3$ the $SiCl_3$ group deviates from the calculated value of 60.0° to 43.5(18)°. However, in $Me_2Ge(SiCl_3)_2$ one of the two $SiCl_3$ torsions, as discussed previously, remains approximately 60.0° while the other twists round 115.8(20)° so the two $SiCl_3$ groups no longer eclipse one another.

The Ge-Si bond length in H_3GeSiH_3 was found to be 236.4(1) pm,[18] 2.9 pm shorter than in $Me_3GeSiCl_3$. This can be attributed to the effect of the addition of electronegative chlorine atoms. These draw electron density away from the silicon atom, allowing the Si-Ge bond length to increase. A similar lengthening is observed in $Me_2Ge(SiCl_3)_2$, where the Ge-Si bond length is 1.7 pm longer than the same bond length in H_3GeSiH_3.

4.5 Conclusion

From the experimental determination of the structure of $Me_2Ge(SiCl_3)_2$ it is possible to see that high level *ab initio* calculations are still not always correct when predicting the global minimum molecular structure. It is also important to notice that, although the calculations correctly predicted the structure of $Me_3GeSiCl_3$, it does not automatically follow that all compounds in the series will be correctly predicted. However, in this case it would be worthwhile for another refinement of the gas-phase data to be carried out modelling freely rotating $SiCl_3$ groups.

4.6 References

1. Hinchley, S. L.; Robertson, Rankin, D. W. H.; du Mont, W. W. *J. Chem. Soc. Dalton Trans.*, 2002, **124**, *8078*.

2. Gaussian 98 (Revision A.7), Frisch, M. J.; Trucks, G. W.; Schlegel, H. B.; Scuseria, G. E.; Robb, M. A.; Cheeseman, J. R.; Zakrzewski, V. G.; Montgomery, J. A.; Stratman, R. E.; Burant, J. C.; Dapprich, S.; Milliam, J. M; Daniels, A. D.; Kudin, K. N.; Strain, M. C.; Farkas, O.; Tomasi, J.; Barone, V.; Cossi, M.; Cammi, R.; Mennucci, B.; Pomelli, C.; Adamo, C.; Clifford, S.; Ochterski, J.; Petersson, G. A.; Ayala, P.Y.; Cui, Q.; Morokuma, K.; Malick, D. K.; Rabuck, A. D.; Raghavachari, K.; Foresman, J. B.; Cioslowski, J.; Ortiz, J. V.; Baboul, A. G.; Stefanov, B. B.; Liu, C.; Liashenko, A.; Piskorz, P.; Komaromi, I.; Gomperts, R.; Martin, R. L.; Fox, D. J.; Keith, T.; Al-Laham, M. A.; Peng, C. Y.; Nanayakkara, A.; Gonzalez, C.; Challacombe, M.; Gill, P. M. W.; Johnson, B. G.; Chen, W.; Wong, M. W.; Andres, J. L.; Gonzales, C.; Head-Gordon, M.; Replogle, E. S.; Pople, J. A. Gaussian, Inc., Pittsburgh PA, **1998**.

3. J. S. Binkley, J. A. Pople and W. J. Hehre, *J. Am. Chem. Soc.*, 1980, **102**, 939.

4. Gordon, M. S.; Binkley, J. S.; Pople, J. A.; Pietro W. J.; Hehre, W. J. *J. Am. Chem. Soc.*, 1982, **104**, 2797.

5. Pietro, W. J.; Francl, M. M.; Hehre, W. J.; DeFrees, D. J.; Pople, J. A.; Binkley, J. S. *J. Am. Chem. Soc.*, 1982, **104**, 5039.

6. Hehre, W. J.; Ditchfield R.; Pople, J. A. *J. Chem. Phys.*, 1972, **56**, 2257.

7. Hariharan, P. C.; Pople, J. A. *Theor. Chim. Acta*, 1973, **28**, 213.

8. Gordon, M. S. *Chem. Phys. Lett.*, 1980, **76**, 163.

9. McLean, A. D.; Chandler, G. S. *J. Chem. Phys.*, 1980, **72**, 5639.

10. Krishnan, R; Binkley, J. S.; Seeger, R.; Pople, J. A. J. Chem. Phys.,1980, **72**, 650.

11. Huntley, C. M.; Laurenson, G. S.; Rankin, D. W. H. *J. Chem. Soc., Dalton Trans.*, 1980, 954.

12. Lewis, J. R.; Brain, P. T.; Rankin, D. W. H. *Spectrum*, 1997, **15**, 7.

13. Cradock, S.; Koprowski, J.; Rankin, D. W.H. *J. Mol. Struct.*, 1981, **77**, 113.

14. Boyd, A. S. F.; Laurenson G. S.; Rankin, D. W. H. *J. Mol. Struct.,* 1981, **71**, 217.

15. Ross, A W.; Fink, M.; Hilderbrandt, R. *International Tables for Crystallography*, Ed. A. J. C. Wilson, Kluwer Academic Publishers, Dordrecht, Boston and London, 1992; Vol. C, p 245.

16. Sipachev, V. A. *J. Mol. Struc. (Theochem)*, 1985, **121**, 143.

17. Mitzel, N. W.; Smart, B. A.; Blake, A. J.; Robertson, H. E.; Rankin, D. W. H. *J. Phys. Chem.* 1996, **100**, 9339; Blake, A. J.; Brain, P. T.; McNab, H.; Miller, H. Morrison, C. A.; Parsons, S.; Rankin, D. W. H.; Robertson, H. E.; Smart, B. A. *J. Phys. Chem.,* 1996, **100**, 12280.

18. Oberhammer, H.; Lobreyer, T.; Sundermeyer, W. *J. Mol. Struc.,* 1994, **323**, 125.

CHAPTER FIVE

Strong intramolecular interactions in trifluorosilylhydrazines? The molecular structures of $F_3SiN(Me)NMe_2$ and $F_3SiN(SiMe_3)NMe_2$ by gas-phase electron diffraction and *ab initio* molecular orbital calculations

5.1 Introduction

The simplest compound that exists with an oxygen linker atom is water. In this case, the H-O-H angle is 104.5°. If the hydrogen atoms are replaced by silyl groups, the angle at the oxygen widens considerably. For example, $O(SiH_3)_2$ has a large Si-O-Si angle (144°)[2] as compared with a much smaller C-O-C angle in $O(CH_3)_2$ (111.4°).[3] The C-O-Si angle in H_3COSiH_3 (120.1°)[4] is also noticeably wider than $O(CH_3)_2$. It might be therefore expected that all silicon substituted oxygen atoms have wide bond angles.

The simplest isolable compounds containing an Si-O-N linkage, $H_3SiONMe_2$ and $H_2Si(ONMe_2)_2$, were studied by Prof Mitzel of the Westfälische Wilhelms-Universität in Münster. However, these compounds were found to have unusually narrow Si-O-N angles compared to their Si-O-C analogues. The Si-O-N angle in $H_3SiONMe_2$ was found to be 102.63(5)°, compared to the Si-N-C angle in $H_3SiCHNMe_2$ of 118.4(1)°.[5] The crystal structure of $H_2Si(ONMe_2)_2$ was found to have Si-O-N angles of 94.2(1) and 96.2(1)° (see Figure 1).[6]

Figure 1 Molecular structure of $H_2Si(ONMe_2)_2$.

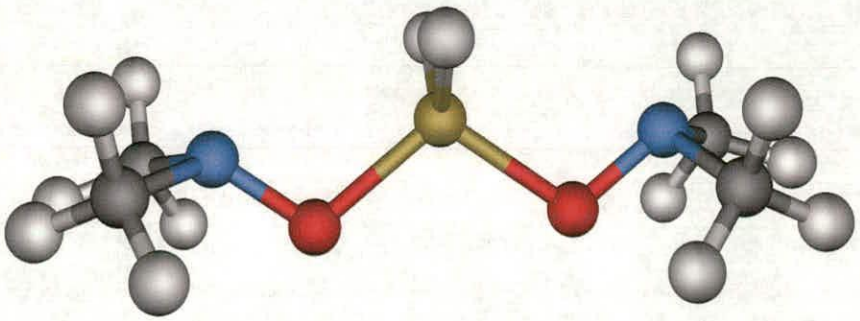

$H_2Si(ONMe_2)_2$ appears to adopt a geometry that supports some sort of interaction between the Si and β-N atoms (see Figure 2). In the case of the hydroxylaminosilanes, the spacer atom is oxygen. The study of this series of compounds was extended to consider if the unusual geometry remained if a different spacer atom was used.

Figure 2 Illustration of interaction indicated by the unusual molecular structures of hydroxylaminosilanes.

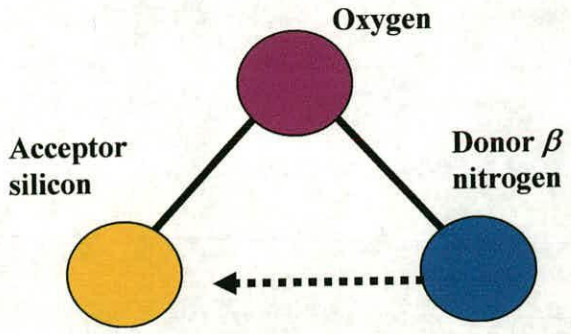

Therefore, instead of an oxygen spacer atom, another nitrogen was included. Examples of the first two compounds studied by Prof. Mitzel were include $SiH_3N(Me)NMe_2$ and $(SiH_3)_2NNMe_2$. These compounds did indeed show the narrow Si-N-N angles with angles of 108.2(1) and 106.0(2)°[7] respectively, although the angles are rather wider than the observed SiON angles..

It was also found that varying the substituents on the silicon, spacer and nitrogen atoms affected the strength of the interaction. Calculations were carried out to investigate this effect further. It was found that in $SiH_3N(R)NMe_2$, changing R from H to Me to SiH_3 resulted in a reduction of ∠NNSi (114.7, 109.1, 104.0° respectively).[7] If R is SiH_3, the smaller electron-withdrawing ability of silicon allows the electron density in the Si-N bond to get closer to the nitrogen atom than would be the case if R = CH_3. This encourages larger ∠SiNN and ∠SiNSi (in $SiH_3N(SiH_3)NMe_2$) than the corresponding ∠CNN and ∠CNSi (in $SiH_3N(CH_3)NMe_2$) which, in turn, promotes smaller ∠NNSi in $SiH_3N(SiH_3)NMe_2$.

In $RN(Me)NMe_2$, varying R from SiH_3 to SiH_2F was found to reduce the ∠SiNN from 109.1 to 103.1° and in $RN(SiH_3)NMe_2$, varying R from SiH_3 to SiH_2F reduces ∠SiNN from 104.0 to 93.9°. This was attributed to the greater electronegativity of the fluorine

Figure 3 The molecular structure of $F_3SiN(Me)NMe_2$ (**1**) showing the atomic numbering.

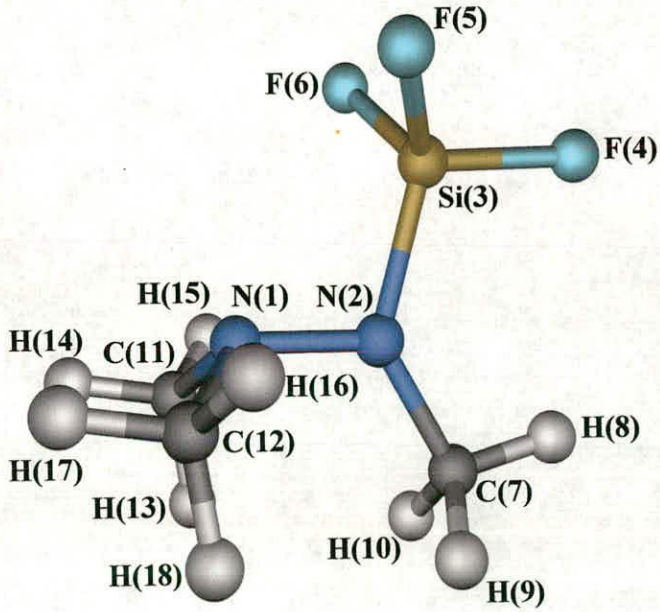

Figure 4 The molecular structure of $Me_2NN(SiF_3)SiMe_3$ showing the atomic numbering.

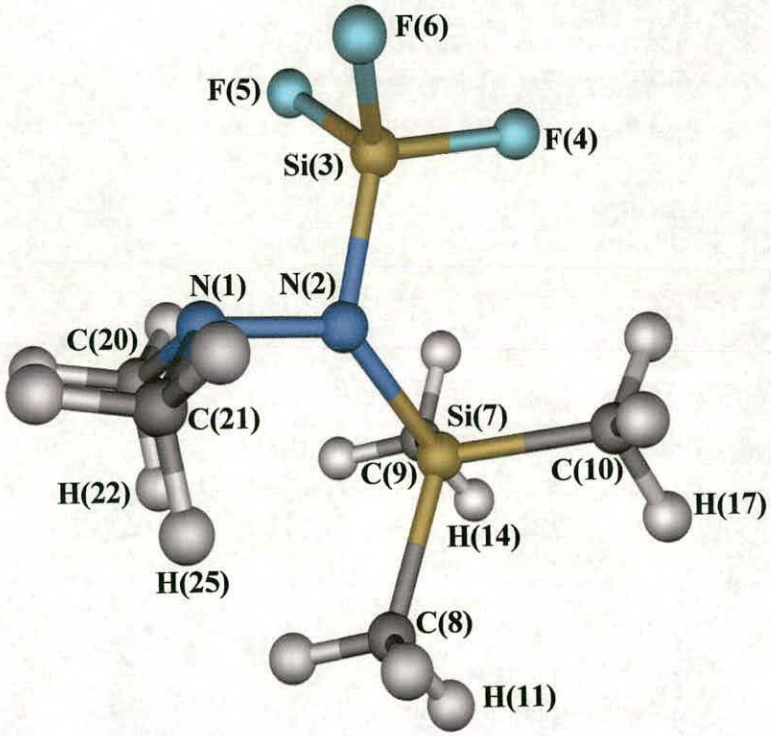

atom increasing the electrophilicity of the acceptor silicon and encouraging a smaller ∠SiNN. In this case, where there are two silicon atoms, the donor-acceptor interaction always takes place between the silicon with more electronegative substituents.

This chapter is concerned with the structures of two compounds in this series, $F_3SiN(Me)NMe_2$ and $F_3SiN(SiMe_3)NMe_2$. These compounds are of interest, as the electronegative effect of three fluorine atoms as opposed to one substituted on the acceptor silicon may prove to be very significant. Also, a possible steric effect may be investigated in $F_3SiN(SiMe_3)NMe_2$.

5.2 Experimental

5.2.1 Synthesis. Samples of $F_3SiN(Me)NMe_2$ (**1**) and $SiF_3N(SiMe_3)NMe_2$ (**2**) were prepared by Krunoslav Vojinović of the Institut für Anorganische und Analytische Chemie, Westfälische Wilhelms-Universität in Münster[8] and no further purification was required prior to the electron diffraction experiment.

5.2.2 Computational studies. All calculations were performed on a Dec Alpha 1000A workstation using the Gaussian 98 program.[9] A search of the torsional potentials of the compound at the HF level of theory using the 3-21G* [10-12] basis set resulted in the location of only one conformer for each of the compounds. Further optimisations were then carried out at HF and MP2(fc) levels of theory using the standard 6-31G* and 6-311G*[13-16] basis sets. Analytical second derivatives of the energies with respect to nuclear coordinates at the HF/6-31G* level gave the force fields, which were then used, without scaling, to provide estimates of the amplitudes of vibration (u) for use in the gas-phase electron diffraction (GED) refinements. Frequency calculations confirmed that the stationary points were minima on their respective potential energy surface. The structures of **1** and **2**, with numbering schemes, are shown in Figures 3 and 4. Cartesian coordinates for the structures of **1** and **2** are given in Appendix D.

5.2.3 Gas-phase electron diffraction experiments. The Edinburgh gas-diffraction apparatus[17] was used to collect data for both compounds. The sample and nozzle temperatures were held at 239 and 293 K respectively for **1** and 273 and 293 K respectively for **2**. An accelerating voltage of 40 kV (electron wavelength *ca.* 6.0 pm) was used and the scattering intensities were recorded at nozzle-to-plate distances of 128.2 and 285.2 mm for **1** and 127.7 and 285.4 mm for **2** on Kodak Electron Image film. Three films were collected at each nozzle-to-plate distance. The weighting points for the off-diagonal weight matrices, correlation parameters and scale factors for the two camera distances for both compounds are given in Table 1. For calibration, to minimise any systematic errors in wavelength and camera distances, the scattering patterns of benzene were also collected and analysed in the same way. The electron-scattering patterns were converted into digital form with a scanning program described elsewhere[18] using a PDS densitometer at the Institute of Astronomy, Cambridge, UK. Data reduction and least-squares refinements were carried out using standard programs[19,20] employing the scattering factors of Ross *et al.*[21]

Table 1 GED experimental conditions for $F_3SiN(Me)NMe_2$(**1**) and $F_3SiN(SiMe_3)NMe_2$ (**2**).

Compound	**1**		**2**	
camera distance / mm	128.18	285.15	127.66	285.38
Δs / nm^{-1}	4	2	4	2
s_{min} / nm^{-1}	100	40	108	40
s_1 / nm^{-1}	120	60	128	60
s_2 / nm^{-1}	272	110	256	102
s_{max} / nm^{-1}	320	130	300	120
correlation parameter	-0.2800	0.2707	-0.2322	0.1397
scale factor	0.696(5)	0.754(1)	0.714(19)	0.868(8)
electron wavelength / pm	6.016	6.016	6.016	6.016

5.3 Results

5.3.1 Computational studies. A search of the potential energy surfaces of $F_3SiN(Me)NMe_2$(**1**) and $F_3SiN(SiMe_3)NMe_2$ (**2**) showed only one minimum for each compound. Partial geometries from the four highest level calculations for **1** and **2** are given in Tables 2 and 3. From these results it is possible to see that both bond lengths and angles of both molecules are quite sensitive to both basis set and level of theory. For example, looking at ∠N(1)N(2)Si(3), an angle very important to this study, the value changes from 109.2 to 105.6° in **1** simply with the inclusion of electron correlation. A similar occurrence is seen in **2** with the same angle changing from 99.4 to 92.8°, again with the inclusion of electron correlation via the MP2 method.

For **1**, using MP2/6-311+G**, basis set convergence appears to have been achieved. The bond lengths can be seen to change little between MP2/6-31G* and MP2/6-311+G**. There is still a slight variation in the values obtained for the angles around the central N(2) atom at the MP2 level when the basis set size is increased and extra functions are added. However, this was predictable due to the unusual electronic nature of the system studied. The calculations also reveal large differences between the angles for atoms lying in the approximate N-N-Si-C plane and those out of it. For example, there is a 5.2° difference between the values calculated at MP2/6-311+G** for ∠N(2)Si(3)F(4) and ∠N(2)Si(3)F(5/6) (108.8 and 114.0° respectively). In order to reflect this deviation from local C_{3v} symmetry, it is important that these differences are included in the model for the refinement of the gas-phase data.

Table 2 Calculated and geometric parameters (r_e structure) for the structure of $F_3SiN(Me)NMe_2$ (**1**) (distances in pm, angles in °).[a]

	Level of theory / Basis set			
Parameters	HF/ 6-31G*	MP2/ 6-31G*	MP2/ 6-311G*	MP2/ 6-311+G**
N(1)-N(2)	140.9	142.9	142.6	142.6
N(1)-C(11/12)	144.4	146.0	146.0	146.1
N(2)-Si(3)	167.4	168.3	167.7	168.1
Si(3)-F(4)	157.5	160.2	159.8	160.1
Si(3)-F(5)	157.3	159.9	159.5	159.8
N(2)-C(7)	144.9	145.4	145.4	145.6
N(2)-N(1)-C(11/12)	113.2	111.7	111.8	111.8
N(1)-N(2)-Si(3)	109.2	105.6	105.5	106.4
N(1)-N(2)-C(7)	120.9	121.9	121.5	121.1
N(2)-Si(3)-F(4)	108.7	107.9	108.5	108.8
N(2)-Si(3)-F(5/6)	113.6	113.8	114.0	114.0
N(2)-C(7)-H(8)	108.3	107.1	107.6	107.8
N(2)-C(7)-H(9/10)	111.8	111.9	111.8	111.7
N(1)-C(11)-H(13)	110.4	110.0	110.0	110.0
N(1)-N(2)-Si(3)-F(4)	180.0	180.0	180.0	180.0
N(1)-N(2)-C(7)-H(9)	-61.0	-61.3	-61.4	-61.3
N(2)-N(1)-C(12)-H(16)	-70.3	-67.7	-68.9	-68.8
Total Energy[b]	-815.0127	-816.3347	-816.6166	-816.7080

[a] See Figure 3 for atom numbering.

[b] Energy in Hartrees and zero-point energy correction applied.

Table 3 Calculated and geometric parameters (r_e structure) for the structure of $Me_2NN(SiF_3)SiMe_3$ (distances in pm, angles in °).[a]

	Level of theory / Basis set			
Parameters	HF/ 6-31G*	MP2/ 6-31G*	MP2/ 6-311G*	MP2/ 6-311+G**
N(1)-N(2)	143.9	146.6	146.2	146.2
N(1)-C(20)	144.7	145.9	145.8	145.9
N(2)-Si(3)	168.3	169.4	168.8	169.0
N(2)-Si(7)	177.7	178.1	177.5	177.9
Si(3)-F(4)	157.9	160.9	160.5	160.7
Si(7)-C(8)	188.7	188.2	187.5	187.6
N(2)-N(1)-C(20)	113.6	112.2	112.4	112.4
N(2)-N(1)-C(21)	113.5	111.5	111.9	111.8
N(1)-N(2)-Si(3)	99.4	92.8	92.2	93.9
N(1)-N(2)-Si(7)	128.1	129.6	128.9	128.2
Si(3)-N(2)-Si(7)	131.8	135.8	137.4	136.2
N(2)-Si(3)-F(4)	110.1	109.0	109.6	109.7
N(2)-Si(3)-F(5)	113.9	115.0	115.1	114.9
N(2)-Si(3)-F(6)	113.5	113.8	114.3	114.2
N(2)-Si(7)-C(8)	111.6	110.8	110.7	110.5
N(2)-Si(7)-C(9)	110.1	110.9	111.4	110.9
N(2)-Si(7)-C(10)	107.6	105.6	105.6	105.8
N(1)-N(2)-Si(3)-F(4)	-176.2	-176.9	-178.4	-178.4
N(1)-N(2)-Si(7)-C(8)	-29.9	-38.6	-42.5	-41.2
C(20)-N(1)-N(2)-Si(7)	-58.6	-52.0	-52.1	-50.9
C(21)-N(1)-N(2)-Si(7)	75.0	77.0	76.6	77.2
Total Energy[b]	-1183.1512	-1184.8200	-1184.1620	-1185.3015

[a] See Figure 4 for atom numbering.

[b] Energy in Hartrees and zero-point energy correction applied.

For **2**, again it appears that basis set convergence has been achieved with MP2/6-311+G**, with the same variations in the values calculated for the angles around the central nitrogen atom at the MP2 level with increasing basis set size. The calculations also reveal the lack of local C_{3v} symmetry within the SiF_3 and $SiMe_3$ groups. At the MP2/6-311+G** level, the N-Si-C angles are predicted to range by 5.1° (from 110.9 to 105.8°) and the N-Si-F angles vary by 5.2° (from 114.9 to 109.7°). Again, it is important that this asymmetry is modelled during the gas-phase refinement in order to ensure that the molecule is not forced to have higher symmetry or local symmetry than it should have.

Appreciable changes in the values calculated for the bond distances in both **1** and **2** were observed when the level of theory was improved from Hartree-Fock to MP2. The N-N distance changed from 140.9 to 142.9 pm in **1** and from 143.9 to 146.6 pm in **2** (HF/6-31G* to MP2/6-31G*). This shows the importance of including correlation for atoms with an electron dense nature (i.e. lone pairs) in order to obtain an accurate prediction of the molecules' geometry. In **1**, basis set convergence has been achieved for most of the bond distances, except the N-Si and Si-F distances, which still change by 0.4 and 0.3 pm respectively (MP2/6-311G* to MP2/6-311+G**). In **2**, the bond distances seem to have converged by the MP2/6-311+G** calculation, with little change in values between this and those calculated for the previous basis set. The largest difference is again in the N-Si distance, which changes by 0.4 pm from 177.5 to 177.9 pm from MP2/6-311G* to MP2/6-311+G**.

Of all the parameters, it is the torsions in **2** that undergo the largest change with variations in level of theory and basis set. The torsion N(1)-N(2)-Si(7)-C(8) can be seen to change by 11.3° from HF/6-31G* to MP2/6-311+G**. This is a large deviation but can be explained by the observation of the low-lying vibrational frequency of 25.9 cm^{-1} (HF/6-31G*), which involves a rotation of the $SiMe_3$ group around the N-Si bond. This high sensitivity of torsion angle to energy is difficult to model in *ab initio* calculations and can explain the variation in the calculated value for the torsion.

5.3.2 Electron diffraction analysis for $F_3SiN(Me)NMe_2$. This molecule presents a challenge in that so many of the bonded distances differ only slightly in value and yet involve heavy atoms. However, there should be enough information in the electron diffraction data to allow refinement of these parameters subject to flexible restraints, using the SARACEN method.[22] It was decided that the best approach was to express the bond distances with similar values in terms of an average value and the differences between them. This helps to overcome the problem of overlapping peaks in the radial distribution curve, as instead of attempting to refine several distances with similar values separately, it is possible to refine their average value with a higher certainty.

The model was written using C_s symmetry for the bond lengths and angles of the heavy-atom skeleton; however, allowing for torsional motions about all C-N and Si-N bonds lowers the overall symmetry to C_1. The structure was defined in terms of 22 independent geometric parameters. These comprised seven bond lengths and differences, eleven angles and four dihedral angles. The bonds lengths *r*NN and *r*NC were expressed in terms of the average of the NN and the average NC distances (p_1) and two difference parameters [*r*NN minus the average *r*NC (p_2) and *r*N(1)C(11/12) minus *r*N(2)C(7) (p_3)]. Also included were the CH distance (p_4) (all were assumed to be equal) and *r*NSi and *r*SiF, which were also expressed as average and difference terms [an average of the NSi and average SiF distances (p_5) and two difference parameters, *r*NSi minus the average SiF distances (p_6) and *r*Si(3)F(4) minus *r*Si(3)F(5/6) (p_7)]. The angles used were ∠N(2)N(1)C(11/12) (p_8), ∠C(11)N(1)C(12) (p_9), an average NCH angle for the two methyl groups attached to N(1) (p_{10}), ∠NNSi (p_{11}), ∠N(2)Si(3)F(4) (p_{12}), ∠N(2)Si(3)F(5/6) (p_{13}), ∠F(4)Si(3)F(5/6) (p_{14}), ∠SiNC (p_{15}), ∠N(2)C(7)H(8) (p_{16}), ∠N(2)C(7)H(9/10) (p_{17}) and ∠H(8)C(7)H(9/10) (p_{18}). The torsions are ϕC(7)-N(2)-N(1)-Si(3) (p_{19}), ϕN(1)-N(2)-C(7)-Si(3) (p_{20}), ϕN(1)-N(2)-Si(3)-C(7) (p_{21}) and ϕN(2)-N(1)-C(11)-Si(3) (p_{22}).

The starting values for the 22 geometric parameters used in the refinement were taken from the *ab initio* results (MP2/6-311+G**). The force field described by a set of symmetry coordinates was converted from the theoretical (HF/6-31G*) Cartesian force fields using the program ASYM40.[23] The model was refined as an r_a structure (i.e. without any perpendicular amplitude corrections). All 22 geometric parameters and eleven groups of amplitudes were refined. Thirteen geometric and two amplitude restraints were applied using the SARACEN method.[22]

The final refinement resulted in $R_G = 0.015$ (R_D=0.013) with very small discrepancies in the difference curves for the combined molecular scattering intensity (Figure 4) and radial distribution (Figure 5). Final refined parameters are listed in Table 4 and interatomic distances and the corresponding amplitudes of vibration in Table 5. The least-squares correlation matrix is given in Table 6.

Figure 4 Experimental and final weighted difference (experimental - theoretical) molecular-scattering intensities for $F_3SiN(Me)NMe_2$.

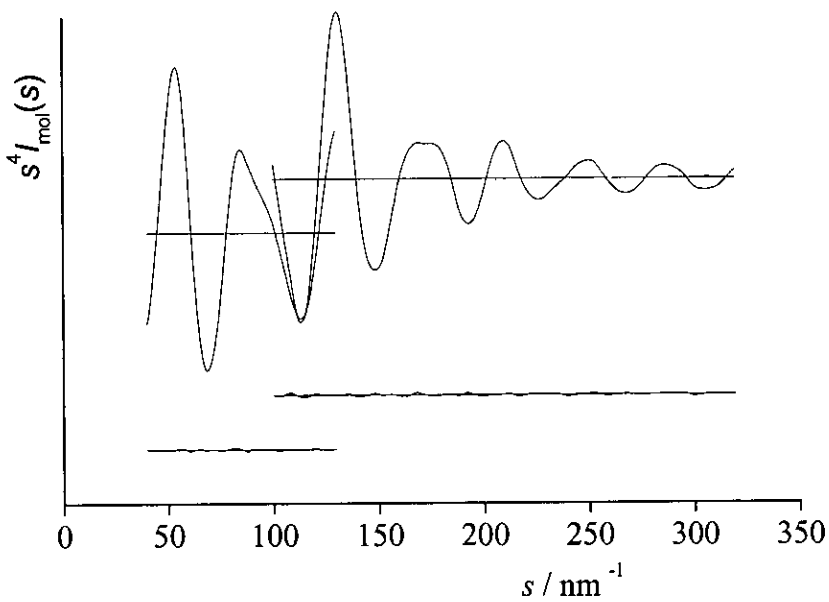

Figure 5 Experimental and difference (experimental - theoretical) radial-distribution curves, $P(r)/r$, for $F_3SiN(Me)NMe_2$. Before Fourier inversion the data were multiplied by $s.\exp(-0.00002s^2)/(Z_{Si}-f_{Si})/(Z_F-f_F)$.

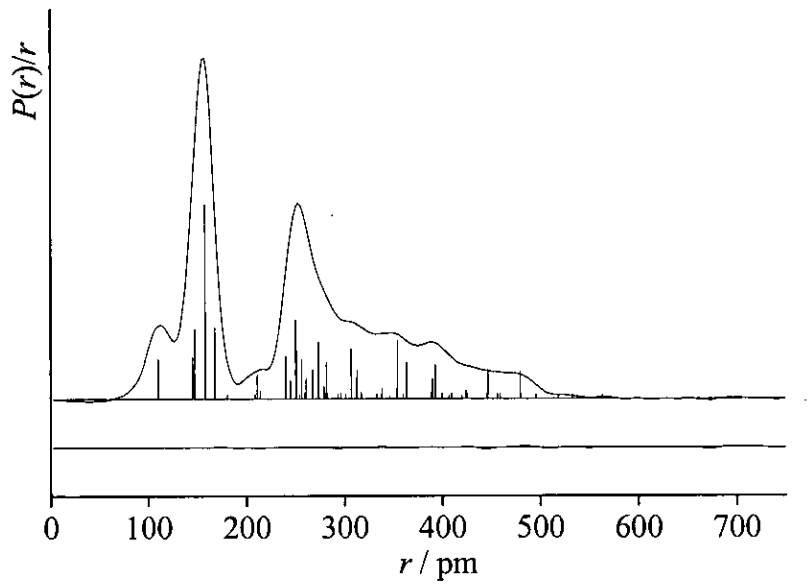

Table 4: Refined and calculated geometric parameters from the GED study of $F_3SiN(Me)NMe_2$ (**1**) (distances in pm, angles in °).[a,b]

	Independent Parameters	MP2/ 6-311+G** (r_e)	GED (r_a)	Restraint
p_1	av *r*NN *r*NC	144.9	145.0(5)	
p_2	*r*NN - av *r*NC	3.5	3.9(13)	3.5(10)
p_3	*r*N(1)C(11/12)-*r*N(1)C(7)	0.5	0.5(2)	0.5(2)
p_4	*r*CH	109.5	110.2(1)	109.5(10)
p_5	av *r*NSi *r*SiF	161.8	162.8(2)	
p_6	*r*NSi – av *r*SiF	8.2	9.7(3)	8.2(20)
p_7	*r*Si(3)F(4) – *r*Si(3)F(5/6)	0.3	0.3(1)	0.3(1)
p_8	∠N(2)N(1)C(11/12)	111.8	110.4(4)	

p_9	∠C(11)N(1)C(12)	112.2	112.3(10)	112.2(10)
p_{10}	av ∠N(1)CH	110.0	109.2(3)	110.0(5)
p_{11}	∠NNSi	106.4	106.5(4)	
p_{12}	∠N(2)Si(3)F(4)	108.8	110.4(3)	108.8(5)
p_{13}	∠N(2)Si(3)F(5/6)	114.0	114.0(2)	114.0(5)
p_{14}	∠F(4)SiF(5/6)	107.1	108.5(7)	
p_{15}	∠SiNC	132.5	126.9(7)	
p_{16}	∠N(2)C(7)H(8)	107.8	107.7(7)	107.8(7)
p_{17}	∠N(2)C(7)H(9/10)	111.7	111.8(3)	111.7(3)
p_{18}	∠H(8)C(7)H(9/10)	108.2	108.7(4)	108.2(4)
p_{19}	C(7)-N(2)-N(1)-Si(3)	0.0	-0.7(6)	
p_{20}	N(1)-N(2)-C(7)-Si(3)	0.0	-0.3(10)	0.1(10)
p_{21}	N(1)-N(2)-Si(3)-C(7)	0.0	-3.5(8)	
p_{22}	60° - N(2)-N(1)-C(11)-Si(3)	16.9	-17.1(30)	
	Dependent Parameters			
p_{23}	N(1)-N(2)	142.6	143.1(5)	
p_{24}	N(2)-C(7)	145.6	146.7(2)	
p_{25}	N(1)-C(11/12)	146.1	147.2(2)	
p_{26}	N(2)-Si(3)	168.1	167.7(3)	
p_{27}	Si(3)-F(4)	160.1	158.1(1)	
p_{28}	Si(3)-F(5/6)	159.8	157.8(1)	
p_{29}	Si(3)···N(1)	249.3	251.0(6)	
p_{30}	∠C(7)-N(1)-N(2)	121.1	126.6(8)	

[a] See Figure 3 for atom numbering.

[b] See text for description of the parameters.

Table 5: Interatomic distances (r_a/pm) and amplitudes of vibration (u/pm) for the restrained GED structure of $F_3SiN(Me)NMe_2$ (**1**).[a,b]

	Atom Pair	r_a / pm	u / pm	Restraint
u_1	F(5)-Si(3)	157.8(1)	3.7(2)	
u_2	F(4)-Si(3)	158.1(1)	3.7 (tied to u_1)	
u_3	F(5)···F(4)	250.0(6)	5.6(6)	6.2(6)
u_4	Si(3)-N(2)	167.7(3)	4.4(3)	4.1(4)
u_5	C(11)-N(1)	147.2(2)	4.2 (tied to u_{11})	
u_6	F(5)···N(2)	273.1(4)	11.0(6)	
u_7	C(11)···N(2)	354.2(5)	12.8(4)	
u_8	F(5)···N(1)	307.0(2)	16.2(4)	
u_9	Si(3)···N(1)	251.0(6)	6.4 (tied to u_3)	
u_{10}	C(11)···N(2)	239.9(6)	4.3(4)	
u_{11}	N(2)-N(1)	145.0(5)	4.0(2)	
u_{12}	H(13)-C(11)	110.2(1)	8.0(2)	
u_{13}	F(6)···F(5)	256.1(11)	4.7 (tied to u_{10})	
u_{14}	C(7)···Si(3)	281.4(9)	10.1 (tied to u_6)	
u_{15}	C(7)-N(2)	146.7(2)	4.2 (tied to u_{11})	
u_{16}	C(7)···F(5)	392.8(7)	14.3(4)	
u_{17}	C(11)···F(5)	363.3(12)	27.4 (tied to u_7)	
u_{18}	C(11)···C(7)	312.9(16)	13.6 (tied to u_8)	
u_{19}	C(11)···F(6)	446.5(7)	14.3(4)	
u_{20}	F(4)···N(2)	267.5(6)	5.6 (tied to u_3)	
u_{21}	C(11)···F(4)	479.5(6)	13.9 (tied to u_{19})	
u_{22}	H(13)···N(1)	210.9(4)	9.7 (fixed)	
u_{23}	C(7)···F(4)	312.4(16)	14.0 (tied to u_8)	
u_{24}	C(7)···N(1)	260.5(10)	5.2 (tied to u_3)	
u_{25}	F(4)···N(1)	390.0(7)	9.9 (tied to u_{16})	

[a] See Figure 3 for atom numbering.

[b] Other amplitudes were included and not refined but fixed at HF/6-31G* values.

Table 6 Least-squares correlation matrix (× 100) for $F_3SiN(Me)NMe_2$(**1**).[a]

	p_2	p_5	p_{14}	p_{18}	p_{19}	p_{20}	p_{21}	u_1	u_3	u_4	u_6	u_7	u_8	u_{10}	u_{11}	u_{19}	k_2
p_1	-98	-	-	-	-	-	-	-	-	-	-	-	-	-	-	-	-
p_5	-	-	-	-	-	-	-	-	-	-	-	50	-58	-	-	-55	-
p_{10}	-	-	94	-	-	-	-	-88	-	-63	-	-	-	-	-76	-	-
p_{11}	-	-	-	-	-54	-62	-	-	73	-	-	-	-	-	-	-	-
p_{12}	-	-78	-	-	-	-	-	-	-	-	-	-	-	-	-	-	-
p_{14}	-	-	-	-	-	-	-	-88	-	-79	-	-	-	-	-64	-	-
p_{16}	-	-	-	-56	-	-	-	-	-	-	-	-	-	-	-	-	-
p_{19}	-	-	-	-	-	59	67	-	-86	-	-61	-	-	-	-	-	-
p_{22}	-	-	-	-	-	-	-	-	-50	-	-	-50	-	-	-	-	-
p_{23}	-	-	-	-	-	-	-	-	-	-	-74	-	-	-	-	-	-
u_1	-	-	-	-	-	-	-	-	-	78	-	-	-	-	85	-	-
u_3	-	-	-	-	-	-	-	-	-	-	60	-	-	58	-	-	-
u_{12}	-	-	-	-	-	-	-	-	-	-	-	-	-	-	-	-	53

[a] Only elements with absolute values ≥50% are shown; k_2 is a scale factor.

5.3.3 Electron Diffraction Analysis for $F_3SiN(SiMe_3)NMe_2$. This is another example of a molecule that has a complicated refinement procedure due to the number of similar distances. The model was written in C_1 symmetry, assuming local C_{3v} symmetry for all methyl groups (in both the $SiMe_3$ and NMe_2 units) and treating all three methyl groups in the $SiMe_3$ group as equivalent. On the basis of the results from the *ab initio* calculations the three Si-F distances were treated as equivalent as they vary by only 0.7 pm. The three Si-C distances were also treated as equivalent as they differ by only 0.7 pm. With these assumptions 42 independent geometric parameters, consisting of seven bond lengths and differences, twelve bond angles and differences and 22 torsions, tilts and rocks were required to build a model of the compound. The bond lengths included were the average of the NN and average NC bond lengths (p_1) and the difference between them (rNN-rNC) (p_2), the average of the two SiN and the SiC distances (p_3), the difference between the average SiN and SiC distances (p_4) and the difference between the two SiN distances (p_5), an average rSiF (p_6) and rCH (p_7). The angles used were ∠N(2)N(1)C(21) (p_8), ∠N(2)N(1)C(20) (p_9) and an average ∠NCH (p_{10}). The NSiF angles were expressed in terms of the average of the three angles (p_{11}) and two differences, ∠N(2)Si(3)F(4) minus ∠N(2)Si(3)F(5) (p_{12}) and ∠N(2)Si(3)F(4) minus ∠N(2)Si(3)F(6) (p_{13}). Also included were ∠SiNSi (p_{14}), ∠N(1)N(2)Si(7) (p_{15}), ∠NSiC

[expressed in terms of an average of the three angles (p_{16}) and two difference parameters, ∠N(2)Si(7)C(8) minus ∠N(2)Si(7)C(9) (p_{17}) and ∠N(2)Si(7)C(10) (p_{18})] and the average ∠SiCH (p_{19}).

A large number of torsions, tilts and rocks were included in order to fully describe the motions of the large substituents. The motions of the methyl groups in $SiMe_3$ were described as a twist, tilt and rock about the local *x*, *y* and *z* axes respectively (p_{20-22}). The local *x*-axis was defined as the Si(7)-C bond, the *y*-axis as in the Si(7)-C(8/9/10)-H(11/14/17) plane and the *z*-axis, by definition, perpendicular to *x* and *y*. Two torsions were included to move two of the methyl groups out of the N-N-Si-C plane (p_{23-24}). A twist, rock and tilt of the $SiMe_3$ group around the local *x*, *y* and *z* axes were also included (p_{25-27}) [local *x*-axis defined as the N-Si(7) bond and the *y*-axis in the N-Si(7)-C(8) plane]. Two out of plane fluorine atoms were placed into position using two torsions along the N-Si bond (p_{28-29}) and a dip angle for the whole SiF_3 into the *xy* plane [defined as N(1)-N(2)-Si(3)] was included (p_{30}). A twist, rock and tilt of the SiF_3 group around the local *x*, *y* and *z* axes was also included (p_{31-33}) [local *x*-axis defined as along the N(2)-Si(3) bond and the *y*-axis in the N(2)-Si(3)-F(4) plane]. Similar torsions about the local *x*, *y* and *z* axes were also included separately for the two methyl groups attached to N(1) (p_{34-39}) [local *x*-axis defined as along the N(1)-C(20/21) bond and *y*-axis in the N(1)-C(20/21)-H(22/25) plane]. The two methyl groups were twisted into position using two separate torsions (p_{40-41}), and a general torsion for the NMe_2 group about the N-N bond was also included. (p_{42}).

The final refinement resulted in an $R_G = 0.025$ (R_D=0.025) with very small discrepancies in the difference curves for the combined molecular scattering intensity (Figure 6) and radial distribution (Figure 7). Final refined parameters are listed in Table 7 and interatomic distances and the corresponding amplitudes of vibration in Table 8. The least-squares correlation matrix is give in Table 9.

Figure 6 Experimental and final weighted difference (experimental - theoretical) molecular-scattering intensities for $F_3SiN(SiMe_3)NMe_2$.

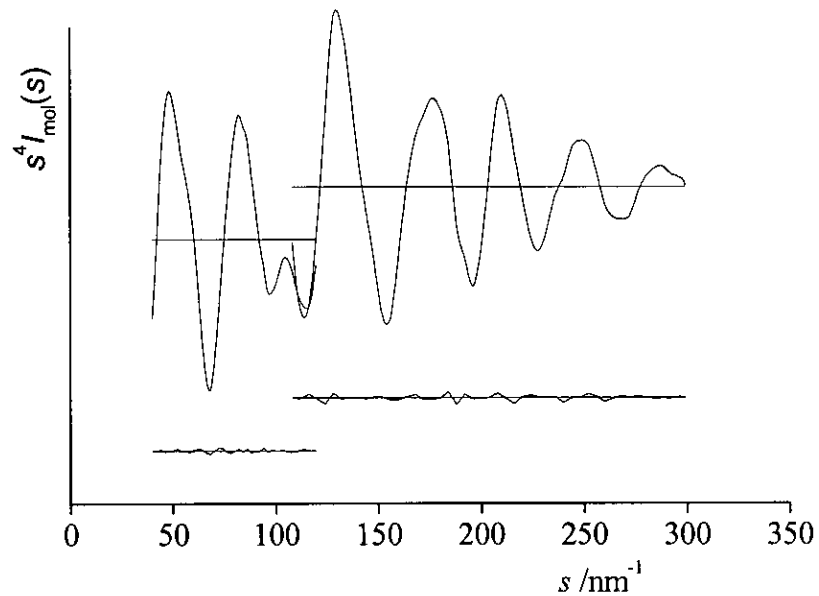

Figure 7 Experimental and difference (experimental - theoretical) radial-distribution curves, $P(r)/r$, for $F_3SiN(SiMe_3)NMe_2$. Before Fourier inversion the data were multiplied by $s.\exp(-0.00002s^2)/(Z_{Si}-f_{Si})/(Z_F-f_F)$.

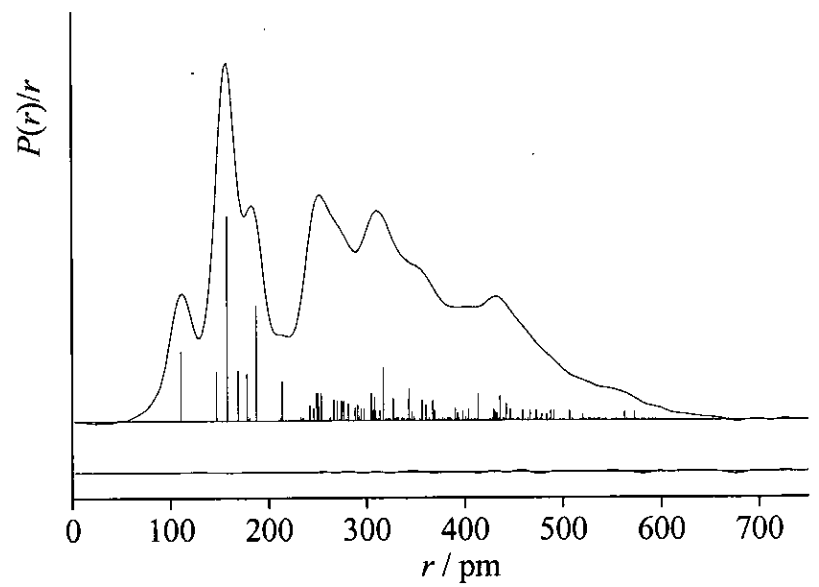

Table 7: Refined and calculated geometric parameters from the GED study of $F_3SiN(SiMe_3)NMe_2$ (**2**) (distances in pm, angles in °).[a,b]

	Independent Parameters	MP2/ 6-311+G** (r_e)	GED (r_a)	Restraint
p_1	av *r*NN *r*NC	146.0	146.3(3)	146.0(20)
p_2	*r*NN - *r*NC	0.3	0.0(5)	0.3(5)
p_3	av *r*SiN *r*SiC	181.8	177.7(2)	
p_4	av *r*SiN – *r*SiC	14.0	14.3(3)	14.0(10)
p_5	*r*Si(7)N(2) – *r*Si(3)N(2)	9.8	7.9(9)	9.8(10)
p_6	*r*SiF	160.3	157.4(1)	
p_7	*r*CH	109.5	110.7(1)	109.5(20)
p_8	∠N(2)N(1)C(21)	111.8	111.3(6)	111.8(5)
p_9	∠N(2)N(1)C(20)	112.4	111.1(6)	112.4(5)
p_{10}	av ∠NCH	109.8	109.9(6)	109.8(5)
p_{11}	av ∠NSiF	112.9	112.4(2)	
p_{12}	∠N(2)Si(7)F(4) - ∠N(2)Si(7)F(5)	-5.2	-5.3(6)	-5.2(5)
p_{13}	∠N(2)Si(7)F(4) - ∠N(2)Si(7)F(6)	-4.5	-5.3(6)	-4.5(5)
p_{14}	∠SiNSi	136.2	132.6(5)	
p_{15}	∠N(1)N(2)Si(7)	128.2	140.3(7)	
p_{16}	av ∠NSiC	109.1	107.0(3)	109.1(5)
p_{17}	∠N(2)Si(7)C(8) - ∠N(2)Si(7)C(9)	0.4	0.4(1)	0.4(1)
p_{18}	∠N(2)Si(7)C(8) - ∠N(2)Si(7)C(10)	5.1	5.1(1)	5.1(1)
p_{19}	av ∠SiCH	111.1	111.8(6)	111.1(5)
p_{20}	ϕH(17)-C(10)-Si(7)-N(2)	177.5	180.1(26)	177.5(25)
p_{21}	methyl tilt	-	-0.8(13)	0.1(10)
p_{22}	methyl rock	-	0.0(13)	0.1(10)
p_{23}	C(10)-Si(7)-N(2)-C(8)	-121.9	-121.5(7)	-121.9(5)
p_{24}	C(10)-Si(7)-N(2)-C(9)	118.7	118.8(7)	118.7(5)
p_{25}	N(1)-N(2)-Si(7)-C(10)	-29.5	-23.7(20)	

p_{26}	tilt $SiMe_3$	-	1.0(8)	0.1(10)
p_{27}	rock $SiMe_3$	-	-0.3(6)	0.1(10)
p_{28}	F(4)-Si(3)-N(2)-F(5)	-116.4	-117.6(6)	-116.4(5)
p_{29}	F(4)-Si(3)-N(2)-F(6)	-118.4	118.4(7)	-118.4(5)
p_{30}	N(1)-N(2)-Si(7)-Si(3)	-	-23.1(26)	
p_{31}	Si(7)-N(2)-Si(3)-F(4)	13.3	14.2(6)	13.3(5)
p_{32}	SiF_3 tilt	-	0.6(5)	0.1(5)
p_{33}	SiF_3 rock	-	-1.9(5)	0.1(5)
p_{34}	$C(20)H_3$ tilt	-	0.1(fixed)	
p_{35}	$C(20)H_3$ rock	-	0.1(fixed)	
p_{36}	60 - N(2)-N(1)-C(20)-H(22)	7.9	7.9(fixed)	
p_{37}	$C(21)H_3$ tilt	-	0.1(fixed)	
p_{38}	$C(21)H_3$ rock	-	0.1(fixed)	
p_{39}	60 - N(2)-N(1)-C(21)-H(25)	-7.9	-7.9(fixed)	-
p_{40}	C(21)-N(1)-N(2)-Si(7)	77.2	77.2(7)	77.2(5)
p_{41}	C(20)-N(1)-N(2)-Si(7)	-50.9	-51.3(13)	
p_{42}	Si(7)-N(1)-N(2)-C(20)	-20.3	-21.7(18)	
	Dependent Parameters			
p_{43}	N(2)-Si(3)	169.0	169.0(6)	
p_{44}	N(2)-Si(7)	177.9	176.9(6)	
p_{45}	Si(7)-C(9/10/11)	187.6	187.3(1)	
p_{46}	∠N(1)N(2)Si(3)	93.9	84.9(4)	
p_{47}	N(1)-N(2)	146.2	146.3(3)	
p_{48}	N(2)-C(20)	145.9	146.3(3)	
p_{49}	∠N(2)Si(3)F(4)	109.7	109.0(5)	
p_{50}	∠N(2)Si(3)F(5)	114.9	113.9(5)	
p_{51}	∠N(2)Si(3)F(6)	114.2	116.0(6)	
p_{52}	∠N(2)Si(7)C(8)	110.5	107.4(8)	
p_{53}	∠N(2)Si(7)C(9)	110.9	109.1(9)	

p_{54}	∠N(2)Si(7)C(10)	105.8	104.4(6)
p_{55}	∠C(20)N(1)C(21)	112.8	114.1(9)
p_{56}	N(1)···Si(3)	230.8	213.5(9)

[a] See Figure 4 for atom numbering.

[b] See text for description of the parameters.

Table 8: Interatomic distances (r_a/pm) and amplitudes of vibration (u/pm) for the restrained GED structure of $F_3SiN(SiMe_3)NMe_2$.

	Atom Pair	r_a / pm	u / pm	restraint
u_1	F(4)-Si(3)	157.4(1)	3.6(3)	3.9(4)
u_2	C(8)-Si(7)	187.3(1)	4.9(3)	5.1(5)
u_3	H(11)-C(8)	110.7(1)	7.2(2)	
u_4	Si(7)···Si(3)	316.8(6)	8.9(5)	7.5(7)
u_5	Si(3)-N(2)	169.0(5)	3.8(tied to u_1)	
u_6	C(20)-N(1)	146.3(3)	4.3(4)	4.6(4)
u_7	Si(7)-N(2)	177.0(6)	4.6(tied to u_2)	
u_8	Si(3)···N(1)	213.5(9)	10.7(5)	9.4(9)
u_9	Si(7)···F(4)	342.1(18)	16.2(fixed)	
u_{10}	Si(7)···N(1)	304.2(7)	6.9(fixed)	
u_{11}	N(2)···N(1)	146.3(3)	4.3(tied to u_6)	
u_{12}	F(5)···F(4)	249.1(10)	8.1(4)	
u_{13}	F(6)···F(4)	250.0(10)	8.1(tied to u_{12})	
u_{14}	F(6)···F(5)	253.7(12)	8.1(tied to u_{12})	
u_{15}	Si(7)···F(5)	412.5(11)	12.3(fixed)	
u_{16}	Si(7)···F(6)	435.4(11)	11.9(fixed)	
u_{17}	C(20)···Si(7)	355.7(41)	15.6(12)	12.8(12)
u_{18}	C(21)···Si(3)	326.5(73)	15.5(tied to u_{17})	
u_{19}	C(20)···Si(3)	308.0(93)	14.4(tied to u_{17})	
u_{20}	C(21)···Si(7)	367.0(46)	12.7(tied to u_{17})	

u_{21}	F(4)···N(2)	265.8(9)	7.1(6)
u_{22}	C(10)···Si(3)	342.5(21)	14.2(fixed)
u_{23}	F(6)···N(2)	276.8(9)	6.9(tied to u_{21})
u_{24}	F(5)···N(2)	273.7(7)	6.8(tied to u_{21})

[a] See Figure 4 for atom numbering.

[b] Other amplitudes were included and not refined but fixed at HF/6-31G* values.

Table 9: Least-squares correlation matrix (× 100) for $F_3SiN(SiMe_3)NMe_2$.[a]

	p_{10}	p_{29}	p_{40}	p_{41}	u_2	u_3	u_6	u_{21}	k_1	k_2
p_2	-	-	-	-	-	-	-	-	55	-
p_{18}	50	-	-	-	-	-	-	-	-	-
p_{24}	-	68	-	66	-	-	-	-	-	-
p_{29}	-	-	-	76	-	-	-	-	-	-
p_{32}	-	-	-	-	-	-	-	53	-	-
p_{39}	-	-	55	-	-	-	-	-	-	-
u_1	-	-	-		53	53	81	-	-	76
u_2	-	-	-	-	-	-	51	-	-	60
u_3	-	-	-	-	-	-		-	-	72
u_6	-	-	-	-	-	-		-	-	53

[a] Only elements with absolute values ≥50% are shown; k_1 and k_2 are scale factors.

5.4 Discussion

5.4.1 Experimental results for $F_3SiN(Me)NMe_2$. In general, the experimental results can be seen to agree well with the highest level *ab initio* calculations (MP2/6-311+G**). There is quite a large difference between the values obtained experimentally and theoretically for ∠SiNC [MP2/6-311+G** 132.5°, GED 126.9(7)°] and ∠NNC(7) [MP2/6-311+G** 121.1°, GED 126.6(8)°]. However, N(2) is shown to be planar in the gas phase as predicted by the calculations, i.e. the values for ∠NNSi, ∠NNC(7) and ∠SiNC add up to 360°. The crystal structure of this molecule has been determined by Prof. N. W. Mitzel[23] and selected geometric parameters are given in Table 10 along with corresponding GED and *ab initio* values.

Table 10 Selected geometrical parameters for $SiF_3N(Me)NMe_2$ as determined by X-ray crystallography (XRD), by *ab initio* calculations (MP2/6-311+G**) and by GED. Distances are given in pm and angles in °.

	XRD	*ab initio*	GED
*r*N(1)N(2)	143.9(2)	142.6	143.1(5)
*r*N(2)Si(3)	164.6(2)	168.1	167.7(3)
*r*N(2)C(7)	144.8(2)	146.1	146.7(2)
∠N(1)-N(2)-Si(3)	104.1(1)	106.4	106.5(4)
∠N(1)-N(2)-C(7)	121.2(2)	121.1	126.6(8)
∠Si(3)-N(2)-C(7)	134.5(1)	132.5	126.9(7)
Si(3)···N(1)	246.6(1)	249.3	251.0(6)

The values obtained for the NNSi angles are fairly similar for the XRD, GED and *ab initio* studies. The other angles around the α-N atom (∠NNC and ∠SiNC) are similar for the calculated and XRD results, but these differ from the GED values. Both the NSi and NC bond distances are seen to be considerably shorter in the crystal structure than in either the *ab initio* and GED structures. However, the N-N distance is seen to be longer in the crystal structure than in the other two methods. Much of the difference between gas- and solid-phase structures can be accounted for by a displacement of the central nitrogen atom away from the other nitrogen in the crystalline phase, but there are clearly other effects of crystal packing on the structure.

5.4.2 Experimental results for $F_3SiN(SiMe_3)NMe_2$. From Table 7 it is possible to see that the structure determined experimentally differs from that calculated *ab initio*. The main difference is in the ∠NNSi angle fundamental to this study, determined by the GED experiment to be 84.9(4)°, a 9° decrease from the MP2/6-311+G** calculated value of 93.9°. The X-ray crystal structure of this compound was determined by Prof. N. Mitzel[23] and selected parameters are given in Table 11 with selected GED and *ab initio* values.

Table 11 Selected geometrical parameters for $F_3SiN(SiMe_3)NMe_2$ as determined by X-ray crystallography (XRD), by *ab initio* calculations (MP2/6-311+G**) and by GED. Distances are given in pm and angles in °.

	XRD	*ab initio* (r_e)	GED (r_a)
*r*N(1)-N(2)	148.7(1)	146.2	146.3(3)
*r*N(2)-Si(3)	166.2(1)	169.0	169.0(6)
*r*N(2)-Si(7)	175.8(1)	177.9	176.9(6)
∠N(1)-N(2)-Si(3)	83.6(1)	93.9	84.9(4)
∠N(1)-N(2)-Si(7)	130.0(1)	128.2	139.8(5)
∠Si(3)-N(2)-Si(7)	145.9(1)	136.2	132.6(5)
Si(3)···N(1)	210.2(1)	230.8	213.5(9)

From Table 11 it can be seen that the gas phase structure resembles some aspects of the crystal structure rather than the predicted *ab initio* structure. The GED value for ∠N(1)N(2)Si(3) is much closer to the X-ray crystal structure than that of the *ab initio* value. However, the other two angles around N(2) [∠N(1)N(2)Si(7) and ∠Si(3)N(2)Si(7)] in the GED structure do not coincide with either the *ab initio* or the XRD values. The gas phase structure has the N-N-Si(Me_3) as the largest whereas both the *ab initio* and XRD results indicate that the angle between the two silicon substituents on the α-N as the largest. However, differences between GED and *ab initio* results are fairly common in this series of compounds.[23,24]

It is also possible to compare the two compounds, to determine the effect of changing the non-acceptor group on the β-N. Both *r*NN and *r*NSi(3) are longer in $F_3SiN(SiMe_3)NMe_2$ than in $F_3SiN(Me)NMe_2$ (by 3.2 and 1.3 pm respectively), which is probably due to the steric effect of the bulky $SiMe_3$ group. There is a very noticeable difference in the values obtained for ∠NNSi(3), which is 21.6° smaller in $F_3SiN(SiMe_3)NMe_2$ than in $F_3SiN(Me)NMe_2$ [84.9(4) and 106.5(4)° respectively].

There is also a large difference in the values obtained for ∠NNC(7) and ∠NNSi(7) in **1** and **2**, which can again be attributed to steric effects from the bulky $SiMe_3$ group. However, whilst the difference between the two angles is still large, 13.2° [∠NNC(7) in $F_3SiN(Me)NMe_2$ is 126.6(8)° and ∠NNSi(7) in $F_3SiN(SiMe_3)NMe_2$ is 139.8(5)°], this shows that the marked decrease in the size of the ∠NNSi(F_3) angles in $F_3SiN(SiMe_3)NMe_2$ is not purely a steric effect and can also be attributed to the different electronic properties of the CH_3 and $SiMe_3$ groups.

5.4.3 Comparison with similar structures. As previously stated, changing the substituents on the acceptor silicon as well as the α-N can have a large effect on the strength of the Si – N interaction. This study can therefore be extended by comparing values obtained for these two molecules with those previously obtained for other compounds. Selected parameters are given in Table 12.

Table 12 Selected parameters calculated at MP2/6-311+G** for $F_3SiN(Me)NMe_2$ (**1**), $FH_2SiN(Me)NMe_2$[7] (**3**), $H_3SiN(Me)NMe_2$[7] (**4**) and $H_3SiN(SiH_3)NMe_2$[7] (**5**). Distances are given in pm and angles in °.[a]

	1	**3**	**4**	**5**
*r*N(1)N(2)	142.6	142.1	142.5	144.9
*r*N(2)Si(3)	168.1	170.8	173.0	174.6
*r*N(2)C/Si(7)	146.1	144.9	145.5	175.3
∠N(1)N(2)Si(3)	106.4	103.1	109.1	104.0
∠N(1)N(2)C/Si(7)	121.1	121.5	118.9	124.7
∠Si(3)N(2)C/Si(7)	132.5	135.4	128.3	131.3
N(1)···Si(3)	249.3	245.7	257.7	251.5

[a] atom numbering as for **1** in Figure 4.

From Table 12, it is possible to see a number of different factors at work in this group of molecules. The molecule with the smallest ∠NNSi (and correspondingly the smallest N···Si distance) is $FH_2SiN(Me)NMe_2$. This can be attributed to the electron withdrawing nature of fluorine increasing the electrophilicity of the acceptor silicon. However, it is interesting to note that the molecule with three fluorines substituted on the acceptor silicon [$F_3SiN(Me)NMe_2$] does not have a smaller ∠NNSi as might have been expected. $H_3SiN(SiH_3)NMe_2$ also has a smaller ∠NNSi than $F_3SiN(Me)NMe_2$, but, the Si···N distance is shorter in the latter case. This can be attributed to a combination of the longer Si-N and N-N distances in $H_3SiN(SiH_3)NMe_2$ increasing the Si···N distance, despite a smaller ∠NNSi. As the Si···N distance is the most important factor in determining the strength of the Si β-N interaction it can be said that the interaction is stronger in $F_3SiN(Me)NMe_2$ than in $H_3SiN(SiH_3)NMe_2$. The N-Si bond length is considerably shorter in the two compounds with fluorine atoms substituted onto the acceptor silicon [$F_3SiN(Me)NMe_2$ 168.1 pm and $FH_2SiN(Me)NMe_2$ 170.8 pm] than in the other three molecules [e.g. $H_3SiN(Me)NMe_2$ 173.0 pm]. It can also be seen that *r*NSi is 2.7 pm shorter in the trifluoro substituted than in the mono substituted compound. This can all be attributed to the electronegative effect of the fluorine atoms, drawing electron density away from the silicon atom and thus decreasing the N-Si bond length.

5.4.4 Further calculations removing donor and acceptor centres. Further calculations were carried out to evaluate the effect of removing either the donor and acceptor centres in both of the compounds (see Figure 9). Cartesian coordinates for the calculated structures are given in Appendix D. It was predicted that removing either the donor (by substituting the nitrogen atom with CH) or the acceptor (by substituting the silicon atom with a carbon atom) will result in larger angles and donor acceptor distances than have been found.

Figure 9 Illustration of removing acceptor (**a**) and donor (**b**) centres.

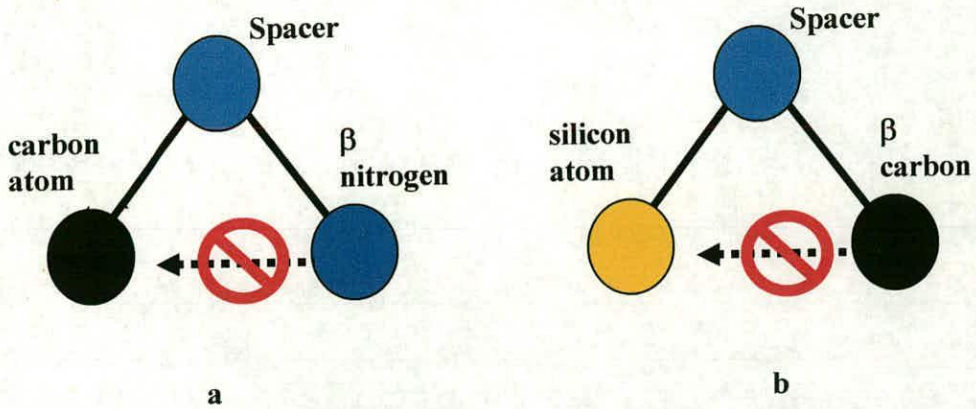

a **b**

Table 13 Selected parameters calculated at MP2/6-311+G** for $F_3SiN(Me)NMe_2$, $F_3CN(Me)NMe_2$, $F_3SiN(Me)CHMe_2$. Distances are given in pm and angles in °.

		no donor	no acceptor
	$F_3SiN(Me)NMe_2$	$F_3SiN(Me)CHMe_2$	$F_3CN(Me)NMe_2$
*r*N/C-N	142.6	147.7	142.2
*r*N-Si/C	168.1	168.0	140.8
*r*N-C	146.1	146.3	146.7
∠N/C-N-Si/C	106.4	119.3	110.2
∠N/C-N-C	121.1	117.0	117.4
∠Si/C-N-C	132.5	123.0	115.1
Σ^a	360.0	359.3	342.7
Si/N···N/C	249.3	272.6	232.1

[a] where Σ represents the sum of the three angles around the α-N [N(2)].

As can be seen from Table 13, there is now a large difference between the values calculated for the main parameters. Looking at ∠N/C-N-Si/C, which is 106.4° in the original molecule, this increases to 110.2° when the acceptor silicon is replaced by a carbon atom and then further increases to 119.3° when the donor nitrogen is replaced by a CH group. Figure 10 shows the change in geometry found on removing the acceptor

silicon. It can clearly be seen from the two perspectives in this figure that the α-N atom (N2) is no longer planar (also illustrated by the fact that the three angles around N2 add up to 342.7° instead of the planar 360°). Instead it more closely resembles a tetrahedral arrangement. This is directly caused by changing the $SiCl_3$ group to a CCl_3 group and so the removal of the acceptor silicon is therefore seen to influence the coordination geometry directly.

Figure 10 Two views of $F_3CN(Me)NMe_2$, the second rotated 90° around the N-N bond.

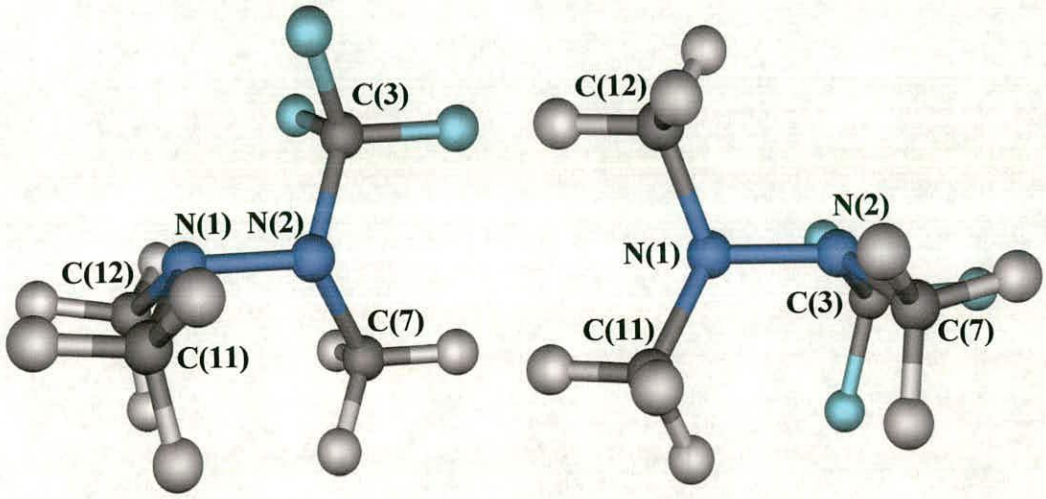

Removing the donor nitrogen and substituting a CH group appears to result in an almost planar geometry at N2 (the sum of the three angles around N2 being 359.3°). After studying a molecular representation of the molecule it can definitely be seen to be non-planar (see Figure 11). As previously mentioned ∠CNSi can be seen to be considerably wider than either ∠NNSi in **1** or ∠SiNC in $F_3SiN(Me)CHMe_2$. This can be compared to the wide angles found in compounds with an C/Si-O-Si linkage as mentioned in the introduction to this chapter.

Figure 11 Two views of $F_3SiN(Me)CHMe_2$, the second rotated 90° around the C-N bond.

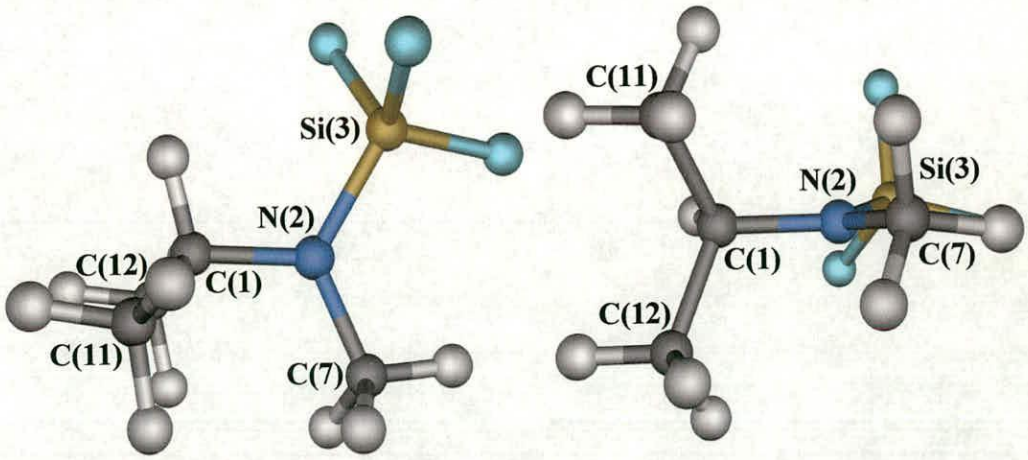

Table 14 Selected parameters calculated at MP2/6-311+G** for $F_3SiN(SiMe_3)NMe_2$, $F_3CN(SiMe_3)NMe_2$, $F_3SiN(SiMe_3)CHMe_2$. Distances are given in pm and angles in °.

	$F_3SiN(SiMe_3)NMe_2$	no donor $F_3SiN(SiMe_3)CHMe_2$	no acceptor $F_3CN(SiMe_3)NMe_2$
*r*N/C-N	146.2	149.2	142.3
*r*N-Si/C	169.0	168.7	139.7
*r*N-Si	177.9	177.6	179.8
∠N/C-N-Si/C	93.9	123.0	108.2
∠N/C-N-$Si(Me)_3$	128.2	114.6	126.4
∠Si/C-N-$Si(Me_3)$	136.2	122.4	123.0
Σ^a	358.3	360.0	357.6
Si/N···N/C	230.8	280.0	228.4

[a] where Σ represents the sum of the three angles around the α-N [N(2)].

Table 14 shows results for a set of $-N(SiMe_3)-$ molecules, again showing the effects of removing donor or acceptor atoms. Summing the three angles around the α-N atom

reveals that both $F_3SiN(SiMe_3)NMe_2$ and $F_3CN(SiMe_3)NMe_2$ are shallow pyramids, whereas $F_3SiN(SiMe_3)CHMe_2$ is planar. There are also great increases in the values calculated for ∠N/C-N-Si/C on removal of the donor and acceptor groups, from 93.0° in $F_3SiN(SiMe_3)NMe_2$ to 108.2° in $F_3CN(SiMe_3)NMe_2$ and123.0° in $F_3SiN(SiMe_3)CHMe_2$. Again, wide angles at nitrogen are associated with neighbouring silyl groups. It can be seen that in the last case ∠CNSi is the smallest angle. The reason for this is illustrated in Figure 12. Unlike the structures of all the other molecules in this series, that of $F_3SiN(SiMe_3)CHMe_2$ has a different orientation at the "donor" end of the molecule, i.e. the $CHMe_2$ group has turned *ca.* 180° compared to $F_3SiN(SiMe_3)NMe_2$ (see Figure 4). This is probably due to the effect of removing the donor interaction between the nitrogen and $Si(F_3)$ atoms, which then allows the -$CHMe_2$ group to rotate to relieve some of the steric crowding around the α-N atom. This was not noticed in the studies of the effects of replacing the acceptor centre in **1** because the steric effect is not so severe as in **2**.

Figure 12 Calculated molecular structure of $F_3SiN(SiMe_3)CHMe_2$.

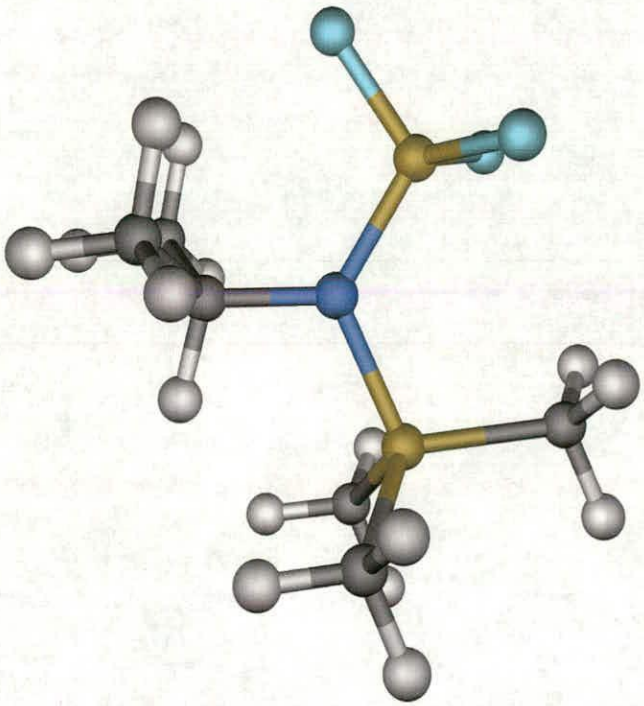

In all cases of removing the donor and acceptor atoms, there is also a decrease in the values calculated for the angles between the $SiMe_3$ group and "donor" groups. For example, in $F_3CN(SiMe_3)NMe_2$, $\angle CNSi(Me_3)$ is calculated to be 123.0° compared to 136.2° in $\angle SiNSi(Me_3)$ in $F_3SiN(SiMe_3)NMe_2$. This is probably simply linked to the increase in $\angle NNC(F_3)$ (108.2°) in $F_3CN(SiMe_3)NMe_2$ (*cf.* $\angle NNSi(F_3)$ of 93.9° in $F_3SiN(SiMe_3)NMe_2$), which causes a decrease in $\angle CNSi$. This is compounded by the fact that there is relatively little change in the $\angle NNSi(Me_3)$ in $F_3CN(SiMe_3)NMe_2$ compared to that of $F_3SiN(SiMe_3)NMe_2$) (126.4 and 128.2° respectively).

5.5 Conclusion

Following on from previous work on silylhydroxylamines and silylhydrazines, $F_3SiN(Me)NMe_2$ and $F_3SiN(SiMe_3)NMe_2$ were also found to have relatively strong attractive interactions between silicon and geminal nitrogen. The interaction in $F_3SiN(SiMe_3)NMe_2$ was found to be stronger than that occurring in $F_3SiN(Me)NMe_2$. This was attributed to both a steric effect (from the $SiMe_3$ group) as well as differing electronic effects from the $SiMe_3$ and Me groups attached to the α-N.

Further calculations were carried out on related compounds to $F_3SiN(Me)NMe_2$ and $F_3SiN(Me)NMe_2$, and these demonstrated the effect of removing the "donor" nitrogen (replacing it with a CH group) and the "acceptor" silicon atom (replacing it with a C atom). This was seen to remove the effects of any interaction, with the bond angles between the "donor" and "acceptor" atoms increasing, along with a corresponding increase in the distance between the two atoms. There was also a change in the coordination geometry of the α-N, most noticeable in $F_3CN(Me)NMe_2$, where there were two pyramidal nitrogen atoms as opposed to one pyramidal and one planar or almost planar nitrogen.

5.6 Further work

This is an area of great interest, with very unusual angles and coordination emerging from the continuing studies. It would be interesting to synthesise and determined the structures of the analogues of $F_3SiN(Me)NMe_2$ and $F_3SiN(Me)NMe_2$ with the donor and acceptor atoms replaced to confirm the structures predicted by the calculations.

Further work could also be carried out into the effect of different spacer atoms. So far, both oxygen and nitrogen have maintained these unusual interactions between silicon and a geminal nitrogen. It would be interesting to discover the effect if using a carbon atom as a spacer would maintain the interaction and also to determine the effects of changing the substituents on this carbon atom.

5.7 References

1. Lukevics, E.; Pudova, O.; Strukokovich, R. *Molecular Structure of Organosilicon Compounds*, Ellis Horwood: Chichester, **1989**.

2. Barrow, M. J.; Ebsworth, E. A. V.; Harding, M. M. *Acta Cryst. B*, **1979**, *35B*, 2093.

3. Kasai, P. H.; Myers, R. J. *J. Chem. Phys.*, **1959**, *30*, 1096.

4. Blake, A. J.; Dyrbush, M.; Ebsworth, E. A.V.; Henderson, S. G. D. *Acta Cryst. C*, **1988**, *44*, 1.

5. Losehand, U.; Mitzel, N. W. *Inorg. Chem.*, **1998**, *37*, 3175.

6. Mitzel, N. W.; Losehand, U. *Angew. Chem. Int. Ed. Engl.*, **1997**, *36*, 2807.

7. Mitzel, N. W. *Chem. Eur. J.*, **1998**, *4*, 692.

8. Vojinović, K.; McLachlan, L. J.; Rankin, D. W. H.; Mitzel, N. W. *Inorg. Chem.*, submitted.

9. Gaussian 98 (Revision A.7), Frisch, M. J.; Trucks, G. W.; Schlegel, H. B.; Scuseria, G. E.; Robb, M. A.; Cheeseman, J. R.; Zakrzewski, V. G.; Montgomery, J. A.; Stratman, R. E.; Burant, J. C.; Dapprich, S.; Milliam, J. M; Daniels, A. D.; Kudin, K. N.; Strain, M. C.; Farkas, O.; Tomasi, J.; Barone, V.; Cossi, M.; Cammi, R.; Mennucci, B.; Pomelli, C.; Adamo, C.; Clifford, S.; Ochterski, J.; Petersson, G. A.; Ayala, P.Y.; Cui, Q.; Morokuma, K.; Malick, D. K.; Rabuck, A. D.; Raghavachari, K.; Foresman, J. B.; Cioslowski, J.; Ortiz, J. V.; Baboul, A. G.; Stefanov, B. B.; Liu, C.; Liashenko, A.; Piskorz, P.; Komaromi, I.; Gomperts, R.; Martin, R. L.; Fox, D. J.; Keith, T.; Al-Laham, M. A.; Peng, C. Y.; Nanayakkara, A.; Gonzalez, C.; Challacombe, M.; Gill, P. M. W.; Johnson, B. G.; Chen, W.; Wong, M. W.; Andres, J. L.; Gonzales, C.; Head-Gordon, M.; Replogle, E. S.; Pople, J. A. Gaussian, Inc., Pittsburgh PA, **1998**.

4. Binkley, J. S.; Pople, J. A.; Hehre, W. J. *J. Am. Chem. Soc.*, **1980**, *102*, 939.

5. Gordon, M. S.; Binkley, J. S.; Pople, J. A.; Pietro, W. J.; Hehre, W. J. *J. Am. Chem. Soc.*, **1982**, *104*, 2979.

6. Pietro, W. J.; Francl, M. M.; Hehre, W. J.; DeFrees, D. J.; Pople, J. A.; Binkley, J. S. *J. Am. Chem. Soc.*, **1982**, *103*, 5039.

7. Hehre, W. J.; Ditchfield, R.; Pople, J. A. *J. Chem. Phys.*, **1972**, *56*, 2257.

8 Hariharan, P. C.; Pople, J. A. *Theor. Chim. Acta*, **1973**, *28*, 213.

9. Gordon, M. S. *Chem. Phys. Lett.*, **1980**, *76*, 163.

10. Krishnan, R; Binkley J. S.; Seeger, R; Pople, J. A. *J. Chem. Phys.*, **1980**, *72*, 650.

12. Huntley, C. M.; Laurenson, G. S.; Rankin, D. W. H. *J. Chem. Soc., Dalton Trans.*, **1980**, 954.

13. Lewis, J. R.; Brain, P. T.; Rankin, D. W. H. *Spectrum*, **1997**, *15*, 7.

14. Cradock, S.; Koprowski, J. *J. Mol. Struct.*, **1982**, *77*, 113.

15. Boyd, A. S. F.; Laurenson, G. S.; Rankin, D. W. H. *J. Mol. Struct.*, **1981**, *71*, 217.

16. Ross, A. W.; Fink M.; Hilderbrandt, R. in *International Tables for Crystallography*, ed. A. J. C. Wilson, Vol. C, Kluwer Academic Publishers, Dordrecht, **1992**, p.245.

17. Huntley, C. M.; Laurenson, G. S.; Rankin, D. W. H. *J. Chem. Soc., Dalton Trans.*, **1980**, 954.

18. Lewis, J. R.; Brain, P. T.; Rankin, D. W. H. *Spectrum*, **1997**, *15*, 7.

19. Cradock, S.; Koprowski, J. *J. Mol. Struct.*, **1982**, *77*, 113.

20. Boyd, A. S. F.; Laurenson, G. S.; Rankin, D. W. H. *J. Mol. Struct.*, **1981**, *71*, 217.

21. Ross, A. W.; Fink M.; Hilderbrandt, R. in *International Tables for Crystallography*, ed. A. J. C. Wilson, Vol. C, Kluwer Academic Publishers, Dordrecht, **1992**, p.245.

22. (a) Blake, A. J.; Brain, P. T.; McNab, H.; Millar, J.; Morrison, C. A.; Parsons, S.; Rankin, D. W. H.; Robertson, H. E.; Smart, B. A. *J. Phys. Chem.*, **1996**, *100*, 12280. (b) Brain, P. T.; Morrison, C. A.; Parsons, S.; Rankin, D. W. H. *J. Chem. Soc., Dalton Trans.*, **1996**, 4589.

23. Vojinović, K.; McLachlan, L. J.; Hinchley, S. H.; Rankin, D. W. H.; Mitzel, N. W. unpublished.
24. Mitzel, N. W.; Losehand, U. *J. Am. Chem. Soc.*, **1998**, *120*, 7320.

CHAPTER SIX

The molecular structure of $ClH_2SiN(Me)NMe_2$ by gas-phase electron diffraction and *ab initio* molecular orbital calculations

6.1 Introdution

At least three major contributions to the strength of the β-donor interactions in silylhydrazines have so far been noted. The previous chapter was concerned mainly with the effects of altering the non-interacting substituents on the α-N (R^{α}). This chapter follows on from this work, and will focus on the effects of altering the substituents on the interacting silicon atom on the α-N (R^{s}).

Previous work carried out by Prof N. W. Mitzel on silylhydroxylamines and silylhydrazines has shown that the strength of the β-donor interaction varies greatly with the nature of the R^{s} substituent[1] and has unearthed β-donor interactions of exceptional strength in $ClH_2SiONMe_2$.[2] The crystal structure was found to have an SiON angle of 79.7(1)° [Si···N distance of 202.8(1) pm], the smallest SiON angle found in the studies so far. This did not match the structure obtained by *ab initio* calculations, which predicted a SiON angle of 91.6° (MP2/6-311G**). It is possible for the crystal structure to vary considerably from the values predicted *ab initio* for various reasons, including, for example, the presence of intermolecular interactions. However, it was found that calculations carried out on silylhydroxylamines generally agree well with the experimental (solid-state) values.[2] The gas-phase structure was determined by electron diffraction (GED) in order to investigate the discrepancy between calculated and experimental solid state values. The GED data indicated that the molecules existed in two conformers [34(5) % *anti* and 66(5) % *gauche*], with the chlorine atom in the SiH_2Cl group in an *anti* or *gauche* position with respect to the nitrogen atom. The crystal structure exists only in the *anti* form. The SiON angle was found to be less extreme in both conformers in the gas phase than occurs in the crystal structure [87.1(9)° *anti* and 104.7(1) *gauche* as compared to 91.6° and 104.5° predicted *ab initio* (MP2/6-311G**)].

The structure of $ClH_2SiN(Me)NMe_2$ was investigated as part of the study into Si β-N interactions in silylhydrazines. Determining the gas-phase structure will allow comparison with calculated and previously determined crystal structure. This will establish if there are differences between the structures obtained experimentally and computationally similar to those found in $ClH_2SiONMe_2$.

6.2 Experimental

6.2.1 Synthesis. A sample of $ClH_2SiN(Me)NMe_2$ (1) was prepared by Prof. N.W. Mitzel (Münster) and no further purification was carried out prior to the electron diffraction experiment.

6.2.2 Computational studies. All calculations were performed on a Dec Alpha 1000A workstation using the Gaussian 98 program.[3] A search of the torsional potentials of the compound at the HF level of theory using the 3-21G* [4-6] basis set resulted in the location of several conformers. Further optimisations of these were carried out at HF and MP2(fc) levels of theory using the standard 6-31G*, 6-311G* and 6-311+G** [7-10] basis sets. Analytical second derivatives of the energy with respect to nuclear coordinates at the HF/6-31G* level for the lowest energy conformer gave the force field, which was then used, without scaling, to provide estimates of the amplitudes of vibration (u) for use in the gas-phase electron diffraction (GED) refinement. A frequency calculation confirmed that the lowest energy stationary point was a minimum on the potential energy surface. The structure of **1**, with numbering scheme, is shown in Figure 1.

6.2.3 Gas-phase electron diffraction experiment. The Edinburgh gas diffraction apparatus[11] was used to collect data. The sample and nozzle temperatures were held at 273 and 293 K. An accelerating voltage of *ca.* 40 kV (electron wavelength *ca.* 6.0 pm) was used and the scattering intensities were recorded at nozzle-to-film distances of 128.1 and 286.7 mm on Kodak Electron Image film. Three films were collected at each nozzle-to-film distance. The weighting points for the off-diagonal weight matrices,

correlation parameters and scale factors for the two camera distances are given in Table 1. The scattering patterns of benzene were also recorded for the purpose of calibration; these were analysed in the same way as the data for **1** to minimise any systematic errors in wavelengths and camera distances. The electron-scattering patterns were converted into digital form using a PDS densitometer at the Institute of Astronomy in Cambridge with a scanning program described elsewhere.[12] Data reduction and least-squares refinements were carried out using standard programs,[13,14] utilising the scattering factors of Ross *et al.*[15]

Figure 1 Molecular structure of $ClH_2SiN(Me)NMe_2$ (**1**) showing the atomic numbering scheme.

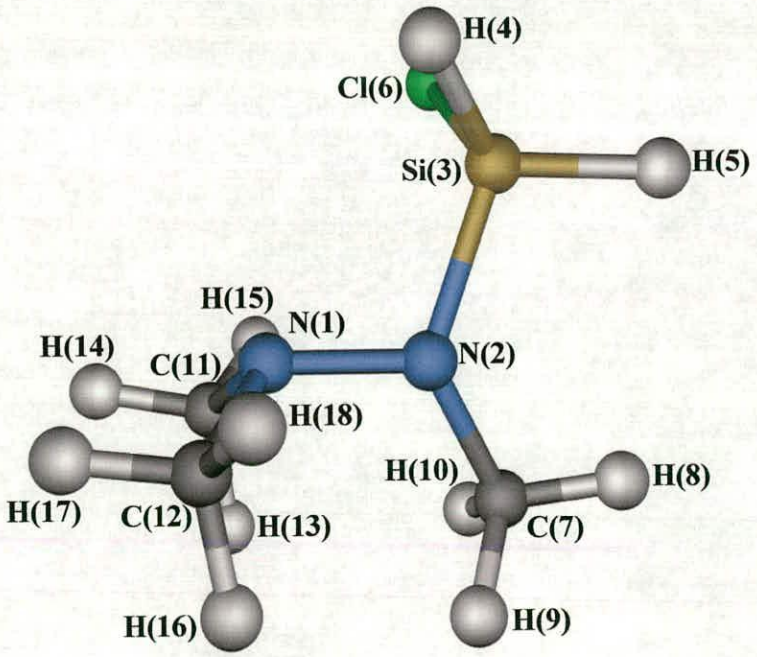

Table 1 GED experimental conditions for $ClH_2SiN(Me)NMe_2$.

camera	weighting functions /nm^{-1}					correlation	scale factor	electron
distance/mm	Δs	s_{min}	s_1	s_2	s_{max}	parameter		wavelength/pm
128.14	4	92	112	272	320	0.0483	0.658(15)	6.016
286.69	2	20	40	110	130	0.1808	0.765(3)	6.016

6.3 Results

6.3.1 Computational studies. A search of the potential energy surface of $ClH_2SiN(Me)NMe_2$ (1) resulted in the location of several minima. The lowest energy structure was found to be C_1 and had ϕCl-Si-N-N of 69.5°. A structure with C_s symmetry was found to exist as a minimum, with a ϕCl-Si-N-N of 180.0°. This structure was found to be 4.68 kJ mol^{-1} higher in energy than the lowest energy form. Therefore, only *ca.* 7% of the higher energy conformer would be present, which is not enough to be detected by GED, so analysis was carried out on the basis of a single conformer. The most important parameters of the lowest energy conformer from the highest level calculation are given in Table 2. Cartesian coordinates for both the C_s and the C_1 structures are given in Appendix E.

The bond lengths and angles in the molecule were found to be quite sensitive to both the basis set and level of theory used. The angle that is fundamental to this study, ∠N(1)N(2)Si(3), can be seen to change from 113.1 to 110.0 on the inclusion of correlation, but this angle is more stable than was found with the two compounds in the previous chapter. Several large changes in the values calculated for the geometrical parameters can be seen after the level of theory was improved from Hartree-Fock to MP2. For example, the N-N distance increases from 141.0 to 142.8 pm and the Si-N distance increases from 170.5 to 171.4 (HF/6-31G* to MP2/6-31G*). There are also several large changes in the values calculated for the angles. As well as the values for ∠NNSi, the values calculated for the angles to the two methyl groups attached to N(1) decrease significantly from 113.9 to 112.7° for ∠N(2)N(1)C(11) and from 113.1 to 110.9° for ∠N(2)N(1)C(12). ∠NSiCl also decreases significantly from 113.9 to 112.8°. This again shows the importance of carrying out calculations that include electron correlation in order to obtain as accurate a prediction as possible.

Table 2 Calculated and geometric parameters (r_e structure) for the structure of $ClH_2SiN(Me)NMe_2$ (distances in pm, angles in °).[a]

	Level of theory / Basis set			
Parameters	HF/ 6-31G*	MP2/ 6-31G*	MP2/ 6-311G*	MP2/ 6-311+G**
N(1)-N(2)	141.0	142.8	143.2	142.8
N(1)-C(7)	145.1	145.9	146.0	145.9
N(2)-C(10)	145.0	146.1	146.2	146.2
N(2)-Si(3)	170.5	171.4	171.8	171.5
Si(3)-Cl(6)	208.7	208.2	208.1	208.0
Si(7)-H(5)	146.8	147.8	148.2	147.2
C(7)-H(8)	108.3	109.2	109.2	109.3
N(2)-N(1)-C(11)	113.9	112.7	12.5	112.6
N(2)-N(1)-C(12)	113.1	110.9	110.8	110.8
N(1)-N(2)-Si(3)	113.1	110.0	110.8	110.2
N(1)-N(2)-C(7)	119.0	118.8	119.0	118.8
N(2)-Si(3)-Cl(6)	113.9	112.8	112.7	112.8
N(2)-Si(3)-H(4)	111.1	110.6	110.4	110.7
N(2)-Si(3)-H(5)	108.0	107.7	106.8	107.6
N(2)-C(7)-H(8)	108.8	108.2	108.8	108.0
N(2)-C(7)-H(9)	111.2	110.8	110.8	110.9
N(2)-C(7)-H(10)	112.8	113.0	113.0	113.0
N(1)-N(2)-Si(7)-C(8)	-174.1	-174.1	-176.1	-174.6
N(1)-N(2)-Si(3)-Cl(6)	-74.3	-69.6	-71.1	-69.5
Total Energy[b]	-977.1636	-978.0939	-978.2358	-978.3379

[a] Atom numbering given in Figure 1.

[b] Energy corrected for zero-point energy.

With MP2/6-311+G**, basis set convergence appears to have achieved, with only the N-N and Si-H bond lengths changing significantly between the top two levels of calculation. However, there is also a large variation in the values calculated for the angles around Si(3) (at the highest level calculated the three angles vary by 5.2°). Large asymmetry is also present in the C(7) methyl group, with the three ∠N(2)C(7)H angles varying by a range of 5°. With such a large asymmetry present in these groups, it is important for this to be reflected in the model for electron diffraction refinement, rather than simply assuming local C_{3v} symmetry for $N(2)C(7)H_3$.

6.3.2 Electron diffraction analysis. The model was written using C_1 symmetry with local C_{3v} symmetry was assumed around the two methyl groups on N(1), but not for the methyl on N(2). The structure was defined in terms of seventeen independent geometric parameters. These comprised six bond lengths and differences, six angles and five torsions. The bonds lengths *r*NN, *r*NC and *r*SiH were expressed in terms of an average of the NN, the average NC distances and the average SiH distances (p_1), and two difference parameters [*r*NN minus the average *r*NC and *r*SiH (p_2) and *r*N(1)C(11/12) minus *r*Si(3)H(4/5) (p_3)]. Also included were the CH distance (all assumed to be equal) (p_4), *r*NSi (p_5) and *r*SiCl (p_6). The three NNC angles were expressed in terms of the average of the three angles (p_7) and two differences, ∠NNC(7) minus ∠NNC(11) (p_8) and ∠NNC(7) minus ∠NNC(12) (p_9). The NSiH/F angles were also expressed in terms of the average of the three angles (p_{10}) and two differences. However, the values for the two differences were fixed within the model, ∠N(2)Si(3)H(4) minus ∠N(2)Si(3)H(5) (-5.2 pm) and ∠N(2)Si(3)H(4) minus ∠N(2)Si(3)Cl(6) (-3.1 pm). Other angles used were ∠N(1)N(2)Si(3) (p_{11}) and ∠N(1)CH (all assumed to be equal) (p_{12}).

The hydrogen atoms on C(7) were twisted into position using two torsion angles, ϕ H(9)-C(7)-N(2)-H(8) and ϕH(10)-C(7)-N(2)-H(8), with fixed values within the model (117.8 and 119.7° respectively). With regard to the $SiClH_2$ group, two torsions were included to move one of the hydrogen atoms and the chlorine out of the N-N-Si-C plane

[ϕ Cl(6)-Si(3)-N(2)-H(4) and ϕH(5)-Si(3)-N(2)-H(4) at fixed values within the model (118.8 and 124.9° respectively)]. Torsions of the C(7) methyl group [ϕH(8)C(7)N(2)N(1)] and the $SiClH_2$ group [ϕH(5)Si(3)N(2)N(1)] (p_{13-14}) were included. The C(7) methyl group was rotated out of the plane using the dihedral angle ϕSi(3)N(2)N(1)C(7) (p_{15}). The two methyl groups attached to N(1) were twisted into position using two separate torsions, ϕC(12)N(1)N(2)Si(3) (p_{16}) and ϕC(11)N(1)N(2)Si(3) (p_{17}).

The starting values for the 17 geometric parameters used in the refinement were taken from the *ab initio* results (MP2/6-311+G**). Force fields described by a set of symmetry coordinates were converted from theoretical (HF/6-31G*) Cartesian force fields using the program ASYM40.[16] The model was refined as an r_a structure (i.e. without any perpendicular amplitude corrections). All 17 geometric parameters and 14 groups of amplitudes were refined. Nine geometric and ten amplitude restraints were applied using the SARACEN method[17] and are listed in Tables 3 and 4.

The final refinement resulted in R_G = 0.033 (R_D=0.040), with very small discrepancies in the difference curves for the combined molecular scattering intensity (Figure 2) and radial distribution (Figure 3). Final refined parameters are listed in Table 3 and interatomic distances and the corresponding amplitudes of vibration in Table 4. The least-squares correlation matrix is give in Table 5.

Table 3: Refined and calculated geometric parameters from the GED study of $ClH_2SiN(Me)NMe_2$ (**1**) (distances in pm, angles in °).[a]

	Independent Parameters	MP2/ 6-311+G** (r_e)	GED (r_a)	Restraint
p_1	av *r*NN *r*NC *r*SiH	145.9	146.0(2)	
p_2	av *r*NC *r*SiH – *r*NN	3.7	3.9(5)	3.7(5)
p_3	*r*NC - *r*SiH	1.1	1.3(5)	1.1(5)

p_4	av *r*CH	109.3	109.3(2)	
p_5	*r*NSi	171.5	169.6(2)	
p_6	*r*SiCl	208.0	206.7(2)	
p_7	av ∠NNC	114.1	114.5(3)	
p_8	∠NNC(11) - ∠NNC(7)	1.8	1.8(2)	1.8(2)
p_9	∠NNC(11) - ∠NNC(12)	-6.2	-6.3(4)	-6.2(4)
p_{10}	av ∠NSiH/Cl	110.4	111.7(4)	
p_{11}	∠NNSi	110.2	109.4(3)	
p_{12}	av ∠NCH	110.6	110.7(5)	110.6(5)
p_{13}	ϕH(8)C(7)N(2)N(1)	0.0	0.8(32)	1.0(30)
p_{14}	ϕH(5)Si(3)N(2)N(1)	0.0	-2.9(15)	
p_{15}	ϕSi(3)N(2)N(1)C(7)	157.7	160.0(14)	157.7(30)
p_{16}	ϕC(12)N(1)N(2)Si(3)	126.2	129.6(22)	126.2(30)
p_{17}	ϕC(11)N(1)N(2)Si(3)	107.2	108.9(20)	107.2(30)
	Dependent Parameters			
p_{18}	*r*NN	142.8	142.8(4)	
p_{19}	*r*NC	146.1	146.1(2)	
p_{20}	*r*SiH	147.2	147.4(5)	
p_{21}	∠NNC(7)	118.8	119.3(4)	
p_{22}	∠NNC(11)	112.6	113.0(3)	
p_{23}	∠NNC(12)	112.6	111.2(3)	
p_{24}	∠SiNC	126.5	127.6(3)	
p_{25}	N···Si	258.2	255.4(4)	

[a] See Figure 1 for atom numbering.

[b] See text for description of the parameters.

Table 4: Interatomic distances (r_a/pm) and amplitudes of vibration (u/pm) for the restrained GED structure of $ClH_2SiN(Me)NMe_2$ (**1**).[a,b]

	Atom Pair	r_a / pm	u / pm	Restraint
u_1	Cl(6)-Si(3)	206.6(2)	5.7(2)	
u_2	C(7)-N(2)	146.1(2)	4.9(2)	
u_3	Si(3)-N(2)	169.2(2)	6.2(2)	
u_4	H(8)-C(7)	108.9(2)	9.6(2)	7.4(7)
u_5	Si(3)···N(1)	256.8(4)	8.8(5)	7.5(8)
u_6	Cl(6)···N(2)	315.3(6)	9.1(5)	8.4(8)
u_7	N(1)-N(2)	142.4(4)	4.8 (tied to u_2)	
u_8	Cl(6)···N(1)	357.7(18)	24.2(7)	
u_9	C(7)···Si(3)	283.1(4)	6.8(4)	7.0(7)
u_{10}	C(11)···Cl(6)	392.7(42)	29.0(29)	28.1(28)
u_{11}	C(7)···Cl(6)	415.7(20)	20.9(13)	20.3(20)
u_{12}	C(11)···Si(3)	356.7(19)	14.3 (tied to u_8)	
u_{13}	C(12)···Si(3)	362.3(19)	14.9 (tied to u_8)	
u_{14}	C(12)··Cl(6)	494.6(19)	22.2 (13)	20.5(20)
u_{15}	H(4)-Si(3)	147.3(5)	8.9 (tied to u_2)	
u_{16}	C(12)···N(2)	238.7(5)	6.8(3)	6.2(6)
u_{17}	C(11)···N(2)	240.1(5)	6.9 (tied to u_{16})	
u_{18}	C(7)···N(1)	249.0(5)	7.0 (tied to u_{16})	
u_{19}	C(12)···C(11)	236.2(13)	7.4 (tied to u_{16})	
u_{20}	C(11)···C(7)	300.1(27)	10.6 (11)	12.3(12)
u_{21}	C(12)···C(7)	301.9(22)	10.1 (tied to u_{20})	
u_{22}	H(15) ···N(1)	210.8(6)	8.5 (tied to u_{23})	
u_{23}	H(13)···N(1)	210.8(6)	8.3(6)	9.8(9)
u_{24}	H(14)···N(1)	210.8(6)	8.4 (tied to u_{23})	

[a] See Figure 1 for atom numbering.

[b] Other amplitudes were included but not refined and fixed at HF/6-31G* values.

Table 5: Least-squares correlation matrix (× 100) for $ClH_2SiN(Me)NMe_2$ (1).[a]

	p_3	p_6	p_{11}	p_{17}	u_2	u_6	u_{11}	u_{20}	u_{24}	k_1	k_2
p_1	87	-	-	-	-	-	-	-	-	-	-
p_2	-	-	54	-	-50	-	-	-	-	-	-
p_5	-	-	-	-	55	-	-	-	-	74	51
p_6	-	-	-	-	-	-	-	-	70	-	-
p_7	-	-	-	-	-	66	-	-	-	-	-
p_{10}	-	-	-	-	-	-	-	-74	-	-	-
p_{12}	-	-75	-	-	-	-	-	-	-	-	-
p_{14}	-	-	-	-	-	-	-50	-	-	-	-
p_{16}	-	-	-	-92	-	-	-	-	-	-	-
u_1	-	-	-	-	52	-	-	-	-	-	62
u_2	-	-	-	-	-	-	-	-	-	70	76
k_1	-	-	-	-	-	-	-	-	-	-	64

[a] Only elements with absolute values ≥50% are shown; k_1 and k_2 are scale factors.

Figure 2 Experimental and final weighted difference (experimental - theoretical) molecular-scattering intensities for $ClH_2SiN(Me)NMe_2$.

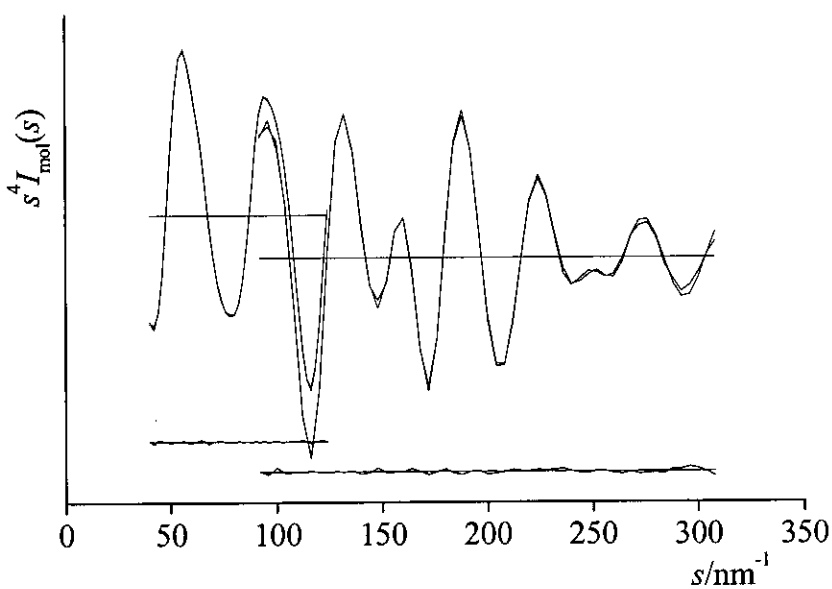

Figure 3 Experimental and difference (experimental - theoretical) radial-distribution curves, $P(r)/r$, for $ClH_2SiN(Me)NMe_2$. Before Fourier inversion the data were multiplied by $s.\exp(-0.00002s^2)/(Z_{Cl}-f_{Cl})/(Z_{Si}-f_{Si})$.

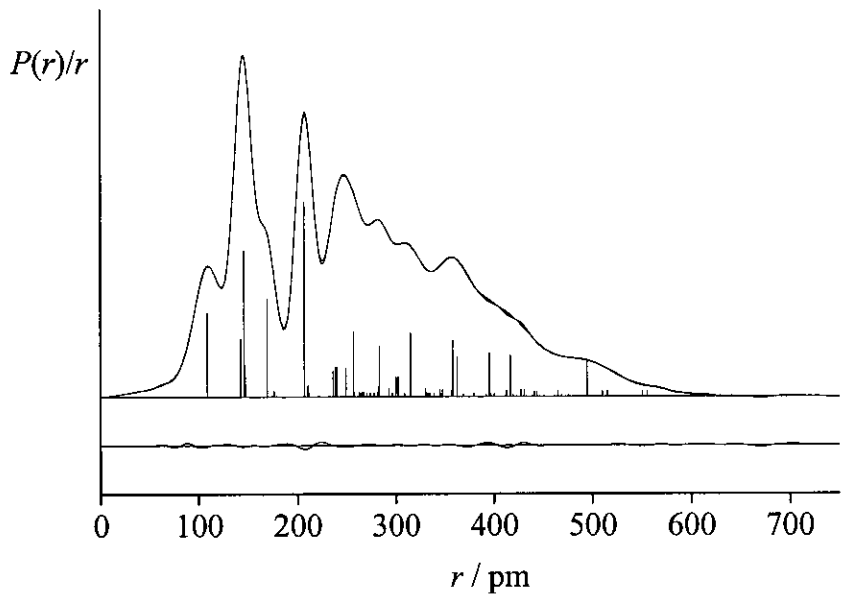

6.4. Discussion

6.4.1 Experimental Results

From Table 3, it can be seen that there is generally good agreement between the values calculated at the MP2/6-311+G** level and those obtained experimentally. The greatest discrepancies are for the NSi and SiCl bond lengths, which are, as usual, overestimated by the MP2 method, even with a large basis set. It is also possible to compare the gas-phase structure with a crystal structure previously determined by Prof Norbert Mitzel. Selected parameters are given in Table 6 with GED and *ab initio* values.

Table 6 Selected geometrical parameters for $ClH_2SiN(Me)NMe_2$ as determined by X-ray crystallography (XRD), by *ab initio* calculations (MP2/6-311+G**) and by GED. Distances are given in pm and angles in °.

	XRD	*ab initio*	GED
*r*N(1)N(2)	143.4(2)	142.8	142.8(4)
*r*N(2)Si(3)	168.5(1)	171.5	169.6(2)
*r*N(2)C(7)	145.5(2)	145.9	146.1(2)
∠N(1)-N(2)-Si(3)	109.9(1)	110.2	109.5(3)
∠N(1)-N(2)-C(7)	119.9(1)	118.8	119.5(4)
∠Si(3)-N(2)-C(7)	127.0(1)	126.5	127.8(3)
ϕN(1)N(2)Si(3)Cl(6)	75.1(1)	69.5	66.6(15)
Si(3)···N(1)	255.7	258.2	255.4(4)

The values obtained using all three methods are closely similar, so we can conclude that there is no major change in the molecule between the gas and solid phases. This is unlike the hydroxylamine analogue of this molecule, $ClH_2SiONMe_2$, which, as mentioned earlier, exists as one conformer in the solid state and two conformers in the gas phase. It can clearly be seen from Table 6 that the dihedral angles in the crystal and gas-phase results indicate the same conformer to be present in both phases.

As discussed in the computational section of this chapter, more than one conformer was located during the search of the potential energy surface of **1**. Figure 4 shows a plot exploring the energy of the system as the dihedral angle N-N-Si-Cl is changed.

Figure 4 Potential energy plot (HF/6-31G*) for the variation of the dihedral angle N-N-Si-Cl in $ClH_2SiN(Me)NMe_2$ (**1**).

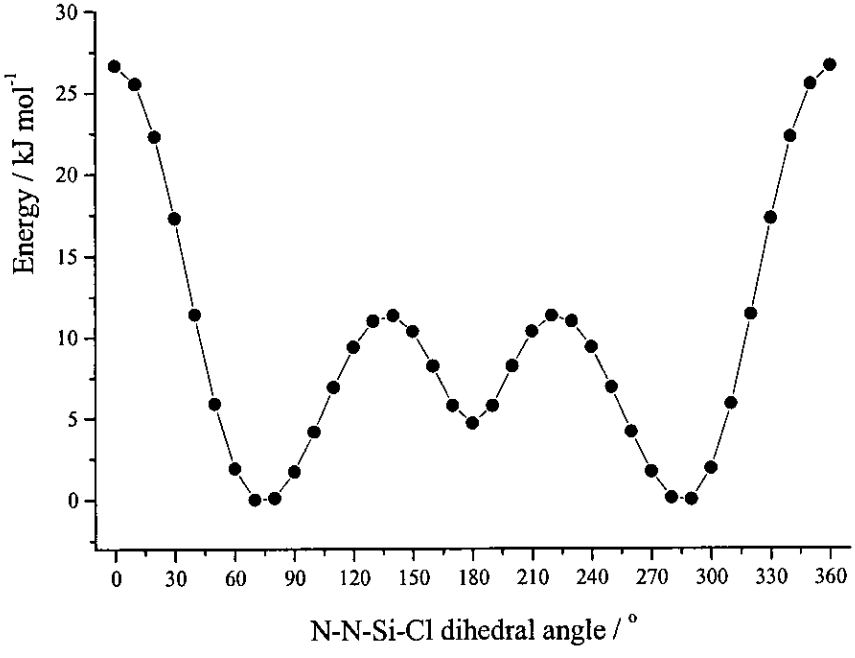

Figure 4 shows the presence of an *anti* conformer as a minimum on the potential energy surface; however, it is 4.68 kJ mol^{-1} higher in energy than the *gauche* conformer. From this, it may have been expected that there may be a small proportion (*ca.* 7 %) of the *anti* conformer present in the gas-phase sample. However, as there is a very good fit of the experimental data to the *gauche* conformer (i.e. negligible discrepancies on the difference curve and low *R* values and errors), it was concluded that addition of a small percentage of a second conformer would not lead to any significant information about its structure, or even its abundance. Refinements were therefore restricted to a single conformer. A check on the possibility that the *anti* conformer was predominant was carried out by introducing a value of 180.0° for ϕNNSiCl. This resulted in a much larger *R* factor (R_G = 0.110 as compared to R_G =0.033 obtained for the *gauche* conformer) and larger discrepancies in the difference curve.

6.4.2 Comparison with similar structures. Further calculations were carried out on related structures to investigate the effect that altering the substitutients on the donor and acceptor groups has on the strength of the Si β-N interaction. The results from these calculations are shown in Table 7.

Table 7 Selected properties calculated at MP2/6-311+G** for $ClH_2SiN(Me)NMe_2$ (**1**), $Cl_3SiN(Me)NMe_2$ (**2**), $FH_2SiN(Me)NMe_2$[1] (**3**) and $F_3SiN(Me)NMe_2$ (**4**). Distances are given in pm and angles in °.[a]

	1	**2**	**3**	**4**
*r*N(1)N(2)	142.8	142.4	142.1	142.6
*r*N(2)Si(3)	171.5	169.0	170.0	168.1
*r*N(2)C(7)	145.9	145.5	144.9	146.1
∠N(1)N(2)Si(3)	110.2	104.6	103.1	106.4
∠N(1)N(2)C(7)	118.8	120.8	121.5	121.1
∠Si(3)N(2)C(7)	126.5	134.6	135.4	132.5
N(1)···Si(3)	258.2	247.3	245.7	249.3

[a] Atom numbering as for **1**, given in Figure 1.

From this Table it can be seen that the molecule with the smallest ∠NNSi (and corresponding smallest N(1)···Si(3) distance) is $FH_2SiN(Me)NMe_2$. As stated in the previous chapter, this is due to the electron-withdrawing fluorine atom increasing the electrophilicity of the acceptor silicon by drawing electron density away from it. Looking at the results for the chlorine analogues of these compounds, it can be seen that $ClH_2N(Me)NMe_2$ has a larger ∠NNSi than $FH_2N(Me)NMe_2$ (by 7.1°). This is expected as chlorine has a smaller electronegativity than fluorine and so it is likely to have a lesser ability to draw electron density towards it. The ∠NNSi is $Cl_3SiN(Me)NMe_2$ is 104.6°, 5.6° narrower than that of $ClH_2N(Me)NMe_2$. Substituting the silicon atom with three chlorine atoms ($Cl_3SiN(Me)NMe_2$) can be to seen increase the electron

withdrawing effect compared with $ClH_2N(Me)NMe_2$, increasing the electrophilicity of the silicon atom, therefore increasing the Si β-N interaction.

It should then follow that $F_3SiN(Me)NMe_2$ has the narrowest ∠NNSi, as increasing the electron-withdrawing nature of the silicon atom's substituents should increase its electrophilicity. However, as mentioned in the previous chapter, ∠NNSi is wider in $F_3SiN(Me)NMe_2$ than in $FH_2SiN(Me)NMe_2$ (106.4 and 103.1° respectively) and, as can be seen from Table 7, wider than $Cl_3SiN(Me)NMe_2$ (106.4 and 104.6° respectively). It is thought that the tri-substituted fluorine compound does not have the smallest ∠NNSi because of back-bonding from the fluorine atoms. It can also be seen that $ClH_2SiN(Me)NMe_2$ is the only compound in Table 7 which has a non-planar α-N (the sum of the three angles around the α-N = 355.5°). However, this was the only calculation carried out using C_1 symmetry. The lowest energy structures for the other three compounds were C_s symmetry and therefore were all planar around the α N. Table 8 shows selected parameters from results of the calculations carried out on the two conformers of $ClH_2SiN(Me)NMe_2$.

Table 8 Selected parameters calculated at the MP2/6-311+G** level for two conformers of $ClH_2SiN(Me)NMe_2$. Distances are given in pm and angles in °.[a]

	gauche	*anti*
*r*N(1)N(2)	142.8	142.3
*r*N(2)Si(3)	171.5	171.2
*r*N(2)C(7)	145.9	145.0
∠N(1)-N(2)-Si(3)	110.2	102.3
∠N(1)-N(2)-C(7)	118.8	121.0
∠Si(3)-N(2)-C(7)	126.5	136.8
ϕN(1)N(2)Si(3)Cl(6)	69.5	180.0
Si(3)···N(1)	258.2	244.9

[a] Atom numbering as for **1**, given in Figure 1.

Table 8 shows considerable differences between the two conformers of $ClH_2SiN(Me)NMe_2$. Perhaps most noticeable is the large difference between the calculated values for ∠NNSi, which is 7.9° smaller in the *anti* conformer than in the *gauche* (102.3 and 110.2° respectively). This can be attributed to the presence of the electron withdrawing element in the *anti* position having a stronger effect than occurs in the *gauche* position. In fact, ∠NNSi for the *gauche* conformer (110.2°) closely resembles that obtained in calculations carried out on $H_3SiN(Me)NMe_2$, which has an ∠NNSi of 109.1°.[1] This shows that having the electronegative atom in the *gauche* position in no way encourages an increase in the strength of the Si β-N interaction. A large difference between conformers was also seen in $ClH_2SiONMe_2$.[2] In this case, the *anti* conformer was calculated (MP2/6-311+G**) to have a SiON angle 12.9° smaller than that in the *gauche* conformer (91.6 and 104.5° respectively). Again, ∠SiON in the *gauche* conformer in $ClH_2SiONMe_2$ closely resembles that of the unsubstituted analogue $H_3SiONMe_2$ (104.5 and 102.5° respectively). This again demonstrates that for the electronegative atom to affect the value of the ∠SiON or ∠SiNN and therefore the strength of the Si β-N interaction it is necessary for it to be in the *anti* position [i.e. ϕN(1)N(2)Si(3)Cl(6) of 180.0°].

6.4.3 Removing the acceptor and donor centres. Further calculations were carried out on $ClH_2Y^SN(Me)Y^NMe_2$, where Y^S is changed from Si to C, and Y^N is changed from N to CH to investigate the structural effects of removing the donor and acceptor groups. As with the examples in the previous chapter, it is expected to have a noticeable effect on the resultant structures. The results from these calculations are given in Table 9. Cartesian coordinates for the calculated structures are given in Appendix E.

Table 9 Selected parameters calculated at the MP2/6-311+G** for $ClH_2SiN(Me)NMe_2$, $ClH_2SiN(Me)CHMe_2$, $ClH_2CN(Me)NMe_2$. Distances are given in pm and angles in °.

		no donor	no acceptor
	$ClH_2SiN(Me)NMe_2$	$ClH_2SiN(Me)CHMe_2$	$ClH_2CN(Me)NMe_2$
*r*N/C-N	142.8	147.4	142.3
*r*N-Si/C	171.5	171.1	140.0
*r*N-C	145.9	146.3	146.0
N/C - N - Si/C	110.2	119.6	113.1
N/C - N - C	118.8	116.0	117.6
Si/C - N - C	126.5	119.5	116.0
Σ^a	355.5	355.1	346.7
Si/C···N/C	258.2	275.4	235.5

[a] where Σ represents the sum of the three angles around the α-N [N(2)].

As seen in the previous chapter, removing the donor or the acceptor atom increases ∠NNSi. Although $ClH_2SiN(Me)NMe_2$ is not itself completely planar at the α-N. From Table 9 it can be seen that there is an even larger shift away from planarity in $ClH_2CN(Me)NMe_2$. Figure 5 shows the geometry of $ClH_2CN(Me)NMe_2$. It is also worth remembering calculations carried out in the previous chapter that revealed similar large shifts from planarity in the case of $F_3SiN(Me)NMe_2$ to marked pyramidal coordination in $F_3CN(Me)NMe_2$ (with the three angles around the α-N adding up to 360.0 and 342.7° respectively). There is also a large difference in the values calculated for the angle between the two groups on the α-N (∠Si/C-N-C). The original compound, $ClH_2SiN(Me)NMe_2$ has the largest angle (∠SiNC 126.5°), which decreases to 116.0° upon removal of the acceptor silicon. This is probably due the increase in the value calculated for ∠NNSi/C, which causes a reduction in the value for ∠Si/CNC. This effect is the same as that observed in the previous chapter, where there was also a reduction in the ∠C/Si-N-N angle caused by a corresponding increase in ∠NNSi/C.

Figure 5 Two views of $ClH_2CN(Me)NMe_2$.

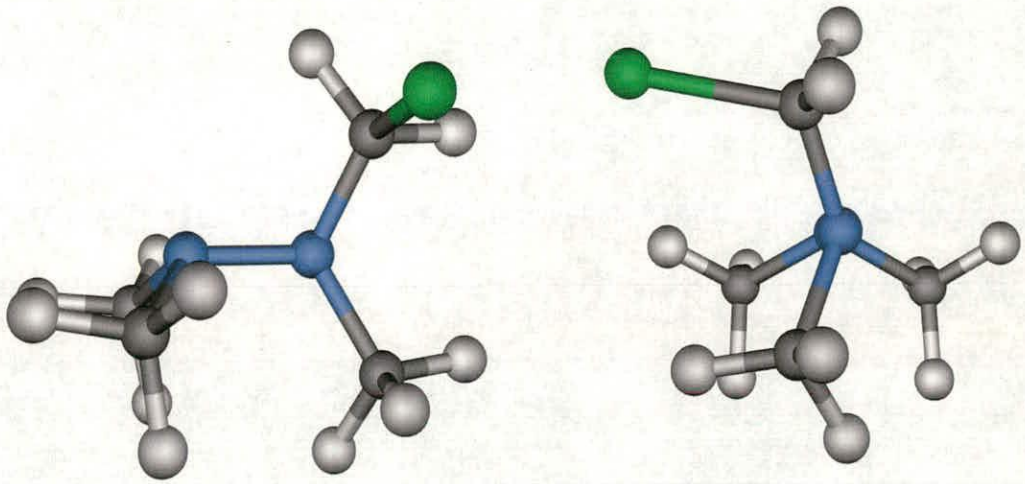

6.5 Conclusions

As compared to the work detailed in the previous chapter, $ClH_2SiN(Me)NMe_2$ was found to have less strong attractive interactions between silicon and geminal nitrogen. However, in investigative calculations, the *anti* conformer [N(1)N(2)Si(3)Cl(6) of 180.0°] (the presence of which was not found in this refinement based on the gas-phase data) was found to have a decreased ∠NNSi when compared to the *gauche* conformer, which was found in the gas-phase experiment.

Upon comparing these results with previous ones from the literature, it was found that this also occurred in the hydroxylaminosilane analogue, $ClH_2SiONMe_2$, where the *anti* conformer was also found to have a considerably decreased ∠SiON when compared to the *gauche* conformer. The effect of the electronegative atom on the Si β-N interaction was therefore only found to occur when the electronegative atom was in an *anti* position.

As in the previous chapter, calculations were carried out on analogous compounds, with the "donor" and "acceptor" centres replaced by other non-interacting elements. Again, this was seen to remove the interaction, illustrated by increased angles between the "donor" and "acceptor" centres. As the α-N was not planar in $ClH_2SiN(Me)NMe_2$, there was a less dramatic change in coordination geometry at this site as compared to the previous chapter. However, there was still a noticeable increase in pyramidal nature at the α-N.

6.6 Further Work

This compound would perhaps benefit from a mixed-conformer electron diffraction refinement to rule out completely the possible presence of a percentage of the *anti* conformer Time pressure has prevented this from being included in this study, and in any case it is thought the be highly unlikely that any useful information would be obtained.

As in the previous chapter, there is plenty of scope for further work on these very interesting compounds, with investigation into different substitutions on both the α- and β-nitrogen atoms as well as the silicon. For example, it would be interesting to investigate substituting the α-N with two bulky groups (e.g. $SiMe_3$). This may destroy the narrow $\angle$NNSi found in this series of compounds, as it would be prevented by steric hindrance.

6.7 References

1. Mitzel, N. W. *Chem. Eur. J.*, **1998**, *4*, 692.

2. Mitzel, N. W.; Losehand, U. *J. Am. Chem. Soc.*, **1998**, *120*, 7320.

3. Gaussian 98 (Revision A.7), Frisch, M. J.; Trucks, G. W.; Schlegel, H. B.; Scuseria, G. E.; Robb, M. A.; Cheeseman, J. R.; Zakrzewski, V. G.; Montgomery, J. A.; Stratman, R. E.; Burant, J. C.; Dapprich, S.; Milliam, J. M; Daniels, A. D.; Kudin, K. N.; Strain, M. C.; Farkas, O.; Tomasi, J.; Barone, V.; Cossi, M.; Cammi, R.; Mennucci, B.; Pomelli, C.; Adamo, C.; Clifford, S.; Ochterski, J.; Petersson, G. A.; Ayala, P.Y.; Cui, Q.; Morokuma, K.; Malick, D. K.; Rabuck, A. D.; Raghavachari, K.; Foresman, J. B.; Cioslowski, J.; Ortiz, J. V.; Baboul, A. G.; Stefanov, B. B.; Liu, C.; Liashenko, A.; Piskorz, P.; Komaromi, I.; Gomperts, R.; Martin, R. L.; Fox, D. J.; Keith, T.; Al-Laham, M. A.; Peng, C. Y.; Nanayakkara, A.; Gonzalez, C.; Challacombe, M.; Gill, P. M. W.; Johnson, B. G.; Chen, W.; Wong, M. W.; Andres, J. L.; Gonzales, C.; Head-Gordon, M.; Replogle, E. S.; Pople, J. A. Gaussian, Inc., Pittsburgh PA, **1998**.

4. Binkley, J. S.; Pople, J. A.; Hehre, W. J. *J. Am. Chem. Soc.*, **1980**, *102*, 939.

5. Gordon, M. S.; Binkley, J. S.; Pople, J. A.; Pietro, W. J.; Hehre, W. J. *J. Am. Chem. Soc.*, **1982**, *104*, 2979.

6. Pietro, W. J.; Francl, M. M.; Hehre, W. J.; DeFrees, D. J.; Pople, J. A.; Binkley, J. S. *J. Am. Chem. Soc.*, **1982**, *103*, 5039.

7. Hehre, W. J.; Ditchfield, R.; Pople, J. A. *J. Chem. Phys.*, **1972**, *56*, 2257.

8 Hariharan, P. C.; Pople, J. A. *Theor. Chim. Acta*, **1973**, *28*, 213.

9. Gordon, M. S. *Chem. Phys. Lett.*, **1980**, *76*, 163.

10. Krishnan, R; Binkley J. S.; Seeger, R; Pople, J. A. *J. Chem. Phys.*, **1980**, *72*, 650.

11. Huntley, C. M.; Laurenson, G. S.; Rankin, D. W. H. *J. Chem. Soc., Dalton Trans.*, **1980**, 954.

12. Lewis, J. R.; Brain, P. T.; Rankin, D. W. H. *Spectrum*, **1997**, *15*, 7.

13. Cradock, S.; Koprowski, J. *J. Mol. Struct.*, **1982**, *77*, 113.

14. Boyd, A. S. F.; Laurenson, G. S.; Rankin, D. W. H. *J. Mol. Struct.*, **1981**, *71*, 217.

15. Ross, A. W.; Fink M.; Hilderbrandt, R. in *International Tables for Crystallography*, ed. A. J. C. Wilson, Vol. C, Kluwer Academic Publishers, Dordrecht, **1992**, p.245.

16. Hedberg, L.; Mills, I. M. *J. Mol. Struct.*, **1993**, *160*, 117.

17. Blake, A. J.; Brain, P. T.; McNab, H.; Millar, J.; Morrison, C. A.; Parsons, S.; Rankin, D. W. H.; Robertson, H. E.; Smart, B. A. *J. Phys. Chem.*, **1996**, *100*, 12280; Brain, P. T.; Morrison, C. A.; Parsons, S.; Rankin, D. W. H. *J. Chem. Soc., Dalton Trans.*, **1996**, 4589.

Appendix A

Supplementary data for of *trans*-1,2-dichloro-1,2-disilylethene and 1-bromo-1-silylethene

Table 1 Calculated coordinates for lowest energy conformer of $(SiH_3)ClCCCl(SiH_3)$ at the MP2/6-31G* level.

Atom	*x*	*y*	*z*
C(1)	0.0000	0.6758	0.0000
C(2)	0.0000	-0.6758	0.0000
Cl(3)	-1.5625	1.4677	0.0000
Si(4)	1.5232	1.8088	0.0000
Cl(5)	1.5625	-1.4678	0.0000
Si(6)	-1.5233	-1.8088	0.0000
H(7)	1.0262	3.2032	0.0000
H(8)	2.3347	1.5519	1.2139
H(9)	2.3347	1.5519	-1.2139
H(10)	-1.0262	-3.2033	0.0000
H(11)	-2.3347	-1.5519	1.2139
H(12)	-2.3347	-1.5519	-1.2139
Energy		-1576.6609 Hartrees	

Table 2 Calculated coordinates for second lowest energy conformer of $(SiH_3)ClCCCl(SiH_3)$ at the MP2/6-31G* level.

Atom	*x*	*y*	*z*
C(1)	0.0765	-0.6947	0.0000
C(2)	0.0000	0.6543	0.0000
Cl(3)	1.6592	-1.4426	0.0000
Si(4)	-1.4002	-1.8921	0.0000
Cl(5)	-1.6164	1.3471	0.0000
Si(6)	1.3393	1.9934	0.0000
H(7)	-0.8443	-3.2639	0.0000
H(8)	-2.2221	-1.6716	1.2140
H(9)	-2.2221	-1.6716	-1.2140
H(10)	2.6958	1.4077	0.0000
H(11)	1.1296	2.8231	1.2108
H(12)	1.1296	2.8231	-1.2108
Energy		-1576.6617 Hartrees	

Table 3 Calculated coordinates for third lowest energy conformer of $(SiH_3)ClCCCl(SiH_3)$ at the MP2/6-31G* level.

Atom	*x*	*y*	*z*
C(1)	0.0000	0.6751	0.0000
C(2)	0.0000	-0.6751	0.0000
Cl(3)	1.5499	1.5035	0.0000
Si(4)	-1.4300	1.9204	0.0000
Cl(5)	-1.5499	-1.5035	0.0000
Si(6)	1.4300	-1.9203	0.0000
H(7)	2.7483	-1.2532	0.0000
H(8)	1.2728	-2.7609	1.2112
H(9)	1.2728	-2.7609	-1.2112
H(10)	-2.7483	1.2532	0.0000
H(11)	-1.2728	2.7609	1.2112
H(12)	-1.2728	2.7609	-1.2112
Energy		-1573.6625 Hartrees	

Table 4 Calculated coordinates for third lowest energy conformer of H_2CCHBr at the MP2/6-31G* level.

Atom	*x*	*y*	*z*
C(1)	0.8285	1.8244	0.0000
C(2)	0.0000	0.7669	0.0000
Br(3)	0.7438	-0.9964	0.0000
Si(4)	-1.8766	0.8632	0.0000
H(5)	-2.2459	2.2988	0.0000
H(6)	-2.4059	0.1925	1.2077
H(7)	-2.4059	0.1925	-1.20772
H(8)	1.9104	1.7271	0.0000
H(9)	0.4153	2.8296	0.0000
Energy		-2937.8677 Hartrees	

Appendix B

Supplementary data for
1,1,1,4,4,4-hexachloro-1,4-disilabutane

Table 1 Calculated coordinates for the two energy minima of $SiCl_3CH_2CH_2SiCl_3$ at the HF/6-31G* level.

	anti			*gauche*		
Atom	*x*	*y*	*z*	*x*	*y*	*z*
C(1)	-0.0148	0.7716	0.0000	-0.1590	0.7559	-0.8112
C(2)	0.0148	-0.7716	0.0000	0.1590	-0.7559	-0.8112
Si(3)	-1.7323	1.5140	0.0000	-1.2588	1.5280	0.4987
Si(4)	1.7323	-1.5140	0.0000	1.2588	-1.5280	0.4987
Cl(5)	1.5950	-3.5527	0.0000	1.8861	-3.3373	-0.2266
Cl(6)	2.7725	-0.9244	1.6603	0.2843	-1.8688	2.2591
Cl(7)	2.7725	-0.9244	-1.6603	2.9042	-0.3668	0.8554
Cl(8)	-1.5950	3.5527	0.0000	-1.8861	3.3373	-0.2266
Cl(9)	-2.7725	0.9244	1.6603	-0.2843	1.8688	2.2591
Cl(10)	-2.7725	0.9244	-1.6603	-2.9042	0.3668	0.8554
H(11)	0.5027	1.1657	-0.8708	-0.6588	0.9833	-1.7499
H(12)	0.5027	1.1657	0.8708	0.7610	1.3352	-0.8255
H(13)	-0.5027	-1.1657	-0.8708	0.6588	-0.9833	-1.7499
H(14)	-0.5027	-1.1657	0.8708	-0.7610	-1.3352	-0.8255
Energy	-3413.1313 Hartrees			-3413.1249 Hartrees		

Table 2 Calculated coordinates for the two energy minima of $CH_3CH_2CH_2CH_3$ at the HF/6-31G* level.

	anti			*gauche*		
Atom	*x*	*y*	*z*	*x*	*y*	*z*
C(1)	-0.5491	0.5324	0.0000	-0.4565	0.6159	0.6472
C(2)	0.5491	-0.5324	0.0000	0.4565	-0.6159	0.6473
C(3)	-0.0004	1.9589	0.0000	-0.1883	1.5974	-0.4950
C(4)	0.0004	-1.9589	0.0000	0.1883	-1.5974	-0.4950
H(5)	0.8032	-2.6898	-0.0001	0.8314	-2.4686	-0.4157
H(6)	-0.6138	-2.1431	0.8771	-0.8412	-1.9443	-0.4755
H(7)	-0.6141	-2.1430	-0.8768	0.3675	-1.1487	-1.4668
H(8)	-0.8032	2.6898	-0.0001	-0.8314	2.4686	-0.4157
H(9)	0.6138	2.1431	0.8771	0.8412	1.9443	-0.4755
H(10)	0.6141	2.1430	-0.8768	-0.3675	1.1487	-1.4668
H(11)	-1.1866	0.3900	0.8703	-0.3312	1.1408	1.5913
H(12)	-1.1865	0.3900	-0.8703	-1.4953	0.2936	0.6147
H(13)	1.1865	-0.3900	-0.8703	1.4953	-0.2936	0.6147
H(14)	1.1866	-0.3900	0.8703	0.3312	-1.1408	1.5913
Energy	-157.2984 Hartrees			-157.2968 Hartrees		

Table 3 Calculated coordinates for the two energy minima of $CH_3CH_2CH_2SiH_3$ at the HF/6-31G* level.

	anti			*gauche*		
Atom	*x*	*y*	*z*	*x*	*y*	*z*
C(1)	-0.5870	0.3984	0.0001	-0.5747	0.4316	0.7089
C(2)	0.5306	-0.6568	0.0000	0.3617	-0.7905	0.7173
Si(3)	0.0239	2.1896	0.0001	-0.1296	1.8306	-0.4904
C(4)	-0.0029	-2.0894	0.0000	0.2792	-1.6455	-0.5479
H(5)	0.8085	-2.8112	-0.0001	0.9208	-2.5174	-0.4672
H(6)	-0.6152	-2.2775	0.8773	-0.7356	-1.9957	-0.7148
H(7)	-0.6155	-2.2775	-0.8771	0.5859	-1.0944	-1.4315
H(8)	-1.1199	3.1270	-0.0008	-1.0095	2.9934	-0.2443
H(9)	0.8480	2.4601	1.1985	1.2734	2.2530	-0.2835
H(10)	0.8493	2.4595	-1.1976	-0.2857	1.4325	-1.9052
H(11)	-1.2276	0.2531	0.8690	-0.5922	0.8723	1.7046
H(12)	-1.2278	0.2531	-0.8687	-1.5963	0.1099	0.5123
H(13)	1.1677	-0.5142	-0.8697	1.3882	-0.4660	0.8692
H(14)	1.1679	-0.5142	0.8695	0.1143	-1.4139	1.5730
Energy		-408.3381 Hartrees			-408.3364 Hartrees	

Table 4 Calculated coordinates for the two energy minima of $SiH_3CH_2CH_2SiH_3$ at the HF/6-31G* level.

	anti			*gauche*		
Atom	*x*	*y*	*z*	*x*	*y*	*z*
C(1)	0.0000	0.7733	0.0000	-0.1386	0.7605	-0.8190
C(2)	0.0000	-0.7733	0.0000	0.1386	-0.7605	-0.8190
Si(3)	-1.7356	1.5313	0.0000	-1.2471	1.4281	0.5676
Si(4)	1.7356	-1.5313	0.0000	1.2471	-1.4281	0.5676
H(5)	1.6646	-3.0084	0.0000	1.5817	-2.8408	0.2901
H(6)	2.4843	-1.0961	1.1988	0.5816	-1.3604	1.8845
H(7)	2.4843	-1.0961	-1.1988	2.5027	-0.6499	0.6394
H(8)	-1.6646	3.0084	0.0000	-1.5817	2.8408	0.2901
H(9)	-2.4843	1.0961	1.1988	-0.5816	1.3604	1.8845
H(10)	-2.4843	1.0961	-1.1988	-2.5027	0.6499	0.6394
H(11)	0.5397	1.1470	-0.8682	-0.6199	1.0319	-1.7573
H(12)	0.5397	1.1470	0.8682	0.8000	1.3116	-0.8053
H(13)	-0.5397	-1.1470	-0.8682	0.6199	-1.0319	-1.7573
H(14)	-0.5397	-1.1470	0.8682	-0.8000	-1.3116	-0.8053
Energy		-659.3774 Hartrees			-659.3751 Hartrees	

Table 5 Calculated coordinates for the two energy minima of $SiCl_3CH_2CH_2CH_3$ at the HF/6-31G* level.

	anti			*gauche*		
Atom	*x*	*y*	*z*	*x*	*y*	*z*
C(1)	-1.4586	0.0000	0.2884	-1.4586	0.0000	0.2884
C(2)	-1.5989	0.0000	1.8208	-1.5989	0.0000	1.8208
Si(3)	0.2872	0.0000	-0.3680	0.2872	0.0000	-0.3680
C(4)	-3.0625	0.0000	2.2619	-3.0625	0.0000	2.2619
H(5)	-3.1392	0.0000	3.3443	-3.1392	0.0000	3.3443
H(6)	-3.5833	0.8778	1.8912	-3.5833	0.8778	1.8912
H(7)	-3.5833	-0.8778	1.8912	-3.5833	-0.8778	1.8912
Cl(8)	0.2582	0.0000	-2.4172	0.2582	0.0000	-2.4172
Cl(9)	1.3156	1.6597	0.2555	1.3156	1.6597	0.2555
Cl(10)	1.3156	-1.6597	0.2555	1.3156	-1.6597	0.2555
H(11)	-1.9580	-0.8704	-0.1332	-1.9580	-0.8704	-0.1332
H(12)	-1.9580	0.8704	-0.1332	-1.9580	0.8704	-0.1332
H(13)	-1.0993	-0.8706	2.2344	-1.0993	-0.8706	2.2344
H(14)	-1.0993	0.8706	2.2344	-1.0993	0.8706	2.2344
Energy		-1785.2167	Hartrees		-1785.2138	Hartrees

Table 6 Calculated coordinates for the two energy minima of $CCl_3CH_2CH_2SiCl_3$ at the HF/6-31G* level.

	anti			*gauche*		
Atom	*x*	*y*	*z*	*x*	*y*	*z*
C(1)	-0.5133	0.6516	-0.0249	-0.3126	0.7823	0.7442
C(2)	0.5960	-0.4100	-0.0399	0.6178	-0.4418	0.6682
C(3)	0.0360	2.0741	-0.0555	-0.3692	1.6478	-0.5105
Si(4)	-0.0061	-2.1783	-0.0038	0.1532	-1.8843	-0.4324
Cl(5)	1.6043	-3.4380	-0.0371	1.3976	-3.4492	-0.0047
Cl(6)	-1.0930	-2.5461	1.6887	-1.7785	-2.4617	-0.0759
Cl(7)	-1.1820	-2.5805	-1.6295	0.3301	-1.4573	-2.4267
Cl(8)	-1.2933	3.2407	-0.2578	-1.5675	2.9456	-0.2871
Cl(9)	0.9708	2.4606	1.4104	1.2222	2.3462	-0.9030
Cl(10)	0.7011	2.2256	-0.8868	-0.6801	1.1023	-1.3816
H(11)	-1.1432	0.5464	0.8498	0.0057	1.4108	1.5669
H(12)	-1.1468	0.5415	-0.8973	-1.3267	0.4674	0.9609
H(13)	1.2136	-0.3015	-0.9292	1.6297	-0.1414	0.4142
H(14)	1.2559	-0.2859	0.8135	0.6784	-0.8667	1.6679
Energy		-2702.0097	Hartrees		-2703.0066	Hartrees

Table 7 Calculated coordinates for the two energy minima of $CCl_3CH_2CH_2CCl_3$ at the HF/6-31G* level.

	anti			*gauche*		
Atom	*x*	*y*	*z*	*x*	*y*	*z*
C(1)	-0.5520	0.5489	-0.0211	-0.3925	0.6420	0.6598
C(2)	0.5420	-0.5217	-0.0383	0.5081	-0.6001	0.6187
C(3)	0.0345	1.9556	-0.0549	-0.3172	1.6268	-0.5031
C(4)	0.0317	-1.9665	-0.0062	0.2090	-1.7069	-0.4047
Cl(5)	1.4360	-3.0570	-0.0430	1.2569	-3.0957	-0.0262
Cl(6)	-0.8945	-2.2843	1.4767	-1.4869	-2.2347	-0.3020
Cl(7)	-0.9921	-2.3165	-1.4183	0.5550	-1.1990	-2.0725
Cl(8)	-1.2654	3.1525	-0.2653	-1.4878	2.9424	-0.2270
Cl(9)	0.9746	2.3279	1.4123	1.3213	2.3004	-0.6939
Cl(10)	0.7055	2.0910	-0.8843	-0.5792	1.1897	-1.4452
H(11)	-1.1782	0.4555	0.8555	-0.1316	1.1822	1.5618
H(12)	-1.1854	0.4496	-0.8929	-1.4283	0.3455	0.7610
H(13)	1.1455	-0.4264	-0.9337	1.5445	-0.3200	0.4840
H(14)	1.1978	-0.4087	0.8140	0.4288	-1.0724	1.5897
Energy		-2451.7698 Hartrees			-2451.7660 Hartrees	

Appendix C

Supplementary data for bistrichlorosilyl-dimethylgermane

Table 1 Cartesian coordinates for lowest energy conformer of $Me_2Ge(SiCl_3)_2$ (HF/6-31G*).

Atom	*x*	*y*	*z*
Ge(1)	0.0000	0.0000	1.0752
C(2)	1.6178	0.0000	2.1616
C(3)	-1.6178	0.0000	2.1616
H(4)	2.4940	0.0000	1.5259
H(5)	-2.4940	0.0000	1.5259
H(6)	1.6347	0.8796	2.7947
H(7)	1.6347	-0.8796	2.7947
H(8)	-1.6347	-0.8796	2.7947
H(9)	-1.6347	0.8796	2.7947
Cl(10)	0.0000	-1.9808	-0.2761
Cl(11)	0.0000	1.9808	-0.2761
Cl(12)	0.0000	-3.6195	0.9713
Cl(13)	0.0000	3.6195	0.9713
Cl(14)	-1.6651	-2.1016	-1.4687
Cl(15)	1.6651	-2.1016	-1.4687
Cl(16)	1.6651	2.1016	-1.4687
Cl(17)	-1.6651	2.1016	-1.4687
Energy		-5487.5832 Hartrees	

Table 2 Cartesian coordinates for lowest energy conformer of $Me_2Ge(SiCl_3)_2$ (HF/6-31G*).

Atom	*x*	*y*	*z*
Ge(1)	-1.0555	-0.3119	0.0000
C(2)	-2.0926	-0.6186	1.6201
C(3)	-2.0926	-0.6186	-1.6201
H(4)	-1.4765	-0.4384	2.4916
H(5)	-1.4765	-0.4384	-2.4916
H(6)	-2.9487	0.0458	1.6414
H(7)	-2.4482	-1.6419	1.6420
H(8)	-2.9487	0.0458	-1.6414
H(9)	-2.4482	-1.6419	-1.6420
Cl(10)	0.8451	-1.8052	0.0000
Cl(11)	-0.3188	1.9677	0.0000
Cl(12)	2.6648	-0.8590	0.0000
Cl(13)	-1.9727	3.1950	0.0000
Cl(14)	0.7868	-3.0184	1.6607
Cl(15)	0.7868	-3.0184	-1.6607
Cl(16)	0.7868	2.4150	-1.6692
Cl(17)	0.7868	2.4150	1.6692
Energy		-5487.5816 Hartrees	

Appendix D

Supplementary data for $F_3SiN(Me)NMe_2$ and $F_3SiN(SiMe_3)NMe_2$

Table 1 Cartesian coordinates for the calculated (MP2/6-311+G**) structure of $F_3SiN(Me)NMe_2$.

Atom	*x*	*y*	*z*
N(1)	-1.3851	0.3841	0.0000
N(2)	0.0000	0.7230	0.0000
Si(3)	0.8451	-0.7299	0.0000
F(4)	2.4148	-0.4131	0.0000
F(5)	0.5515	-1.6529	1.2714
F(6)	0.5515	-1.6529	-1.2714
C(7)	0.4333	2.1134	0.0000
H(8)	1.5255	2.1227	0.0000
H(9)	0.0872	2.6456	-0.8925
H(10)	0.0872	2.6456	0.8925
C(11)	-2.0566	0.8457	1.2129
C(12)	-2.0566	0.8457	-1.2129
H(13)	-2.1283	1.9433	1.2685
H(14)	-3.0683	0.4321	1.2231
H(15)	-1.5111	0.4729	2.0820
H(16)	-2.1283	1.9433	-1.2685
H(17)	-3.0683	0.4321	-1.2231
H(18)	-1.5111	0.4729	-2.0820
Energy		-816.8556 Hartrees	

Table 2 Cartesian coordinates for the calculated (MP2/6-311+G**) structure of $F_3SiN(SiMe_3)NMe_2$

Atom	*x*	*y*	*z*
N(1)	-0.4907	1.5375	0.0231
N(2)	-0.0177	0.1620	-0.1247
Si(3)	-1.5660	-0.5045	-0.0005
F(4)	-1.4732	-2.1072	-0.0809
F(5)	-2.3199	-0.2071	1.3815
F(6)	-2.5603	-0.0767	-1.1793
Si(7)	1.6529	-0.4438	-0.0334
C(8)	2.8250	0.7256	-0.9147
C(9)	2.1945	-0.6450	1.7516
C(10)	1.6370	-2.1081	-0.8836
H(11)	3.8334	0.2956	-0.8872
H(12)	2.5492	0.8606	-1.9648
H(13)	2.8797	1.7111	-0.4430
H(14)	3.1778	-1.1270	1.8023
H(15)	2.2685	0.3141	2.2732
H(16)	1.4874	-1.2741	2.3027
H(17)	2.6516	-2.5217	-0.9034
H(18)	1.2872	-2.0197	-1.9167
H(19)	0.9892	-2.8235	-0.3706
C(20)	0.0198	2.1743	1.2324
C(21)	-0.2448	2.3286	-1.1809
H(22)	1.1085	2.3351	1.1929
H(23)	-0.4733	3.1440	1.3436
H(24)	-0.2244	1.5501	2.0939
H(25)	0.8240	2.5169	-1.3488
H(26)	-0.7635	3.2851	-1.0685
H(27)	-0.6609	1.7997	-2.0397
Energy		-1185.5274 Hartrees	

Table 3 Cartesian coordinates for the calculated (MP2/6-311+G**) structure of $F_3CN(Me)NMe_2$.

Atom	*x*	*y*	*z*
N(1)	-1.2016	-0.4341	0.0846
N(2)	-0.1186	0.2960	-0.4783
C(3)	1.1078	-0.2126	-0.0089
F(4)	2.1217	0.4324	-0.6108
F(5)	1.3072	-0.0559	1.3325
F(6)	1.2270	-1.5145	-0.2592
C(7)	-0.2236	1.7596	-0.4792
H(8)	0.5564	2.1677	-1.1212
H(9)	-1.1916	2.0239	-0.9084
H(10)	-0.1391	2.2000	0.5218
C(11)	-1.8001	0.1805	1.2702
C(12)	-2.1933	-0.6953	-0.9515
H(13)	-2.3392	1.1162	1.0510
H(14)	-2.5133	-0.5364	1.6843
H(15)	-1.0295	0.3708	2.0183
H(16)	-2.6829	0.2229	-1.3181
H(17)	-2.9618	-1.3503	-0.5322
H(18)	-1.7060	-1.2004	-1.7860
Energy		-565.6172 Hartrees	

Table 4 Cartesian coordinates for the calculated (MP2/6-311+G**) structure of $F_3SiN(Me)CHMe_2$.

Atom	*x*	*y*	*z*
C(1)	1.5187	-0.4940	0.0842
N(2)	0.4005	0.4459	-0.1354
Si(3)	-1.1793	-0.1090	0.0035
F(4)	-2.2017	0.9494	-0.6182
F(5)	-1.3642	-1.5133	-0.7396
F(6)	-1.6874	-0.3862	1.4994
C(7)	0.7393	1.8653	-0.2483
H(8)	-0.1466	2.4294	-0.5472
H(9)	1.1068	2.2786	0.6974
H(10)	1.5021	2.0178	-1.0178
C(11)	2.3805	-0.6340	-1.1715
C(12)	2.3529	-0.1086	1.3062
H(13)	2.8825	0.3077	-1.4136
H(14)	3.1543	-1.3917	-1.0121
H(15)	1.7665	-0.9335	-2.0248
H(16)	2.8974	0.8247	1.1335
H(17)	3.0901	-0.8898	1.5151
H(18)	1.7166	0.0149	2.1875
H(19)	1.0684	-1.4750	0.2834
Energy		-800.8731 Hartrees	

Table 5 Cartesian coordinates for the calculated (MP2/6-311+G**) structure of $F_3CN(SiMe_3)NMe_2$

Atom	*x*	*y*	*z*
N(1)	-1.0208	1.3623	-0.0094
N(2)	-0.3536	0.1135	-0.1533
C(3)	-1.3031	-0.9044	-0.0341
F(4)	-0.6939	-2.1070	-0.1113
F(5)	-1.9777	-0.8901	1.1419
F(6)	-2.2460	-0.8708	-0.9956
Si(7)	1.4154	-0.1754	-0.0088
C(8)	2.3153	1.3843	-0.5302
C(9)	1.8532	-0.6122	1.7603
C(10)	1.9427	-1.5423	-1.1747
H(11)	3.3859	1.2001	-0.3770
H(12)	2.1697	1.5972	-1.5931
H(13)	2.0535	2.2766	0.0417
H(14)	2.9167	-0.8638	1.8456
H(15)	1.6493	0.2195	2.4423
H(16)	1.2766	-1.4777	2.1030
H(17)	3.0270	-1.4857	-1.3262
H(18)	1.4612	-1.4320	-2.1515
H(19)	1.7043	-2.5364	-0.7910
C(20)	-0.7293	2.0408	1.2473
C(21)	-0.8943	2.2130	-1.1860
H(22)	0.3021	2.4209	1.3198
H(23)	-1.4126	2.8904	1.3383
H(24)	-0.9183	1.3520	2.0726
H(25)	0.1058	2.6521	-1.3108
H(26)	-1.6206	3.0264	-1.0931
H(27)	-1.1429	1.6222	-2.0693
Energy		-934.2834 Hartrees	

Table 6 Cartesian coordinates for the calculated (MP2/6-311+G**) structure of $F_3SiN(SiMe_3)CHMe_2$

Atom	*x*	*y*	*z*
C(1)	-0.2383	1.7918	0.0002
N(2)	-0.0337	0.3136	-0.0002
C(3)	-1.3099	-0.7904	-0.0002
F(4)	-1.3003	-1.7727	1.2662
F(5)	-2.7366	-0.0659	-0.0013
F(6)	-1.2990	-1.7741	-1.2655
Si(7)	1.6676	-0.1972	0.0001
C(8)	1.7381	-2.0687	-0.0005
C(9)	2.5033	0.4761	-1.5376
C(10)	2.5024	0.4751	1.5386
H(11)	2.7893	-2.3784	0.0004
H(12)	1.2665	-2.5042	0.8854
H(13)	1.2681	-2.5035	-0.8876
H(14)	2.4586	1.5687	-1.5917
H(15)	3.5614	0.1908	-1.5540
H(16)	2.0329	0.0732	-2.4405
H(17)	2.4576	1.5676	1.5935
H(18)	3.5606	0.1899	1.5554
H(19)	2.0316	0.0715	2.4410
C(20)	-0.9407	2.2686	1.2709
C(21)	-0.9395	2.2695	-1.2708
H(22)	-0.4015	1.9214	2.1569
H(23)	-1.9668	1.8926	1.3139
H(24)	-0.9795	3.3630	1.2923
H(25)	-0.3994	1.9231	-2.1566
H(26)	-1.9655	1.8933	-1.3152
H(27)	-0.9785	3.3639	-1.2914
H(28)	0.7644	2.2386	0.0008
Energy		-1169.5507 Hartrees	

Appendix E

Supplementary data for $ClH_2SiN(Me)NMe_2$

Table 1 Cartesian coordinates for the two lowest energy calculated (MP2/6-311+G**) structures of $ClH_2SiN(Me)NMe_2$.

	anti			*gauche*		
Atom	*x*	*y*	*z*	*x*	*y*	*z*
N(1)	-1.3958	0.7733	0.0000	1.1997	0.4936	-0.3822
N(2)	0.0000	0.4946	0.0000	0.5321	-0.6847	0.0702
Si(3)	0.0297	-1.2175	0.0000	-1.0423	-0.7690	-0.6037
Cl(4)	2.0187	-1.8039	0.0000	-0.9989	-0.5403	-2.0497
H(5)	-0.5826	-1.7929	1.2081	-1.6207	-2.0690	-0.2257
H(6)	-0.5826	-1.7929	-1.2081	-2.3261	0.6780	0.1598
C(7)	0.9749	1.5679	0.0000	0.9829	-1.3164	1.3059
H(8)	1.9678	1.1124	0.0000	0.4221	-2.2460	1.4349
H(9)	0.8934	2.2012	-0.8922	2.0455	-1.5746	1.2468
H(10)	0.8934	2.2012	0.8922	0.8190	-0.6904	2.1922
C(11)	-1.8167	1.4712	1.2130	1.3283	1.5047	0.6656
C(12)	-1.8167	1.4712	-1.2130	2.4910	0.1625	-0.9762
H(13)	-1.4200	2.4970	1.2692	2.0288	1.2099	1.4641
H(14)	-2.9090	1.5206	1.2269	1.6974	2.4254	0.2062
H(15)	-1.4717	0.9057	2.0811	0.3457	1.6970	1.1008
H(16)	-1.4200	2.4970	-1.2692	3.2103	-0.2424	-0.2453
H(17)	-2.9090	1.5206	-1.2269	2.9155	1.0736	-1.4072
H(18)	-1.4717	0.9057	-2.0811	2.3355	-0.5704	-1.7698
Energy	-978.4926 Hartrees			-978.4958 Hartrees		

Table 2 Cartesian coordinates for the two lowest energy calculated (MP2/6-311+G**) structures of $ClH_2CN(Me)NMe_2$.

Atom	*x*	*y*	*z*
N(1)	0.9762	-0.5060	0.2737
N(2)	0.0810	0.5737	0.0158
C(3)	-1.5105	0.1941	0.5203
Cl(4)	-2.3147	1.4210	0.3859
H(5)	-2.2341	-0.9303	-0.4163
H(6)	-1.5043	-0.3720	1.8722
C(7)	0.5038	1.6388	-0.8871
H(8)	-0.2866	2.3933	-0.9145
H(9)	1.4161	2.1257	-0.5259
H(10)	0.6741	1.2855	-1.9116
C(11)	1.4024	-1.1777	-0.9521
C(12)	2.1142	-0.0711	1.0774
H(13)	2.0610	-0.5545	-1.5791
H(14)	1.9491	-2.0828	-0.6742
H(15)	0.5183	-1.4601	-1.5277
H(16)	2.7806	0.6254	0.5424
H(17)	2.6958	-0.9537	1.3575
H(18)	1.7410	0.4128	1.9820
Energy		-618.5374 Hartrees	

Table 3 Cartesian coordinates for the two lowest energy calculated (MP2/6-311+G**) structures of $ClH_2SiN(Me)CHMe_2$.

Atom	*x*	*y*	*z*
C(1)	-1.3989	0.3875	-0.4584
N(2)	-0.4834	-0.6321	0.0840
Si(3)	1.0899	-0.7876	-0.5696
Cl(4)	1.6676	-2.0661	-0.1339
H(5)	1.0236	-0.6157	-2.0266
H(6)	2.4183	0.6744	0.0990
C(7)	-0.7366	-1.0523	1.4619
H(8)	-0.0901	-1.9004	1.7051
H(9)	-0.5408	-0.2565	2.1921
H(10)	-1.7722	-1.3860	1.5796
C(11)	-2.7889	-0.1971	-0.7157
C(12)	-1.4722	1.6400	0.4201
H(13)	-3.2789	-0.4829	0.2203
H(14)	-3.4240	0.5467	-1.2080
H(15)	-2.7175	-1.0800	-1.3565
H(16)	-1.9683	1.4250	1.3719
H(17)	-2.0507	2.4187	-0.0873
H(18)	-0.4715	2.0291	0.6288
H(19)	-0.9830	0.6852	-1.4301
Energy		-962.5148 Hartrees	

Appendix F

Conformational Analysis with Both Experimental and Computational Data for Both Gaseous and Crystalline Phases: Unexpected Interactions in *N*-Methyldichloroacetamide

Conformational Analysis with Both Experimental and Computational Data for Both Gaseous and Crystalline Phases: Unexpected Interactions in *N*-Methyldichloroacetamide

Sarah L. Hinchley,[†] Heather E. Robertson,[†] Lorna J. McLachlan,[†] Carole A. Morrison,[†] David W. H. Rankin,*[,†] Stephen J. Simpson,[‡] and Emrys W. Thomas[§]

School of Chemistry, University of Edinburgh, West Mains Road, Edinburgh, EH9 3JJ, United Kingdom, Chemistry Department, School of Sciences, University of Salford, Salford, Greater Manchester, M5 4WT, United Kingdom, and Division of Biological Sciences, School of Environment and Life Sciences, University of Salford, Salford, Greater Manchester, M5 4WT, United Kingdom

Received: August 20, 2003; In Final Form: November 6, 2003

The structure of *N*-methyldichloroacetamide ($MeNHCOCHCl_2$) has been elucidated in the gaseous and solid states experimentally by gas electron diffraction and X-ray crystallography, and computationally with ab initio and plane-wave DFT methods. Although the main structural parameters generally agree well, the orientation of the $CHCl_2$ group relative to the carbonyl oxygen was found to be very different in the solid and gas phases. X-ray crystallography and solid-state plane-wave DFT methods indicate that the bond torsion angle ϕ(HCCO) is 180.0°, while ab initio and gas electron diffraction methods return ϕ(HCCO) as −13.1° and −31.8(22)°, respectively. Further investigation of this phenomenon was carried out by using various computational methods. The possibility of intermolecular H···O and Cl···O bonds, which would stabilize the solid-state structure, was investigated by both solid-state plane-wave DFT and single-point ab initio methods. Ab initio SCRF calculations were also employed to evaluate solvent effects on the structure, using the Onsager reaction field model.

Introduction

Rotational isomerism in several α-halo-substituted acetic acids and their derivatives has been intensively studied by ab initio, spectroscopic, and diffraction methods.[1−6] With regard to 2,2-dichloroacetic acid,[7] its methyl ester,[8] and acyl chloride,[9] several studies indicate clearly the presence of two low-energy conformers derived from rotational isomerism of the dichloromethyl group. They are syn conformers in which the HCCO torsion angle is ~0°, and gauche conformers in which this torsion angle is ~140° (with eclipsing of Cl and O atoms). A slight preference for the syn form is shown, particularly for the ester and acyl chloride. With regard to the *N*-methylamide of dichloroacetic acid, however, the available evidence (based on an IR study) indicates the presence of just one conformer in dilute tetrachloromethane solution, with stabilization of another conformer in the presence of added H-bond acceptors.[10] As chloramphenicol, an important antibiotic drug, contains the $-NHCOCHCl_2$ moiety, understanding of the conformations of such species, as free molecules, in solution, and in the solid phase, is important. In the absence of definitive structural data on this particular amide, a combined gas-phase electron diffraction, X-ray diffraction, and ab initio study has been undertaken to determine conformational preferences of the dichloromethyl group. This work complements a parallel modeling study[11] of the solution conformation of chloramphenicol.

Experimental Section

Synthesis. *N*-Methyldichloroacetamide (melting point 348 K, lit. mp 346−348 K) was prepared according to literature methods[12] by aminolysis of ethyl dichloroacetate in 30% w/v aqueous methylamine, followed by double re-crystallization from diethyl ether. A sample was provided for use in the gas electron diffraction apparatus without further purification.

Theoretical Methods. All geometry optimization and frequency calculations were performed on a dual-processor Pentium III 1000-MHz workstation with the Gaussian 98program.[13] The MP2/6-311++G** force-field calculations were performed with resources of the EPSRC National Service for Computational Chemistry Software, on a cluster of 6 HP ES40 computers. Each Alphaserver ES40 machine has four 833 MHz EV68 CPUs and 8 GB of memory. All MP2 calculations were frozen core [MP2(fc)]. The solvation calculations were performed on a single-processor NT Pentium 4 1.5 GHz workstation. Plane-wave DFT calculations were carried out with CASTEP version 2.2[14]on a Linux 800 MHz dual-processor PC.

Geometry Optimizations. An extensive search of the torsional potential of $MeNHCOCHCl_2$ was undertaken at the HF/3-21G*[15−17] level to locate all minima. Two different orientations of the N−C(O) bond were investigated, syn with ϕ(CNCO) = 0° and anti with ϕ(CNCO) = 180°. For each of these conformers, four possible orientations of the $CHCl_2$ group relative to the carbonyl oxygen were investigated, giving ϕ(HCCO) = 0°, 60°, 120°, and 180°. This gives eight possible structures: *syn0*, *syn60*, *syn120*, *syn180*, *anti0*, *anti60*, *anti120*, and *anti180*. For the syn structures investigated, two conformers, *syn0* and *syn120*, were found. For the anti structures (ϕ(CNCO) = 180°), two conformers were also located, *anti0* and *anti120*. For both the syn and anti conformers, the structures were of C_1 symmetry due to nonplanarity at the nitrogen atom, but one (*anti120*) was very close to C_s symmetry. Further geometry optimizations were undertaken for all the conformers at the HF and MP2 levels with the standard 6-31G*[18−20] basis set, and at

* Address correspondence to this author. E-mail: d.rankin@ed.ac.uk.
† School of Chemistry, University of Edinburgh.
‡ School of Sciences, University of Salford.
§ School of Environment and Life Sciences, University of Salford.

10.1021/jp036478h CCC: $27.50
Published on Web 12/10/2003

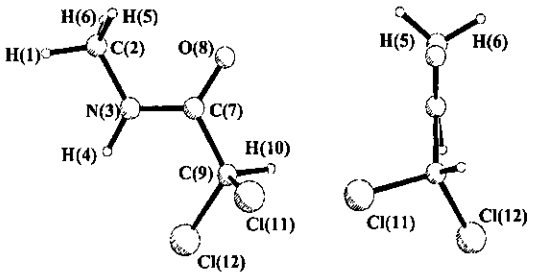

Figure 1. Molecular structure of $MeNHCOCHCl_2$ showing (a) a perspective view and (b) a view along the C(7)−N(3) bond.

the MP2 level with the 6-311G*,[21,22] 6-311+G*, and 6-311++G** basis sets. The lowest energy structure of $MeNHCOCHCl_2$ and the atom numbering scheme are shown in Figure 1.

Frequency Calculations. Numeric second derivatives of the energy with respect to nuclear coordinates calculated at the MP2/6-311++G** level for $MeNHCOCHCl_2$ gave the force field. This was used to provide estimates of the amplitudes of vibration (u) and the curvilinear corrections (k) for use in the gas electron diffraction (GED) refinements. This improved level of theory and large basis set were used for the force-field calculation, because a large change in ϕ(HCCO) was observed on the inclusion of diffuse functions. The analytic force fields calculated at the HF/6-31G* level were used to calculate the frequencies for all the optimized structures, which in turn provided information about the nature of stationary points.

Solvation Calculations. Self-consistent reaction field calculations were performed at the B3LYP/6-31G** level[23] with use of the Onsager model.[24] Two different solvent systems were investigated: tetrachloromethane (TCM) and dimethyl sulfoxide (DMSO). The solute was set to occupy a fixed spherical cavity of radius a_0 = 407 pm for both TCM and DMSO within the solvent field. Dielectric constants of ϵ = 2.23 and 46.7 were used for TCM and DMSO, respectively. In this model the molecular dipole interacts with the dielectric continuum, leading to a net stabilization that should be observable for each solvent system. A full potential search of the bond torsion ϕ(HCCO) at 20° intervals (0° to 360°) was performed for both tetrachloromethane and dimethyl sulfoxide.

Single-Point Energy Calculations. The crystal structure coordinates were used for ab initio molecular orbital (ab initio MO) single-point energy calculations to evaluate ab initio the strengths of the interactions within the solid-state structure. A monomer of *N*-methyldichloroacetamide and two dimers with different interactions were calculated with two different methods, MP2/6-311++G** and PW91PW91/6-311++G**. The strengths of the interactions would be overestimated by both MP2 and DFT methods unless Basis Set Superposition Error (BSSE) was corrected for. This was done by using the Counterpoise (CP) correction.[25] The first dimer investigated showed interlayer Cl···O bonding (Figure 2a), and the second displayed two intralayer H···O bonds (Figure 2b).

Plane-Wave DFT Calculations. A series of plane-wave DFT (PW-DFT) calculations were carried out on *N*-methyldichloroacetamide to investigate further the strengths of the interactions between the molecules in the solid phase. A generalized gradient approximation (GGA-PBE) was used for the exchange and correlation potential.[26] The wave function was generated by using a series of pseudopotentials and delocalized plane waves expressed at an energy cutoff of 300 eV.

Crystal Lattice Calculation. This calculation used the lattice vectors and atomic coordinates from the low-temperature crystal

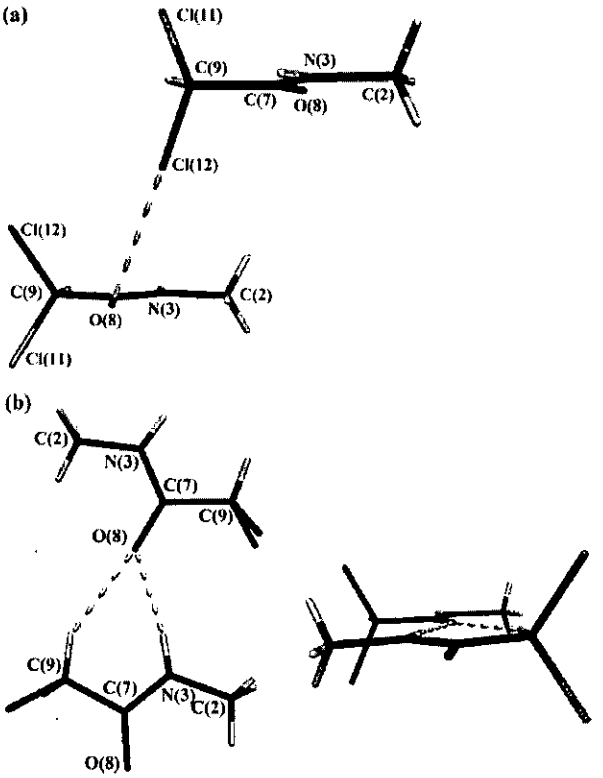

Figure 2. Solid-state dimer models used for the ab initio MO single point energy calculations of (a) the interlayer Cl···O interaction and (b) the intralayer H···O interactions.

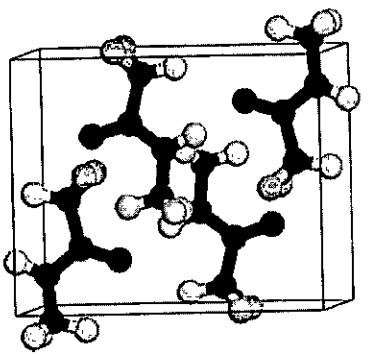

Figure 3. X-ray crystallographic structure of *N*-methyldichloroacetamide.

structure reported later in this paper. The unit cell volume and atom positions were allowed to optimize until convergence was achieved (changes in energy per atom to within 2.0×10^{-5} eV and forces within 0.05 eV $Å^{-1}$). The symmetry-reduced k-point sets used to sample the reciprocal space were generated by using Monkhurst−Pack grids[27] (dimensions 2 × 2 × 3, giving 2 k-points in the symmetry-reduced first Brillouin zone). A diagram of the unit cell is given in Figure 3.

Supercell Calculations. These two calculations involved an isolated molecule of *N*-methyldichloroacetamide in a 1200 × 1200 × 1200 pm^3 unit cell, the first being a single-point energy calculation, the second being a geometry optimization. The purpose of the periodic (PW-DFT) calculation was to investigate the properties of the intermolecular interactions within a periodic environment to contrast with results obtained from the ab initio MO single-point calculations. The starting geometry for the isolated molecule was taken from the optimized geometry of

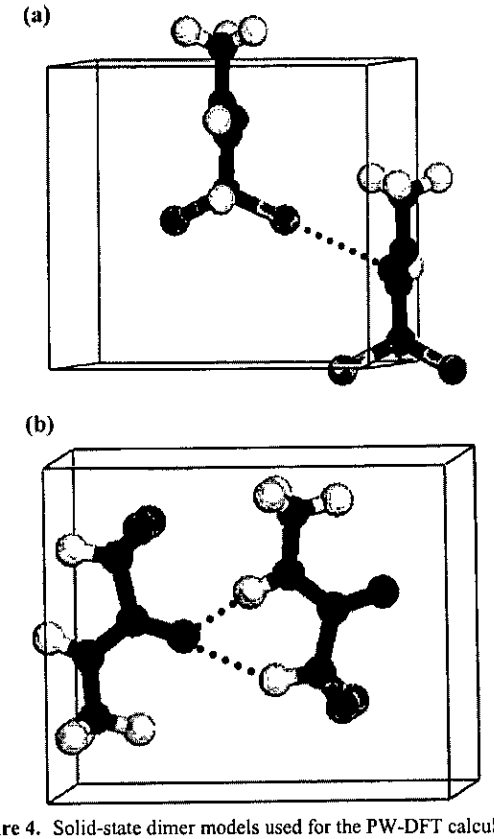

Figure 4. Solid-state dimer models used for the PW-DFT calculations of (a) the Cl···O interaction and (b) the H···O interactions.

the first calculation. The same energy cutoff and convergence criteria were used as in the crystal lattice. Integrations over the symmetrized Brillouin zone were performed using one *k*-point positioned at the Γ-point.

H···O and Cl···O Interactions. Calculations were carried out to determine the strengths of the two types of interactions, namely the combined strength of the hydrogen bonds and the Cl···O interaction. In the two models, two molecules were removed from the unit cell to destroy the hydrogen bonds in the first calculation and the Cl···O interaction in the second [see Figure 4, panels a and b]. The energies of the interactions were obtained by comparing the energy per molecule from these calculations with those from the optimized crystal lattice calculation. A cutoff energy of 300 eV was used, the same as for the supercell and crystal lattice calculations to allow comparison, and *k*-point sampling grids of 2 × 3 × 2.

Electron Diffraction Measurements. Data were collected with the Edinburgh gas diffraction apparatus.[28] An accelerating voltage of ca. 40.0 kV (electron wavelength ca. 6.0 pm) was used, while maintaining the sample and nozzle temperatures at 403 and 410 K, respectively. Scattering intensities were recorded at nozzle-to-plate distances of 98 and 252 mm on Kodak Electron Image films. The weighting points for the off-diagonal weight matrixes, correlation parameters, and scale factors for the two camera distances are given in Table S1 (Supporting Information), together with electron wavelengths, which were determined from the scattering patterns of benzene vapor, recorded immediately after the compound patterns and analysed in exactly the same way to minimize systematic errors in wavelengths and camera distances. The electron-scattering patterns were converted into digital form by using a PDS densitometer at the Institute of Astronomy, Cambridge University, UK with a scanning program described elsewhere.[29] Data reduction and least-squares refinements were carried out with standard programs,[30,31] employing the scattering factors of Ross et al.[32]

X-ray Diffraction Measurements. A suitable crystal was mounted on a glass fiber with epoxy resin and cooled in a stream of nitrogen gas on a Siemens P4 diffractometer. Careful centering of 29 reflections in the 2θ range 10−25° gave a unit cell. Data were collected with use of variable scan rates with three check reflections monitored every 100 reflections. Programs XSCHNS and SHELXL were used for data collection and refinement. Atomic coordinates and thermal parameters have been deposited at the Cambridge Crystallographic Database. Details of data collection for $MeNHCOCHCl_2$ are given in Table S2 of the Supporting Information.

Results

Theoretical Methods. The eight possible structures of $MeNHCOCHCl_2$ described previously in the Experimental Section were investigated ab initio. Of the four syn conformers studied, only two were returned as minima on the potential energy surface at the HF/6-31G* level. It was observed that *syn180* collapsed to the same structure as *syn120* with ϕ(HCCO) = 118°, and *syn60* collapsed to the *syn0* structure with ϕ(HCCO) = 0°. The lowest lying frequency for *syn120* was just 15 cm^{-1}, and this motion is associated with the HCCO torsion, compared to the next frequency of 104 cm^{-1} (methyl torsion). For *syn0*, the lowest lying frequency was 25 cm^{-1} for the HCCO bond torsion, with one at 32 cm^{-1} (methyl torsion). At the HF/6-31G* level, *syn120* was found to be 11.7 kJ mol^{-1} less stable than *syn0*. *Syn120* and *syn0* were both taken to a higher level of theory with the same basis set (MP2/6-31G*), at which point both returned the *syn0* structure. From this we concluded that there is only one syn conformer, with ϕ(HCCO) ≈ 0°.

The anti conformers were investigated in the same manner as the syn ones. At the HF/6-31G* level two conformers, *anti0* and *anti120*, were minima on the potential energy surface, with *anti60* and *anti180* collapsing back to *anti0* and *anti120*, respectively, as in the syn case. ϕ(HCCO) was 3° for *anti0* and 149° for *anti120*. At the MP2/6-31G* level, both conformers were returned. A summary of ϕ(CNCO), ϕ(HCCO), and molecular energies at the HF/6-31G* and MP2/6-311++G** levels for all four conformers is given in Table 1. The molecular geometry of the lowest energy conformer of $MeNHCOCHCl_2$ at the MP2/6-311++G** level (*syn0*) is given in Table 2. The molecular geometries calculated at the HF/6-31G*, MP2/6-31G*, MP2/6-311G*, MP2/6-311+G*, and MP2/6-311++G** levels to compare the effects of improving basis set and level of theory and the effect of inclusion of polarization and diffuse functions on the structural parameters are given in Table S3 in the Supporting Information.

At the highest level of theory and basis set investigated (MP2/6-311++G**), the anti conformers were at least 15 kJ mol^{-1} higher in energy than the syn conformer. At room temperature an energy difference of 15 kJ mol^{-1} would correspond to 99.7% of the lower energy conformer and 0.3% of the higher energy conformer being observed in the gas-phase electron diffraction experiment. The tiny amount of the higher energy conformer would be undetectable in the GED experiment. Thus the results of the ab initio calculations for the *syn0* structure will be the only ones analyzed here unless otherwise stated.

The C−N bond associated with the sp^3 carbon [C(2)−N(3)] varies little with increased level of theory and bigger basis set. However, the C−N bond with the sp^2 carbon [C(7)−N(3)]

TABLE 1: Comparison of Energies for the Four Conformers of MeNHCOCHCl$_2$ (all C_1) at the HF/6-31G* and MP2/6-311++G Levels and Torsion Angles ϕ(CNCO) and ϕ(HCCO)[a,b]**

level of theory	parameter	*syn0*	*syn120*	*anti0*	*anti120*
HF/6-31G*	energy[c]	−1164.8827	−1164.8784	−1164.8754	−1164.8727
	ϕ(CNCO)	0.1	7.1	−173.3	−179.7
	ϕ(HCCO)	−0.1	118.1	2.6	149.4
	ΔE[e]	0.0	+11.3	+19.2	+26.3
MP2/6-311++G**	energy[d]	−1166.0029		−1165.9972	−1165.9942
	ϕ(CNCO)	3.1		−169.6	178.4
	ϕ(HCCO)	−13.1		1.62	150.5
	ΔE[e]	0.0		+15.0	+22.8

[a] See text for conformer definitions. [b] Energies in hartrees. [c] Corrected for zero point energy. [d] Not corrected for zero point energy. [e] Energy in kJ mol^{-1}.

TABLE 2: Refined and Calculated Geometric Parameters for MeNHCOCHCl$_2$ (distances in pm, angles in deg) from the GED Study[a,b]

no.	parameter	MP2/6-311++G** (r_e)	GED (r_{h1})	restraint
		independent parameters		
p_1	(C−H mean + N−H)/2	105.1	105.1(4)	105.1(5)
p_2	C−H mean − N−H	8.3	8.4(6)	8.3(5)
p_3	[C(7)−C(9) + C(7)−N(3) + C(2)−N(3)]/3	144.6	145.8(2)	144.6(4)
p_4	C−C − [(C(7)−N + C(2)−N)/2]	13.1	11.9(4)	13.1(4)
p_5	C(2)−N(3) − C(7)−N(3)	10.3	9.9(4)	10.3(4)
p_6	C=O	122.4	124.7(3)	
p_7	C−Cl mean	177.7	178.4(2)	
p_8	H−C−H mean	109.1	107.6(10)	109.1(10)
p_9	C(2)−N(3)−C(7)	120.3	118.7(10)	120.3(18)
p_{10}	H(4)−N(3)−C(7)	119.0	118.9(8)	119.0(7)
p_{11}	N(3)−C(7)=O(8)	124.4	123.0(4)	
p_{12}	N(3)−C(7)−C(9)	115.9	118.0(6)	
p_{13}	C(7)−C(9)−H(10)	107.4	107.4(4)	107.4(3)
p_{14}	Cl(11)−C(9)−Cl(12)	111.4	110.7(2)	
p_{15}	H(10)−C(9)−Cl(11)	108.1	108.0(12)	108.1(10)
p_{16}	[C(7)−C(9)-Cl(11) + C(7)−C(9)−Cl(12)]/2	110.9	112.7(2)	
p_{17}	C(7)−C(9)−Cl(11) − C(7)−C(9)−Cl(12)	2.1	4.1(9)	2.1(10)
p_{18}	O(8)=C(7)−C(9)−H(10)	−13.1	−31.8(22)	
p_{19}	H(1)−C(2)−N(3)−C(7) (methyl torsion)	−173.0	−173.1(24)	−173.0(20)
p_{20}	C(2)−N(3)−C(7)=O(8)	3.1	2.0(24)	3.1(31)
p_{21}	H dip	10.7	10.5(24)	10.7(20)
		dependent parameters		
p_{22}	N(3)−C(7)	135.1	136.9(3)	
p_{23}	C(2)−N(3)	145.4	146.8(3)	
p_{24}	C(7)−C(9)	153.3	153.7(3)	
p_{25}	N(3)−H(4)	100.9	100.9(5)	
p_{26}	C(2)−N(3)−H(4)	119.8	121.5(13)	
p_{27}	O(8)=C(7)−C(9)	119.4	119.0(6)	
p_{28}	C(7)−C(9)−Cl(11)	112.0	110.7(5)	
p_{29}	C(7)−C(9)−Cl(12)	109.9	114.7(5)	

[a] Numbers in parentheses are the estimated standard deviations of the last digits. [b] See text for parameter definitions.

lengthens by 1.5 pm on increasing the level of theory, decreases by 3 pm on going from a double-ζ to triple-ζ basis set, then lengthens by 2.9 pm on the inclusion of diffuse functions (6-311+G*). Whereas we can say that C(2)−N(3) has converged with respect to basis set and level of theory, i.e., its value changes little on improving both, we cannot say this for the C(7)−N(3) bond length, which fluctuates wildly. Having observed this fluctuation for the C(7)−N(3) bond length, it is interesting to observe the C(7)−O(8) bond length behavior. The inclusion of electron correlation has a large effect on this distance, as expected (HF/6-31G* = 119.6 pm, MP2/6-31G* = 123.1 pm). Improving the basis set to triple-ζ reduces the bond length by 1 pm to 122.1 pm, and the inclusion of diffuse functions does not affect the parameter much (0.3 pm longer). Thus the C−O bond appears to be reaching convergence, whereas the C−N bond does not. Another unexpected feature is the lack of sensitivity of the C−Cl bonds to the inclusion of electron correlation and improvement of basis set. The biggest variation by either bond is 0.3 pm, whereas we expected a much bigger change upon the inclusion of electron correlation and diffuse functions.

Although the C−Cl bond distances are seemingly unaffected by changes in basis set and level of theory for this molecule, the C−C−Cl bond angles are slightly affected, mainly upon the inclusion of diffuse functions. Here, a decrease of 1.3° is observed for C(7)−C(9)−Cl(11), while an increase of 0.9° is observed for C(7)−C(9)−Cl(12). The Cl−C−Cl angle remains very stable, varying little upon the inclusion of electron correlation or change in basis set. The bond angles around N(3) differ by as much as 3.4° (MP2/6-31G*) but N(3) is calculated to be planar in all but the 6-311+G* and 6-311++G** cases. At the MP2/6-311+G* level the sum of the angles around N(3) is 359.7°, indicating only a very slight deviation from planarity at nitrogen, and at the MP2/6-311++G** level the sum is 359.1°. The range of angles at the MP2/6-311+G* level is the smallest (120.3−119.6°; 0.7°). A much wider range of bond angles is observed about C(7), with the largest at the MP2/6-311G* level (125.8−115.2°; 10.6°). Again the carbonyl carbon

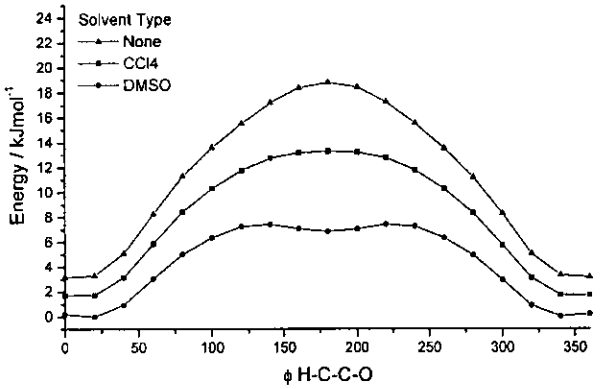

Figure 5. Effect of various solvents on the fluid-phase structure of *N*-methyldichloroacetamide.

is returned as planar at all levels except MP2/6-311++G**, and even in this case the sum of angles around C(7) is 359.7°, individual angles ranging from 124.4° [N(3)−C(7)−O(8)] to 115.9° [N(3)−C(7)−C(9)]. The H−C−H angles are also unaffected by the change in basis set and level of theory, and are hardly distorted from the perfect tetrahedral angle of 109.5° (109.1°, MP2/6-311++G**). This indicates that the methyl group is not distorted by either steric or electronic effects.

One parameter that does vary wildly with the inclusion of electron correlation, the increase in basis set size, and functionality is the bond torsion about C(7)−C(9). ϕ(HCCO) changes from −0.1° to −5.2° upon the inclusion of electron correlation with the 6-31G* basis set. The bond torsion then changes to 0.2° when the basis set is increased to 6-311G*. The most dramatic effect is seen upon the inclusion of diffuse functions, when ϕ(HCCO) changes from 0.2° to −13.1°, a change of 13.3°. ϕ(CNCO) does not vary so much on including electron correlation, or with increased basis set size. However, on going from a 6-311+G* basis set to a 6-311++G** basis set, a 2.1° increase is observed. Along with the slightly pyramidal nature of the nitrogen, this serves to remove the planarity of the CN(H)C(O)C backbone of the molecule.

Solvent Effect Calculations. It was observed that the orientation of the $CHCl_2$ group relative to the carbonyl group was very different between the solid and gaseous structures. One of the techniques used to try to account for this different orientation was solvation modeling. The conformation observed in the solid state is relatively polar and could in principle originate from a similar conformer preferentially stabilized in the polar media used during the synthesis of the amide. A full potential energy surface scan of the ϕ(HCCO) bond torsion was performed at the B3LYP/6-31G** level with tetrachloromethane and dimethyl sulfoxide as solvents. The results (Figure 5) indicate that the most stable conformer of *N*-methyldichloroacetamide has ϕ(HCCO) between −20° and 20° in the media studied. The calculations in DMSO, however, show stabilization of a higher energy conformer with ϕ(HCCO) ~ 180°. This conformer is calculated to be 6.9 kJ mol^{-1} higher in energy than the global minimum at the B3LYP/6-31G** level, corresponding to a 94.2:5.8 mixture of conformers at room temperature. On this basis solvent stabilization seems to be an unlikely explanation for the $CHCl_2$ rotameric state in the solid. It is also worth noting the absence of solvent molecules in the crystal structure itself.

Single-Point Energy Calculations. The results of the ab initio MO single-point energy (MP2 and DFT) calculations for the monomer and two dimers of the solid-state structure are given in Table 3. All energies quoted hereafter are those corrected for BSSE by using the CP correction. Solid-state calculations, as they are plane wave in nature, do not account for dispersion forces in long-range interactions. By using the exchange component and the gradient-corrected correlation functional of Perdew and Wang for the ab initio MO DFT calculation and comparing the results to the MP2 calculations, we can evaluate the effect of this omission on the different interaction energies. From the MP2/6-311++G** calculations, the interlayer Cl···O nonbonded interaction (X-ray, 304.5 pm) was determined to be 13.1 kJ mol^{-1}. This is a reasonably high intermolecular interaction energy and may help to explain the different orientation of the $CHCl_2$ group in the solid state compared to the gas phase. The intralayer H···O interactions (X-ray, 204.1 and 244.9 pm) were determined to correspond to an energy of 37.1 kJ mol^{-1}. This indicates that both the hydrogen bonds are also strong but the individual values cannot be resolved further. One of the hydrogen atoms involved in the bonding is the H of the $CHCl_2$ group, another indication as to why this particular group orientates itself in the way it does in the solid-state structure.

TABLE 3: Single Point Energy Calculations for Monomer and Two Different Dimers of $MeNHCOCHCl_2$ at the MP2/6-311++G and PW91PW91/6-311++G** Levels with Counterpoise Correction Calculations**

molecule/interaction	energy/ hartrees	interaction energy/ kJ mol^{-1} uncorrected[a]	interaction energy/ kJ mol^{-1} corrected[b]
MP2/6-311++G**/Cl···O		−18.9	−13.1
monomer	−1165.9291		
donor + ghost	−1165.9309		
acceptor + ghost	−1165.9314		
dimer	−2331.8655		
MP2/6-311++G**/H···O		−57.6	−37.1
donor + ghost	−1165.9320		
acceptor + ghost	−1165.9341		
dimer	−2331.8802		
PW91PW91/6-311++G**/Cl···O		−9.6	−6.9
monomer	−1167.6261		
donor + ghost	−1167.6264		
acceptor + ghost	−1167.6268		
dimer	−2335.2558		
PW91PW91/6-311++G**/H···O		−39.8	−36.4
donor + ghost	−1167.6267		
acceptor + ghost	−1167.6274		
dimer (H···O)	−2335.2673		

[a] E_{uncorr} = dimer − (2 × monomer) (uncorrected for basis set superposition error). [b] $E_{corr} = E_{uncorr}$ − (donor − monomer) − (acceptor − monomer) (corrected for basis set superposition error).

The DFT calculations (PW91PW91/6-311++G**) return a Cl···O interaction energy of 6.9 kJ mol^{-1} compared to the MP2 value of 13.1 kJ mol^{-1}. This indicates that some energy is "missing" from the DFT calculations of the nonbonded interactions. This missing energy is the effect of the dispersion forces, which, as mentioned previously, are neglected in the DFT calculations. The H···O calculated energy for two bonds is 36.4 kJ mol^{-1} compared to 37.1 kJ mol^{-1} calculated by the MP2 method. These energies are very similar, implying that the effects of the dispersion forces are negated by some other factor(s) for first-row atoms, but that they become important for interactions involving second-row atoms and beyond.

To ensure that the relative energies calculated by the two methods were consistent, the energy difference between the solid and gaseous structures was calculated at the MP2/6-311++G** and PW91PW91/6-311++G** levels (Table 3). The energy differences for the MP2 and DFT methods were 14.1 and 15.3 kJ mol^{-1}, respectively, with both returning the gaseous structure

TABLE 4: Geometric Parameters from Various Stages of Solid-State Plane Wave DFT Calculations[a,b]

parameter	X-ray	plane wave DFT	supercell (optimized)[c]	Cl···O interaction[d]	H···O interaction[d]
C=O	123.0	124.2	122.1	122.1	122.1
C−C	153.1	152.1	152.9	152.9	152.9
C−Cl	177.0	176.6	176.2	176.2	176.2
C−H(Cl_2)	99.0	109.1	109.1	109.1	109.1
N−C(H_3)	145.9	144.1	143.9	143.9	143.9
N−C(O)	131.5	133.1	135.3	135.3	135.3
N−H	87.0	103.6	101.7	101.7	103.6
O···H(1)	204.1	189.0			189.0
O···H(2)	244.9	240.6			240.6
Cl···O	304.5	311.7		311.7	
energy/molecule (hartree)		−2077.9193	−2077.3444	−2077.3985	−2077.8885

[a] Distances in pm. [b] ϕ(HCCO) always 180.0°. [c] Energy for single point supercell = −2077.3013 hartrees. [d] Single point energies.

as the more stable conformer. These energies are reasonably consistent and provide confidence for our previous assertions regarding interaction energies.

Solid-State Calculations. *Crystal Lattice Calculation.* The calculated structure, both geometry and unit cell vectors, agrees well with that obtained for the low-temperature crystal structure. The calculated unit-cell volume obtained is within 3.6 % of the crystal structure. There is good agreement between the calculated molecular geometry and that obtained experimentally in the low-temperature crystal structure. The largest difference between the values obtained for the non-hydrogen bond distances in the calculated and low-temperature crystal structures is 2 pm. The calculated distances for the nonbonded interactions do not match as well, with a difference of 15 pm for H···O(1) between calculated and observed values.

Supercell Calculations. The results from the two supercell calculations show that the geometry of the molecule changes little between the solid and gas phases in this orientation. The largest change is observed in the C=O bond length, which decreases by 2 pm from the crystal lattice to the supercell optimized calculation. This can be attributed to the fact that the oxygen atom is no longer involved in any intermolecular interactions, either to hydrogen or to chlorine atoms. The N−C(=O) bond distance is seen to increase in value from 133.1 to 135.3 pm between the calculation of the crystal lattice and supercell optimized calculation. This is also due to the destruction of the intermolecular interactions allowing the molecule to relax.

H···O and Cl···O Interactions. To study the H···O and Cl···O interactions, two of the four molecules were removed from the unit cell. Geometry optimizations were then not possible because the molecules would reorientate in a way that was not meaningful. The molecular geometries of the remaining molecules were therefore frozen and the energy recalculated. Relevant structural parameters from the above stages are given in Table 4, as well as those for the X-ray structure for comparison. The energy values obtained in these calculations are discussed later in this paper.

Gas-Phase Electron Diffraction Refinement. On the basis of the ab initio calculations described above, electron-diffraction refinements were carried out with use of a model of C_1 symmetry to describe the vapor. In accord with the calculations, the assumption of local C_{3v} symmetry for the methyl group was made.

The structure of $MeNHCOCHCl_2$ was finally defined in terms of 21 independent geometric parameters, comprising 7 bond lengths and differences, 10 bond angles and differences, and 4 torsion parameters [Table 2; atom numbering shown in Figure 1]. See the Supporting Information for the parameter definitions.

TABLE 5: Comparison of Geometrical Parameters for *N*-Methyldichloroacetamide from the X-ray Diffraction, Gas Electron Diffraction, and Theoretical Structures[a]

parameter	MP2/6-311++G**	GED	X-ray
C(2)−N(3)	145.4	146.8(3)	145.8(4)
N(3)−C(7)	135.1	136.9(3)	131.5(3)
C(7)=O(8)	122.4	124.7(3)	123.0(3)
C(7)−C(9)	153.3	153.7(3)	153.1(4)
C−Cl(11)	177.5	178.4(2)	177.0(2)
C−Cl(12)	177.8	178.4(2)	177.0(2)
C(2)−N(3)-C(7)	120.3	118.7(10)	121.7(2)
N(3)−C(7)=O(8)	124.4	123.0(4)	125.0(2)
N(3)−C(7)-C(9)	115.9	118.0(6)	114.5(2)
O(8)=C(7)−C(9)	119.4	119.0(6)	120.5(2)
C(7)−C(9)−Cl(11)	109.9	110.7(5)	108.7(1)
C(7)−C(9)−Cl(12)	112.0	114.7(5)	108.7(1)
Cl(11)−C(9)−Cl(12)	111.3	110.7(2)	110.5(1)
C(2)−N(3)−C(7)=O(8)	3.1	2.0(24)	0.0
O(8)=C(7)−C(9)−H(10)	−13.1	−31.8(22)	180.0

[a] See Figure 1 for atom numbering.

The starting parameters for the r_{h1} refinement[33] were taken from the theoretical geometry optimized at the MP2/6-311++G** level. Theoretical (MP2/6-311++G**) Cartesian force fields were obtained and converted into force fields described by a set of symmetry coordinates with use of the SHRINK program.[33] All geometric parameters were then refined.

In total all 21 geometric parameters and 16 groups of vibrational amplitudes were refined. Flexible restraints were employed during the refinement with use of the SARACEN method.[34] Altogether, 14 geometric and 9 amplitude restraints were employed. These are listed in Table 5.

In the final refinement, R factors were $R_G = 0.041$ and $R_D = 0.048$. The radial distribution curve and the molecular scattering intensity curves are shown in Figures 6 and 7, respectively. Final refined parameters are listed in Table 2, interatomic distances and the corresponding amplitudes of vibration in Table S4 (Supporting Information), and the least-squares correlation matrix in Table S5 (Supporting Information). Experimental coordinates from the GED analysis are given in Table S6 (Supporting Information). Figure 1 shows a perspective view of $MeNHCOCHCl_2$ in the optimum refinement of the GED data, as well as a view down the (O−)C−N bond

X-ray Crystallography. Solid-state structural analysis of $MeNHCOCHCl_2$ was carried out with low-temperature single-crystal X-ray diffraction at 233 K. The solid structure was found to possess the orthorhombic space group *Pnma* with four molecules per unit cell. The structure was solved by direct methods[35] and all non-hydrogen atoms were treated as aniso-

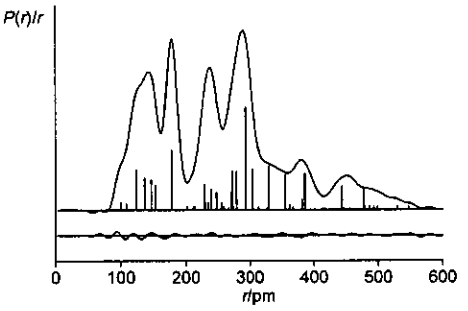

Figure 6. Experimental and difference (experimental − theoretical) radial-distribution curves, $P(r)/r$, for $MeNHCOCHCl_2$. Before Fourier inversion the data were multiplied by $s \exp(-0.00002s^2)/(Z_{Cl} - f_{Cl})/(Z_C - f_C)$.

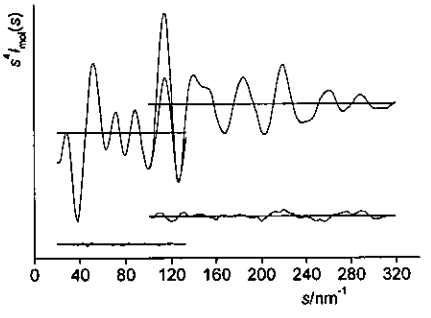

Figure 7. Experimental and final weighted difference (experimental − theoretical) molecular-scattering intensities for $MeNHCOCHCl_2$.

tropic. In the solid state $MeNHCOCHCl_2$ adopts a planar heavy-atom structure with ϕ(HCCO) = 180°. The atoms C(2), N(3), C(7), O(8), and C(9) lie on a mirror plane that relates Cl(11) and Cl(12). The methyl group was modeled as two groups related by a 180° rotation at equal occupancy. The crystal structure is the same as shown in Figure 4. The geometrical parameters determined by the X-ray crystallographic study of *N*-methyldichloroacetamide are listed in Table 5, along with the equivalent parameters from the gas electron diffraction and ab initio study.

Discussion

The structural properties of *N*-methyldichloroacetamide have been investigated in the gas phase by gas-phase electron diffraction and ab initio methods, in the fluid phase by ab initio solvent-inclusion methods, and in the solid phase by X-ray crystallography, ab initio, and plane-wave density functional methods.

In general, the experimental gas-phase and theoretical structures agree well with each other. Theoretical bond lengths were generally found to be within 1−2 pm of the experimental values, and the bond angles were also within 1−2° of the experimental values. The main difference between the structures occurs in the HCCO bond torsion. The value of ϕ(HCCO) is calculated to be −13.1° for the free molecule at the MP2/6-311++G** level, whereas a value of −31.8(22)° is returned by the GED experiment. However, if the structure is constrained to the value calculated at the MP2/6-311++G** level, the *R* factor rises significantly (0.105 compared to 0.041), indicating that the goodness of fit for the experimental data has deteriorated significantly with the imposition of the ab initio value. Given the large variation of this torsion angle, by ~15°, during the calculations, this difference between the experimental and ab initio value for this parameter is not surprising. Examination of the correlation matrix (Table S5) indicates that this parameter is not heavily correlated with any others, and during the refinement procedure the parameter was very stable, barely changing from the final reported value on refinement of other parameters. Another test was to constrain the HCCO torsion angle to the value obtained from the GED study and recalculate the molecular structure at the MP2/6-311++G** level to evaluate the energy difference between the two. This energy difference was found to be just 1.2 kJ mol^{-1}. Figure 5 shows the energy differences for the torsional variation at the B3LYP level. It can be seen that the potential is very flat for ϕ(HCCO) between −20° (340°) and 20°. Both these pieces of evidence indicate that it is relatively easy for the molecule to deviate from the equilibrium structure as calculated ab initio to the GED structure, which *is* corrected for the effects of vibrations at the temperature of the experiment.

Although parameters determined in the gaseous and solid phases are not directly comparable because of the differences in diffraction techniques, most of the X-ray crystallographic parameters agree well with those in the gas phase. However, there are significant differences between the N(3)−C(7) bond distances [GED, 136.9(3) pm; X-ray, 131.5(3) pm], and the N(3)−C(7)−C(9) and C(7)−C(9)−Cl(11/12) bond angles. GED determines the N−C−C bond angle to be 118.0(6)°, significantly larger than the value of 114.5(2)° for the crystal, while the C−C−Cl(12) bond angle was found to be 114.7(5)° by GED and only 108.7(1) by X-ray crystallography.

The shortening of the N−C bond has been observed previously for other acetamides.[36,37] In acetamide,[36] the C−N bond was determined to be 138.0(4) pm in the gas phase compared to 133.4(17) pm in the crystal structure.[38] In *N*-methylacetamide,[37] the gaseous C−N bond length was found to be 138.6 pm, nearly 10 pm longer than the solid-state value of 129.0 pm.[39] The shortening of these bonds in all cases can be attributed to the intermolecular hydrogen bonding in the solid structures. In the cases of acetamide and *N*-methylacetamide, the C=O bond length was also consistently shorter in the gas-phase structures than in the solid-phase ones. For example, in acetamide the gaseous C=O bond was 122.0(3) pm compared to 126.0(11) pm in the solid state. The difference was not so dramatic in *N*-methylacetamide (gas, 122.5 pm; solid, 123.6 pm), while in *N*-methyldichloroacetamide the C=O bond length is actually determined to be longer in the gas phase than in the solid phase [gas, 124.7(3) pm; solid, 123.0(3) pm]. The gaseous C=O bond length is much longer in *N*-methyldichloroacetamide than in *N*-methylacetamide and acetamide [124.7(3) pm cf. 122.5 and 122.0(3) pm]. This can be attributed to the electron-withdrawing effect of the two chlorine atoms on the $CHCl_2$ group adjacent to the C=O bond, weakening it and making it longer. The solid-phase C=O bond length is similar to that in *N*-methylacetamide, while both these are much less than that in acetamide.

The torsion angle ϕ(HCCO) in the gaseous structure was also investigated in a solvent field at the B3LYP/6-31G** level to gauge the effects of tetrachloromethane and dimethyl sulfoxide (DMSO) on the conformation of the molecule. When no solvent is present, there is a definite maximum in the curve at ϕ(HCCO) ~ 180°, confirming that this structure is not real in the gas phase. Using CCl_4 as a solvent results in a very broad maximum at ϕ(HCCO) ~ 150° to 200°, implying that CCl_4 does not change the preferred conformation of the molecule, or predispose it to form the observed solid-state conformation about the C−C bond. However, using DMSO as a solvent does result in a minimum at ϕ(HCCO) ~ 180°. This minimum is significantly higher in

energy than that observed for ϕ(HCCO) ~ 20° (6.9 kJ mol^{-1}), corresponding to a 94.2:5.8 mixture of conformers at room temperature and a 97.6:2.4 mixture at 223 K (the temperature at which the crystal was formed). Of course, the conformation adopted in the crystal depends on the total energy of the system, which depends on the sum of all interactions. Nevertheless, the calculations do show that a second conformation, with ϕ(HCCO) = 180°, is possible.

Further investigation of the solid-state structure was undertaken with ab initio molecular orbital and plane-wave DFT methods to investigate whether there are solid-state interactions that would favor molecular crystal formation with ϕ(HCCO) = 180° (as opposed to the gaseous ϕ(HCCO) = −30°). These intermolecular bonds should ideally involve the hydrogen and chlorine atoms of the $CHCl_2$ group to help explain the conformation observed. Examination of the crystal structure reveals possible interlayer Cl···O bonding (Figure 2a) involving chlorine from the $CHCl_2$ group, and two possible intralayer H···O bonds (Figure 2b) involving the hydrogen of the $CHCl_2$ group and the amide hydrogen, both with the carbonyl oxygen.

Two different dimers were chosen to describe the interactions to be investigated ab initio, using ab initio MO single-point energy calculations on the crystal coordinates. One dimer described the single Cl···O interaction while the other described the two H···O bonds, although it is impossible to resolve them further. Both MP2 and DFT methods (MP2/6-311++G**/PW91PW91/6-311++G**) were used to analyze any differences between the two methods, especially for the Cl···O interactions. Although the Cl···O interaction may be classically regarded as repulsive, it has been previously observed that weak Cl···O interactions may be important in stabilizing a structure. For example, the solid-state structure of oxalyl chloride[40] is anti, with weak Cl···O interactions, while the gaseous structure was found to be a mixture of anti and gauche conformers in an approximate 50:50 mixture (varying with temperature).[41] Therefore, although not contributing much energy, these interactions can be important and cannot be ignored altogether from the theoretical study. From Table 3 it can be seen that the interaction energy for the Cl···O bond was 13.1 kJ mol^{-1} for MP2 and 6.9 kJ mol^{-1} for DFT. For the H···O interactions, the energy was very similar from both MP2 and DFT methods (37.1 and 36.4 kJ mol^{-1}, respectively). The substantial difference between the MP2 and DFT methods for the Cl···O interaction can be attributed to the lack of modeling of dispersion forces by DFT. It is anticipated that a significant proportion of the Cl···O bond will be van der Waals in nature, which is not modeled in current DFT functionals. The pure ab initio method (in this case MP2) gives a more rigorous approximation of the forces, and so the interaction energy is higher. This is especially significant for interactions involving atoms in the second row and higher.

The solid-state interactions were also investigated under periodic boundary conditions by PW-DFT and compared to the energies obtained from the ab initio MO investigation. These calculations are especially interesting as they involve optimizing the structure under periodic conditions, where the surrounding molecules influence the molecular structure. In this case the Cl···O interaction energy was calculated to be just 2.4 kJ mol^{-1}, while the H···O interactions were predicted to be 46.5 kJ mol^{-1}. Comparing with the ab initio MO values (PW91PW91, 6.9 and 36.4 kJ mol^{-1}; MP2, 13.1 and 37.1 kJ mol^{-1}) it appears that under periodic conditions the H···O interactions have much more influence on the structure than the Cl···O interaction. Closer observation of the solid-state structure reveals that the H···O interactions form a chain across the molecules, with each interaction further stabilizing the next one. These synergistic interactions help to stabilize the overall solid-state structure, with the energy gained from the solid-state H···O interactions (between 36 and 46 kJ mol^{-1}) overcoming the energy lost by rotating the $CHCl_2$ group from ϕ(HCCO) = −31° to ϕ(HCCO) = 180° upon crystallization (~15 kJ mol^{-1}). We believe that this is the reason for the dramatic conformational change observed on going from that gas to the solid phase. The increase in energy of hydrogen bonding by ~10 kJ mol^{-1} from the dimer system to the periodic system has been observed previously for urea.[42] In this case, Dannenberg et al. demonstrated that as the urea dimer was extended to form an infinite one-dimensional chain, the strength of intermolecular interaction increased by almost 10 kJ mol^{-1}.

Other molecules containing the dichloroacetamido moiety have also been investigated to examine the correlation between the HCCO torsion angle and intermolecular hydrogen bonding in the solid phase. A search of the Cambridge Structural Database (CSD)[43,44] reveals 14 structures with the $NHCOCHCl_2$ moiety, 12 of which possess the torsion ϕ(HCCO) ~ 180°. Close examination of the crystal structures of dichloroacetylaminoisobutyric acid[45] and chloramphenicol[46] both reveal hydrogen bonding between the carbonyl oxygen on one molecule and the N−H and $CHCl_2$ hydrogen atoms on an adjacent molecule. Both these structures yield ϕ(HCCO) ~ 180°. It is observed that for the 12 structures with ϕ(HCCO) ~ 180°, hydrogen bonding between both the H of the $CHCl_2$ group and the H of the amido group to the adjacent carbonyl is always present. Thiamphenicol[47] is a close relative of chloramphenicol, simply replacing the NO_2 group with a SO_2CH_3 group. In this case, hydrogen bonding is also observed at the carbonyl oxygen and $CHCl_2$ hydrogen, but involving one of the S=O bonds and the sulfonyl methyl group. In this case, ϕ(HCCO) is ~0°, which serves to facilitate the observed bonding. Thus it appears that the $CHCl_2$ group orientates itself in the solid state to optimize hydrogen bonding, and hence stabilization of the crystal structure. In the one remaining structure from the CSD, no bonding between the $CHCl_2$ group and any other group is present, and in this case ϕ(HCCO) was observed to be −45°, close to that observed in our gas-phase structure.

Conclusions

The structure of *N*-methyldichloroacetamide has been elucidated in the gas and solid phases. The gas-phase structure was found to be that with ϕ(HCCO) = −31.8(22)°, similar to the most energetically favorable conformer by ab initio calculations. The solid state was found to consist of a conformer with ϕ(HCCO) = 180.0°. This was also found to be energetically favorable, by further theoretical investigations of the crystal structure, because of solid-state interactions that are not possible for the gaseous conformation. The combined use of gas- and solid-phase experimental and theoretical techniques, including the relatively new plane-wave DFT method, has facilitated the structural investigation of this apparently straightforward but nevertheless fascinating molecule.

Acknowledgment. We thank the U.K. Computational Chemistry Facility (admin: Department of Chemistry, King's College London, Strand, London WC2R 2LS) for the computing time on Columbus and Dr. Svein Samdal (University of Oslo) for helpful discussions. C.A.M. is grateful to the Royal Society for the award of a University Research Fellowship.

Supporting Information Available: Parameter descriptions for the GED model of $MeNHCOCHCl_2$ (text); nozzle-to-plate

distances (mm), weighting functions (nm^{-1}), correlation parameters, scale factors, and electron wavelengths (pm) used in the gas electron diffraction study of $MeNHCOCHCl_2$; X-ray crystal structure data collection, processing, solution, and refinement for $MeNHCOCHCl_2$; molecular geometry of the lowest energy (*syn0*) C_1 structure of $MeNHCOCHCl_2$ at the HF/6-31G*, MP2/6-31G*, MP2/6-311G*, and MP2/6-311+G* levels of theory; interatomic distances (*r*/pm) and amplitudes of vibration (*u*/pm) for the restrained GED structure of $MeNHCOCHCl_2$; least-squares correlation matrix (×100) for $MeNHCOCHCl_2$; experimental GED coordinates for $MeNHCOCHCl_2$ (all tables). This material is available free of charge via the Internet at http://pubs.acs.org.

References and Notes

(1) Samdal, S.; Seip, R. *J. Mol. Struct.* **1997**, *413*−*414*, 423.

(2) Gundersen, S.; Novikov, V. P.; Samdal, S.; Seip, R.; Shorokov, D. J.; Sipachev, V. A. *J. Mol. Struct.* **1999**, *485*−*486*, 97.

(3) Gundersen, S.; Samdal, S.; Seip, R.; Shorokov, D. J. *J. Mol. Struct.* **1999**, *477*, 225.

(4) Fausto, R.; Teixeira-Dias, J. J. C. *J. Mol. Struct.* **1986**, *144*, 225.

(5) Fausto, R.; Teixeira-Dias, J. J. C. *J. Mol. Struct.* **1986**, *144*, 241.

(6) Tormena, C. F.; Amadeu, N. S.; Rittner, R.; Abraham, R. J. *J. Chem. Soc., Perkin Trans. 2* **2002**, 773.

(7) Kulbida, A.; Fausto, R. *J. Chem. Soc., Faraday Trans.* **1993**, *89*, 4257.

(8) Litvinov, O. A.; Zuev, M. B.; Naumov, V. A.; Volden, H. V.; Hagen, K. *J. Phys. Chem.* **1993**, *97*, 10674.

(9) Shen, Q.; Hilderbrandt, R.; Hagen, K. *J. Mol. Struct.* **1980**, *71*, 161.

(10) Ginzburg, I. M. *Zh. Obsch. Khim.* **1983**, *53*, 2563.

(11) Thomas, E. W. Manuscript in preparation.

(12) Liler, M. *J. Chem. Soc. B* **1969**, 385. Molday, R. S.; Kallen, R. G. *J. Am. Chem. Soc.* **1972**, *94*, 6739.

(13) Frisch, M. J.; Trucks, G. W.; Schlegel, H. B.; Scuseria, G. E.; Robb, M. A.; Cheeseman, J. R.; Zakrzewski, V. G.; Montgomery, J. A., Jr.; Stratmann, R. E.; Burant, J. C.; Dapprich, S.; Millam, J. M.; Daniels, A. D.; Kudin, K. N.; Strain, M. C.; Farkas, O.; Tomasi, J.; Barone, V.; Cossi, M.; Cammi, R.; Mennucci, B.; Pomelli, C.; Adamo, C.; Clifford, S.; Ochterski, J.; Petersson, G. A.; Ayala, P. Y.; Cui, Q.; Morokuma, K.; Malick, D. K.; Rabuck, A. D.; Raghavachari, K.; Foresman, J. B.; Cioslowski, J.; Ortiz, J. V.; Baboul, A. G.; Stefanov, B. B.; Liu, G.; Liashenko, A.; Piskorz, P.; Komaromi, I.; Gomperts, R.; Martin, R. L.; Fox, D. J.; Keith, T.; Al-Laham, M. A.; Peng, C. Y.; Nanayakkara, A.; Gonzalez, C.; Challacombe, M.; Gill, P. M. W.; Johnson, B.; Chen, W.; Wong, M. W.; Andres, J. L.; Gonzalez, C.; Head-Gordon, M.; Replogle, E. S.; Pople, J. A. *Gaussian 98*, Revision A.7; Gaussian, Inc.: Pittsburgh, PA, 1998.

(14) Segall, M. D.; Lindan, P. L. D.; Probert, M. J.; Pickard, C. J.; Hasnip, P. J.; Clark, S. J.; Payne, M. C. *J. Phys. Condens. Matter* **2002**, *14* (11), 2717−2743.

(15) Binkley, J. S.; Pople, J. A.; Hehre, W. J. *J. Am. Chem. Soc.* **1980**, *102*, 939.

(16) Gordon, M. S.; Binkley, J. S.; Pople, J. A.; Pietro, W. J.; Hehre, W. J. *J. Am. Chem. Soc.* **1982**, *104*, 2797.

(17) Pietro, W. J.; Francl, M. M.; Hehre, W. J.; DeFrees, D. J.; Pople, J. A.; Binkley, J. S. *J. Am. Chem. Soc.* **1982**, *104*, 5039.

(18) Hehre, W. J.; Ditchfield, R.; Pople, J. A. *J. Chem. Phys.* **1972**, *56*, 2257.

(19) Hariharan, P. C.; Pople, J. A. *Theor. Chim. Acta* **1973**, *28*, 213.

(20) Gordon, M. S. *Chem. Phys. Lett.* **1980**, *76*, 163.

(21) McLean, A. D.; Chandler, G. S. *J. Chem. Phys.* **1980**, *72*, 5639.

(22) Krishnan, R.; Binkley, J. S.; Seeger, R.; Pople, J. A. *J. Chem. Phys.* **1980**, *72*, 650.

(23) (a) Becke, A. D. *J. Chem. Phys.* **1993**, *98*, 5648. (b) Lee, C.; Yang, W.; Parr, R. G. *Phys. Rev. B* **1988**, *37*, 785.

(24) (a) Wong, M. W.; Frisch, M. J.; Wiberg, K. B. *J. Am. Chem. Soc.* **1991**, *113*, 4776. (b) Wong, M. W.; Wiberg, K. B.; Frisch, M. J. *J. Am. Chem. Soc.* **1992**, *114*, 523. (c) Wong, M. W.; Wiberg, K. B.; Frisch, M. J. *J. Am. Chem. Soc.* **1992**, *114*, 1645.

(25) van Duijneveldt, F. B.; van Duijneveldt-van de Rijdt, J. G. C. M.; van Lenthe, J. H. *Chem. Rev.* **1994**, *94*, 1873.

(26) Perdew, J. P.; Burke, K.; Ernzerhof, M. *Phys. Rev. Lett.* **1997**, *77*, 3865.

(27) Monkhurst, H. J.; Pack, J. D. *Phys. Rev. B* **1976**, *13*, 5188.

(28) Huntley, C. M.; Laurenson, G. S.; Rankin, D. W. H. *J. Chem. Soc., Dalton Trans.* **1980**, 954.

(29) Lewis, J. R.; Brain, P. T.; Rankin, D. W. H. *Spectrum* **1997**, *15*, 7.

(30) Cradock, S.; Koprowski, J.; Rankin, D. W. H. *J. Mol. Struct.* **1981**, *77*, 113.

(31) Boyd, A. S. F.; Laurenson, G. S.; Rankin, D. W. H. *J. Mol. Struct.* **1981**, *71*, 217.

(32) Ross, A. W.; Fink, M.; Hilderbrandt, R. *International Tables for Crystallography*; Wilson, A. J. C., Ed.; Kluwer Academic Publishers: Dordrecht, The Netherlands, , 1992; Vol. C, p 245.

(33) Sipachev, V. A. *J. Mol. Struct. (THEOCHEM)* **1985**, *121*, 143.

(34) Brain, P. T.; Morrison, C. A.; Parsons, S.; Rankin, D. W. H. *J. Chem. Soc., Dalton Trans.* **1996**, 4589. Blake, A. J.; Brain, P. T.; McNab, H.; Miller, J.; Morrison, C. A.; Parsons, S.; Rankin, D. W. H.; Robertson, H. E.; Smart, B. A. *J. Phys. Chem.* **1996**, *100*, 12280.

(35) Sheldrick, G. M. *Acta Crystallogr.* **1990**, *A46*, 467.

(36) Kitano, M.; Kuchitsu, K. *Bull. Chem. Soc. Jpn.* **1973**, *46*, 3048.

(37) Kitano, M.; Fukuyama, T.; Kuchitsu, K. *Bull. Chem. Soc. Jpn.* **1973**, *46*, 384.

(38) Hamilton, W. C. *Acta Crystallogr.* **1965**, *18*, 866

(39) Katz, J. L.; Post, B. *Acta Crystallogr.* **1960**, *13*, 624.

(40) Groth, P.; Hassel, O. *Acta Chem. Scand.* **1962**, *16*, 2311.

(41) Hagen, K.; Hedberg, K. *J. Am. Chem. Soc.* **1973**, *95*, 1003.

(42) Masunov, A.; Dannenberg, J. J. *J. Phys. Chem. B* **2000**, *104*, 806.

(43) CONQUEST, Cambridge Crystallographic Data Centre, Cambridge, 2001.

(44) CSD Version 5.34: Allen, F. H.; Kennard, O. *Chem. Design Autom. News* **1993**, *8*, 31.

(45) Valle, G.; Bonora, G. M.; Toniolo, C. *Gazz. Chim. Ital.* **1984**, *114*, 481.

(46) Chatterjee, C.; Dattagupta, J. K.; Saha, N. N.; Saenger, W.; Muller, K. *J. Cryst. Mol. Struct.* **1979**, *9*, 295.

(47) Ghosh, M.; Basak, A. K.; Mazumdar, S. K.; Párkányi, L.; Kálmán, A. *Acta Crystallogr.* **1987**, *C43*, 1552.

Appendix G

Publications

Highly asymmetric coordination in alkenes: gas-phase structures of trans-1,2-dichloro-1,2-disilylethene and 1-bromo-1-silylethene.
McLachlan L. J; Hinchley S. L; Rankin D. W H; Morrison C. A; Robertson H. E; Mitzel N. W; Rudinger C.; Schmidbaur H. *Inorg. Chem.* **2003**, *42(20)*, 6539.

Conformational Analysis with Both Experimental and Computational Data for Both Gaseous and Crystalline Phases: Unexpected Interactions in N-Methyldichloroacetamide
Hinchley, S. L.; Robertson, H. E.; McLachlan, L. J.; Morrison, C. A.; Rankin, D. W. H.; Simpson, S. J.; Thomas, E. W. *J. Phys. Chem.*, **2004**, *108(1)*, 185.

Strong intramolecular secondary Si···N bonds in trifluorsilylhydrazines
Vojinović, K.; McLachlan, Lorna J.; Rankin, D. W.H.; Mitzel, N. W., *manuscript submitted.*

Molecular structures of bistrichlorosilyldimethylgermane $[Me_2Ge(SiCl_3)_2]$ *and trimethyltrichlorosilylgermane* $(Me_3GeSiCl_3)$ *by gas electron diffraction and ab initio calculations.*
McLachlan, L.J.; Hinchley, S. L.; Robertson, H. E.; Rankin, D. W. H.; Sepaala, E.; du Mont, W. W., *manuscript in* preparation.

Appendix H

Courses and conferences attended

Courses attended

- Unix 1, 2000
- Unix 2, 2000
- HTML – publishing on the web, 2000
- More HTML – forms and scripts, 2000
- Fortran programming, 2001
- C programming, 2001
- Computers in Chemistry, 2002
- Exotic instruments, 2002
- Dr. C. A. Morrison's Computational chemistry lectures, 2000
- BCA/ICG Intensive course in crystallography, Durham, 2001
- Departmental colloquia, 2000 – 2003
- Inorganic section meetings, 2000 – 2003.

Conferences attended

9th European Symposium on Molecular Structure
Blaubeuren, Germany, June 2001
Poster presentation: "Freely Rotating Silyl Groups – or is it just more spin?"

Universities of Scotland Inorganic Conference (USIC),
University of St. Andrews, U.K., September 2001
Poster presentation: as above
Prize – best poster

19th Austin Symposium on Molecular Structures
Austin, U.S.A., March 2002
Poster presentation: "β-N interations in Silyl Hydrazines?"

Universities of Scotland Inorganic Conference
University of Edinburgh, U.K., September 2002.
Member of organising committee

Exploring Modern Computational Chemistry
University of Nottingham, U.K., August 2002.
Poster presentation: "Why Theoreticians Need Experimentalists"

10^{th} European Symposium on Molecular Structure,
St. Petersburg, Russia, July 2003
Poster presentation: "Interactions in Silyl Hydrazines"

Universities of Scotland Inorganic Conference,
University of Strathclyde, U.K., September 2003
Poster presentation: as above